

1 of 3

RECEIVED

SEP 27 1993

OSTL
ISL 1670

Application of an Electrochemical Quartz Crystal Microbalance to
the Study of Electrocatalytic Films

by

Gordon, James

PHD Thesis submitted to Iowa State University

Ames Laboratory, U.S. DOE

Iowa State University

Ames, Iowa 50011

Date Transmitted: September 1, 1993

PREPARED FOR THE U.S. DEPARTMENT OF ENERGY

UNDER CONTRACT NO. W-7405-Eng-82.

RECEIVED

DISTRIBUTION OF THIS DOCUMENT IS UNLIMITED

DISCLAIMER

This report was prepared as an account of work sponsored by an agency of the United States Government. Neither the United States Government nor any agency thereof, nor any of their employees, makes any warranty, express or implied, or assumes any legal liability or responsibility for the accuracy, completeness or usefulness of any information, apparatus, product, or process disclosed, or represents that its use would not infringe privately owned rights. Reference herein to any specific commercial product, process, or service by trade name, trademark, manufacturer, or otherwise, does not necessarily constitute or imply its endorsement, recommendation, or favoring by the United States Government or any agency thereof. The views and opinions of authors expressed herein do not necessarily state or reflect those of the United States Government or any agency thereof.

This report has been reproduced directly from the best available copy.

AVAILABILITY:

To DOE and DOE contractors: Office of Scientific and Technical Information
P.O. Box 62
Oak Ridge, TN 37831

prices available from: (615) 576-8401
FTS: 626-8401

To the public: National Technical Information Service
U.S. Department of Commerce
5285 Port Royal Road
Springfield, VA 22161

Application of an Electrochemical Quartz Crystal
Microbalance to the study of electrocatalytic films

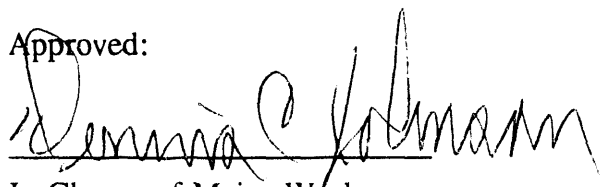
by

James Samuel Gordon, Jr.

A Dissertation Submitted to the
Graduate Faculty in Partial Fulfillment of the
Requirements for the Degree of
DOCTOR OF PHILOSOPHY

Department: Chemistry
Major: Analytical Chemistry

Approved:

A handwritten signature in black ink, appearing to read "Dennis C. Johnson", is written over a horizontal line.

In Charge of Major Work

For the Major Department

For the Graduate College

Iowa State University
Ames, Iowa

1993

Application of an Electrochemical Quartz Crystal
Microbalance to the study of electrocatalytic films

James Samuel Gordon, Jr.

Under the supervision of Dennis C. Johnson
From the Department of Chemistry
Iowa State University

An Electrochemical Quartz Crystal Microbalance (EQCM) was applied to the study of the deposition and composition of electrodeposited pure lead dioxide (PbO_2) and bismuth-doped lead dioxide films (Bi-PbO_2) that are active toward anodic oxygen-transfer reactions. Mass-to-charge ratio ($\Delta m/\Delta q$) values obtained for the electrodeposited films were concluded to indicate that within Bi-PbO_2 films Bi is incorporated as Bi^{+5} in the form of BiO_2A^- , where A represents an electrolyte anion (ClO_4^- or NO_3^-). No such anion incorporation is observed in the electrodeposition of PbO_2 . For the deposition of both PbO_2 and Bi-PbO_2 , the effect of changes in hydration between the Au oxide and the depositing film resulted in higher than expected initial $\Delta m/\Delta q$ values. X-ray diffraction (XRD) and X-ray photoelectron spectroscopy (XPS) were also used to study these films. XPS data indicate that for the Bi-PbO_2 films the ratio of $[\text{Bi}^{+3}]/[\text{Pb}^{+2}]$ in the films was identical to that in the deposition solutions. No difference was observed between the PbO_2 and Bi-PbO_2 films in the XRD spectra. This is evidence that the rutile structure of PbO_2 is retained even with the incorporation of Bi.

The EQCM was applied also to studies of the formation and dissolution of Au oxide and preoxide structures formed on the Au substrate electrodes in acidic media. The preoxide structures were concluded to be AuOH and resulted in increased surface mass because of hydrogen bonding to water molecules adjacent to the electrode surface. An average of 32 water molecules was concluded to be associated with each AuOH formed on the electrode surface.

In addition, various methods were explored for the formation of stable Au films on the quartz wafers. The most effective of these methods is the use of Ti as an interlayer between the Au and quartz. Criteria were established also to substantiate the stability of the vapor deposited Au films.

DEDICATION

To: The One who created all things, both in the heavens and on the earth,
visible and invisible...the One who is before all things, and in Whom all
things are held together...Our great God and Savior, Jesus Christ.

TABLE OF CONTENTS

ACKNOWLEDGEMENTS	iv
GENERAL INTRODUCTION	1
 PAPER I. ELECTROCATALYSIS OF ANODIC OXYGEN-TRANSFER REACTIONS: APPLICATION OF AN ELECTROCHEMICAL QUARTZ CRYSTAL MICROBALANCE TO A STUDY OF PURE AND BISMUTH-DOPED BETA-LEAD DIOXIDE FILM ELECTRODES	 30
INTRODUCTION	31
EXPERIMENTAL	33
RESULTS AND DISCUSSION	37
CONCLUSIONS	72
REFERENCES	74
 PAPER II. APPLICATION OF AN ELECTROCHEMICAL QUARTZ CRYSTAL MICROBALANCE TO A STUDY OF THE DEPOSITION OF PbO_2 AND Bi-PbO_2 FILMS ON GOLD ELECTRODES	 76
INTRODUCTION	77
EXPERIMENTAL	79
RESULTS AND DISCUSSION	81
CONCLUSIONS	116
REFERENCES	125

PAPER III. APPLICATION OF AN ELECTROCHEMICAL QUARTZ CRYSTAL MICROBALANCE TO A STUDY OF WATER ADSORPTION AT GOLD SURFACES IN ACIDIC MEDIA	126
INTRODUCTION	127
EXPERIMENTAL	130
RESULTS AND DISCUSSION	131
CONCLUSIONS	148
REFERENCES	153
GENERAL CONCLUSIONS	155
LITERATURE CITED	157
APPENDIX	161

ACKNOWLEDGEMENTS

First and foremost, I want to thank my Heavenly Father for creating all of the chemistry occurring around us. Next, how can I thank my wife? She has been my constant love and companion during my time at ISU. Her encouragement and challenges have carried me through the depths of despair and strengthened me to the heights of joy. She is truly a Proverbs 31 woman. To my parents I owe my very life and am grateful that they aimed me in such an excellent direction in my youth. Their constant guidance and example has, at times, meant the difference between continuing and quitting. Seeing that they "practice what they preach" has made all the difference.

I have learned a great deal from many friends and colleagues at ISU. I regret the limited space to only mention a few, but please know that I cherish all of you. To Dr. Larry Larew, I say thank you for making me feel at home in the Johnson group and for helping me get started with the EQCM. To Dr. Brian Wels, thank you for your friendship and all of the help during my early years. You made the lab an enjoyable place to be. To Dr. Joseph Vitt and David Dobberpuhl, thank you for all of our lengthy discussions. You provided me with a lot of insights and asked great questions, not all of them about chemistry. I hope that I returned the favor from time to time. To my good friend Jianren Feng, thank you for your cheerful smile, words of encouragement, and, especially, for your example of hard work. I will greatly miss our racquetball games. To my dear friend Leslie Perkins, our lunches and racquetball games were special times. You were a ray of sunshine on some pretty cloudy days. And to my newest friend Dr.

Kirk Kawagoe, thanks for the constant reality checks of perspective during my last few steps. Your knowledge and insight have been a great help in accomplishing this work. It has been a privilege to work with Bill LaCourse, Rich Roberts, Peter Vandeberg, Doug Williams, Lupe Anderson, Kim Pamplin, Jisheng Ge, Theo Clark, Linda Houk, and Anna Tudos. Thanks for all of your friendships. I want to especially thank Dr. Porter for allowing me the use of their Edwards thermal vaporization chamber. Without that, there would have been no dissertation. Also, I want to thank Victor Young for his help with the x-ray diffraction work.

I am forever indebted to Dr. Dennis Johnson for what he has taught me as a teacher, researcher, and friend. His character and enthusiasm command the greatest respect not only from me but from all of his students. I count it the highest of honors to have worked under his direction. If I become only half the teacher he is, my students will be fortunate.

To the secretaries and staff, especially Allis Dethrow and Norma Sandvick, I say thank you. I couldn't have made it through without all of your help.

Lastly, I want to thank Ames Laboratory for bankrolling this research. This work was performed at Ames Laboratory under contract no. W-7405-eng-82 with the U. S. Department of Energy Office of Basic Energy Sciences. The United States government has assigned the DOE Report number IS-T 1670 to this thesis.

GENERAL INTRODUCTION

Explanation of Thesis Format

This dissertation includes a general introduction section which gives the background information about the goals of the research and experimental techniques. Three research papers comprise the body of the dissertation and will be discussed below. Following these papers are general conclusions from this work and future plans. The literature cited in the general introduction follows the conclusions. Lastly, the appendix provided is concerned with the general operation of the EQCM as discussed below.

Paper I includes results from EQCM studies of anodic oxygen-transfer redox reactions. This work was done in conjunction with Dr. Larry Larew and Dr. Yun-Lin Hsiao and was published in the *Journal of the Electrochemical Society*, **137**, 3071 (1990). The instrumental design was provided by Dr. Dan Buttry from the University of Wyoming. Paper II includes results from EQCM studies of the deposition and composition of PbO_2 and Bi-doped PbO_2 film electrodes. Paper III includes results from EQCM studies of the adsorption of water at gold electrodes. Appendix I is a condensed operations manual for the EQCM. It includes necessary program instructions to perform basic electrochemical experiments with the EQCM. It was written to meet the Department of Energy regulations on standard operations procedure manuals for all laboratory equipment.

Anodic Oxygen-Transfer Reactions

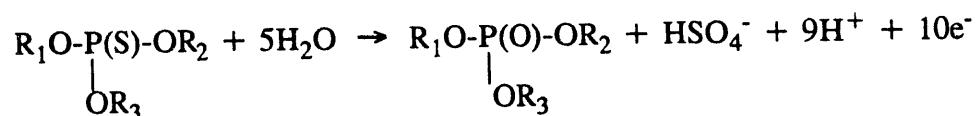
The research in this laboratory is focused on a two-fold development of electrochemical techniques for the oxidation of various organic and inorganic compounds. One area of interest, and the primary focus of this work, is in the development and characterization of electrode materials for use in the oxidative destruction of various organic toxins. The second area of interest involves the continued development and optimization of liquid chromatography with electrochemical detection, specifically, pulsed electrochemical detection schemes [1-3]. In our research, these two diverse areas are related in that both are concerned with the same type of electrochemical reaction - "anodic oxygen-transfer reactions." As the name implies, the oxidative mechanism of these reactions involves the transfer of at least one oxygen atom from the solvent (water) to the reactant.

In this work, electrode materials were studied which exhibit electrocatalytic activity toward anodic oxygen-transfer reactions. "Electrochemical incineration" is a term that has been used to describe this process because of the similar effects produced in typical incineration reactions. Reactions of interest include such simple model reactions as the conversion of dimethyl sulfoxide to dimethyl sulfone, as represented by:

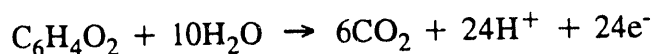
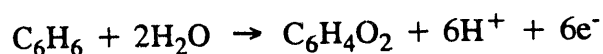


as well as more significant reactions such as the oxidative desulfurization of

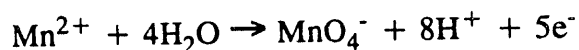
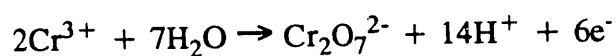
thiophosphate pesticides, as represented by:



where R_1 , R_2 and R_3 represent alkyl groups; and the partial and complete degradation of benzene, as represented by:



Oxidation of inorganic species is also of interest, as represented by:



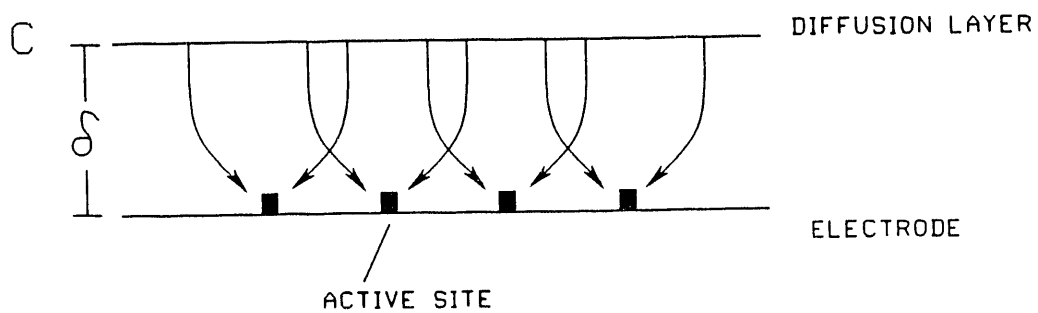
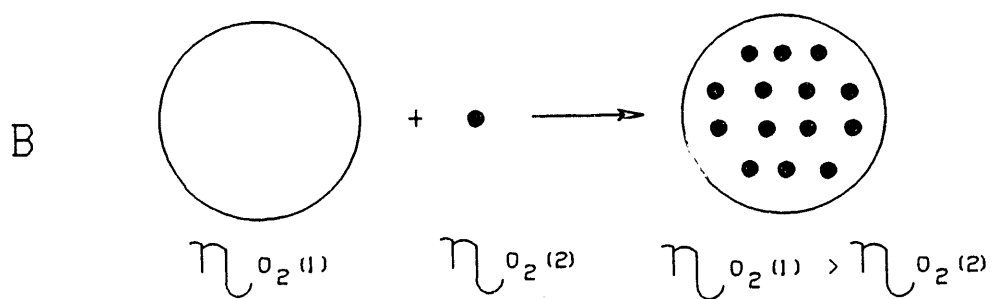
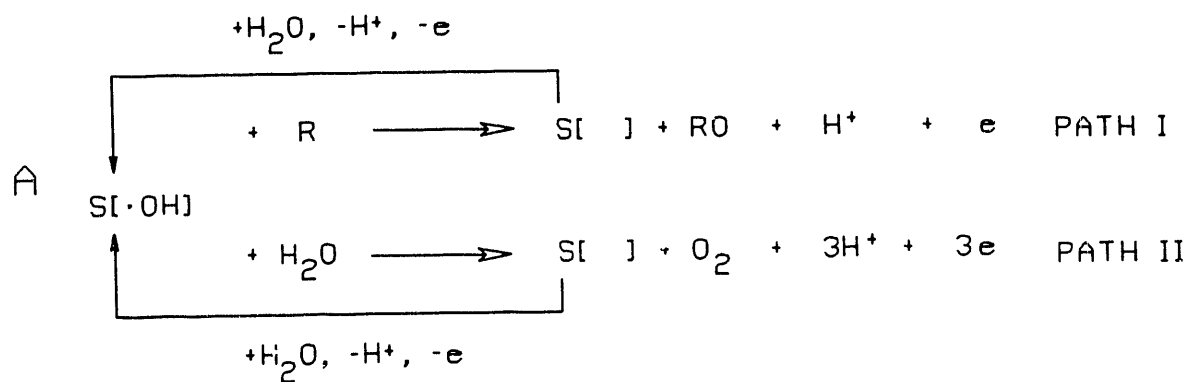
Thermodynamic calculations support the conclusion that virtually all organic compounds can be oxidized at potentials easily accessed at common anode materials, including Pt, Au, C and PbO_2 . Furthermore, it is a trivial task to write the balanced equations for these anodic oxygen-transfer reactions and this often leads to the conclusion that such reactions can be made to occur with great facility. Nevertheless, experimental observations demonstrate that these reactions do not occur at appreciable rates at these common electrode materials without using high electrode potentials or current densities. Under these conditions, the electrochemical conversion is very inefficient and costly.

Therefore, motivation for this work is the development of electrode materials applicable for direct and indirect electrochemical incineration of organic toxins at nominal potentials and current densities. Direct electrochemical incineration requires that the reactant undergo oxidation at the electrode surface. Indirect electrochemical incineration can be accomplished by using inorganic species which have large positive E° values, e.g. MnO_4^- and CrO_4^- , to serve as strong chemical oxidizers. The reactant undergoes a homogeneous oxidation reaction with the chemical oxidizer rather than at the electrode surface. However, once the chemical oxidizer is converted to its reduced form, its reoxidation is an anodic oxygen-transfer reaction and, currently, suffers the same economical and efficiency problems as in direct degradation.

Dimethyl sulfoxide (DMSO) was the model compound used for this work because its oxidation represents the simplest oxygen-transfer process requiring the transfer of only one oxygen atom and two electrons. Also, DMSO is uncharged in both the oxidized and reduced forms. Therefore, there are no electrostatic interactions to affect the electrode kinetics.

A schematic representation of the oxidative mechanism is shown in Figure 1A. In order to oxidize the reactant (**R**) to the desired product (**RO**), it is necessary first to produce the required oxygen species, in the form of surface adsorbed hydroxyl radicals ($\text{S}[\cdot\text{OH}]$), by the discharge of water at the electrode surface [4]. When the electrode potential is made sufficiently positive to produce the hydroxyl species, **R** undergoes oxidation to produce **RO** (Figure 1A, Path I). However, if the discharge of water occurs too vigorously, a competition arises between the formation of the desired product **RO** and

Figure 1. (A) The competitive oxidation mechanism for a generic anodic-oxygen transfer redox reaction. (B) An illustration of a modified or "doped" electrode surface showing the active sites as filled circles. The oxygen evolution overpotential of the matrix electrode material [η_{O_2} (1)] is greater than that of the active site material [η_{O_2} (2)]. (C) An illustration showing how under curvilinear diffusion virtually any active site is accessible by any of the analyte molecules.



the formation of O_2 (Figure 1A, Path II).

To overcome the undesirable production of O_2 , electrode materials were used that require the application of large positive potentials to evolve O_2 , i.e. materials having a large oxygen-evolution overpotential (η_{O_2}). Atomic scale defect sites having much smaller η_{O_2} were introduced into the electrode surface to produce the necessary $S[\cdot OH]$. Figure I.1B shows an illustration of a modified or "doped" electrode surface. The small black spots are exaggerated representations of the imbedded defect sites referred to as "active sites". Curvilinear diffusion, as depicted in Figure 1C, permits the reactant molecule an equal chance of diffusing to virtually any active site, provided the intersite distance is small compared to the diffusion layer thickness (δ). Therefore, virtually the entire electrode surface appears as active area toward oxidation of the reactant species. However, the production of O_2 is restricted to the area of the individual active sites. The net result is that the rate of the desired oxidation is much greater than the rate of production of O_2 .

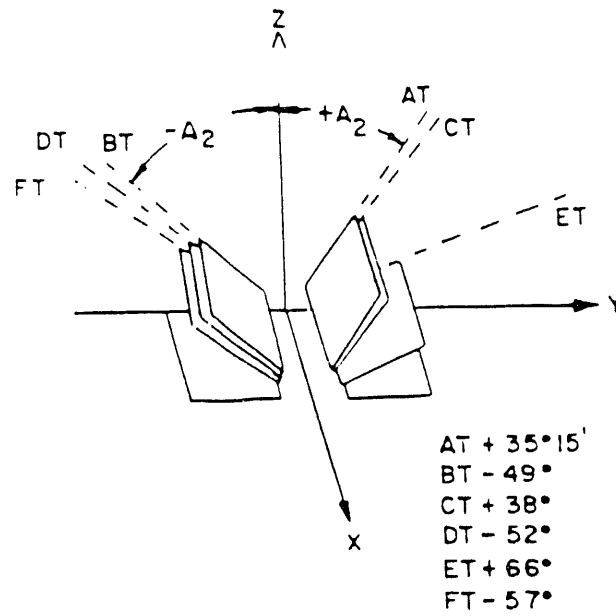
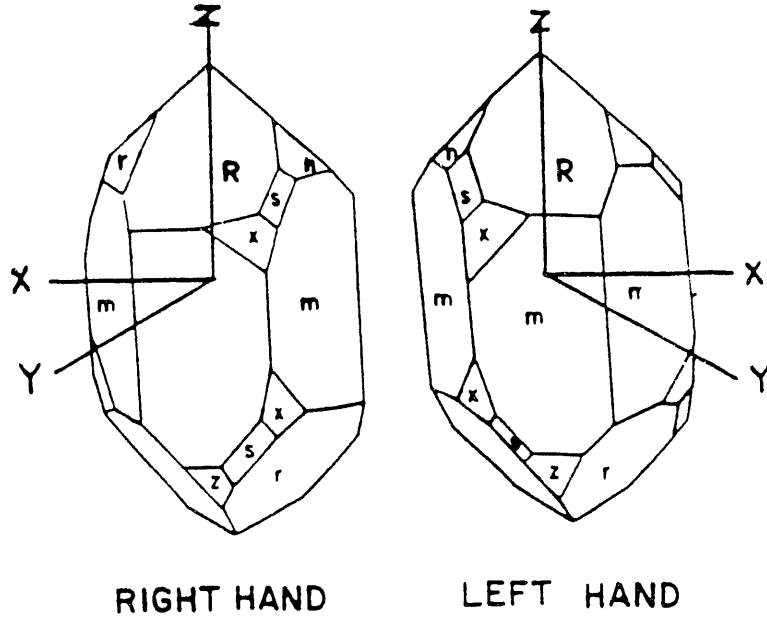
Here, PbO_2 films served as the electrode material having a large positive η_{O_2} . The PbO_2 films were doped with Bi(III) [5-7] to produce the active defect sites necessary for electrocatalysis. Other metallic [8-9] and anion species, such as As(V) [10], Cl^- [11] and Acetate [12] have been shown also to exhibit electrocatalysis of oxygen-transfer reactions when used as doping agents. Along with electrochemical techniques [13, 14], surface science techniques [15, 16] have been employed to characterize these electrodes. This work introduces an Electrochemical Quartz Crystal Microbalance (EQCM) to the study.

Quartz Wafers as Mass Sensors

Quartz is one of several ionic crystalline "piezoelectric" solids. In 1880, Pierre and Jacques Curie [17] performed experiments showing that pressure applied to a small piece of quartz produces an electrical potential difference between the deformed surfaces. The term "piezoelectric" meaning "pressure electric" was given by the Curies to appropriately characterize this phenomenon. They also found the converse to be true. The application of an electrical potential across a piece of quartz causes it to deform.

Single quartz crystals are cut at precise angles according to different axis orientations to obtain thin wafers having particular deformation characteristics. The proper orientation for cutting a crystal of quartz is shown in Figure 2 to obtain a wafer designated as an "AT-cut wafer". These are among the most popular of the quartz wafers since their piezoelectric response has virtually a zero temperature coefficient for the temperature range normally encountered under typical laboratory conditions. For high frequency applications (> 5 MHz), the AT-cut wafers are typically $< 500\ \mu\text{m}$ thick and exhibit deformations parallel to the surface of the wafer, i.e. shear-mode deformations. Oscillation is established within the crystals by depositing metallic films, e.g., Au via thermal vaporization, on each side and applying an oscillating electric field to these contacts. The oscillating wave within the crystal has a node at the thickness center with antinodes at the faces (Figure 3C).

Figure 2. A diagram of a piece of α quartz showing the angles and orientation of cutting the crystal to obtain wafers with various oscillation and temperature sensitivity characteristics

α QUARTZ CRYSTAL STRUCTURE

Sauerbrey Equation

The basic premise for the quartz crystal microbalance is that any change in mass on the wafer surface inversely affects its resonant oscillation frequency. Sauerbrey [18] first derived the relationship between the frequency of oscillation of a quartz wafer and a change in mass on the wafer's surface:

$$\Delta f = \left(\frac{-2f_q^2}{v_q \rho_q} \right) \frac{\Delta m}{A} \quad (1)$$

The change in frequency (Δf) is related to the change in mass per unit area ($\Delta m/A$) by a series of constants related to the quartz: the resonant frequency of the quartz wafer (f_q), the shear wave velocity of quartz ($v_q = 3340 \text{ m s}^{-1}$), and the density of the quartz ($\rho_q = 2.648 \text{ g cm}^{-3}$). For 5.0 MHz crystals equation (1) becomes:

$$\Delta f = -(56 \text{ Hz cm}^2 \mu\text{g}^{-2})(\Delta m) \quad (2)$$

When a quartz crystal oscillates at its fundamental frequency, equation (3) is an accurate description of the relationship between the thickness of the crystal (t_q) and the wavelength of the acoustic transverse wave in the crystal (λ_q).

$$t_q = \frac{\lambda_q}{2} \quad (3)$$

The effect of the two electrodes is considered to be negligible. Equation (3) can be rewritten because $\lambda_q f_q = v_q$, where v_q is the shear wave velocity of quartz and f_q is the oscillation frequency of the quartz wafer.

$$f_q t_q = \frac{v_q}{2} \quad (4)$$

Using equation (4), the relationship between changes in the frequency and changes in the thickness of the quartz is given in equation (5):

$$\frac{\Delta f_q}{f_q} = \frac{-\Delta t_q}{t_q} \quad (5)$$

where Δt_q and Δf_q are the changes, respectively, in thickness and frequency of the quartz crystal. In obtaining equation (5), it is assumed that density and the velocity of the acoustic wave are the same for both the deposited material and the quartz. This assumption is made on the basis that relatively thin films are deposited. The minus sign indicates that an increase in the thickness of the quartz produces a decrease in its oscillation frequency.

The change in thickness of the quartz (Δt_q) can be represented by a change in mass of the quartz crystal electrode surface per unit area divided by the density of quartz ($\Delta m/A\rho_q$). By solving equation (4) for t_q , the equivalent expression for Δt_q and t_q are substituted into equation (5). The result is solved for Δf , and Sauerbrey's equation is obtained:

$$\Delta f_q = \left(\frac{-2f_q^2}{Av_q\rho_q} \right) \Delta m \quad (6)$$

Equation (6) reduces the general form of the Sauerbrey equation:

$$\Delta f_q = -K\Delta m \quad (7)$$

where $K = \frac{2f_q^2}{Av_q\rho_q}$

Highlighted History of Analytical Applications

Quartz Crystal Microbalances (QCM) have been used for years as mass sensitive detectors. King was the first to realize the usefulness of the QCM as a detector in gas chromatography (GC) [19]. This detector was based on the partitioning of analyte gases into GC column material coated onto Au QCM electrodes as in a typical GC separation. King referred to these coated crystals as "Piezoelectric Sorption Detectors". A simplified variation of this technique allowed the development of partition detectors for atmospheric gases. Different coatings have been employed to detect a variety of species including CO [20], CO₂ [21], SO₂ [22], and NO₂ [23]. Quantitation was typically down to ppb concentration levels. Olin [24] developed a mass detector for airborne particulate matter. Automobile emissions and laboratory aerosols were examined with the concentrations being measured to 5% accuracy within 10 sec. These and other QCM applications have been reviewed recently by Guilbault [25].

For liquid chromatographic detectors, the QCM began as an *ex situ* detector. King [26] coated effluent from the column onto Au QCM electrodes and allowed the solvent to evaporate. A quantitative determination of the analyte was performed by measuring the frequency of the crystal before and after coating. The entire process took about 10 sec. Early attempts at *in situ* detection using a single crystal suffered from drifts in the oscillation frequency caused by changes in eluent density. This was overcome by using a dual-crystal system [27] in which a reference crystal was exposed to the same mobile phase as the indicating crystal but without the analyte. Recently, Buttry and Lasky [28]

used this concept to develop a real-time glucose biosensor by immobilizing hexokinase onto the crystal surface. The system has a dynamic range of ca. 0.1 to 20mM with a response time of less than 10 sec. Guilbault recently reviewed the use of piezoelectric crystals as biosensors [29].

The first QCM applications to electrochemical studies involved deposition of metallic species [30]. However, as with all the early work, the frequency measurements were made *ex situ*, i.e., before and after deposition of the metal of choice. While effective for correlating the total charge passed to the total mass gained, the process was cumbersome. Nomura tried the first *in situ* EQCM experiments in 1981 [31] after determining that the crystal's oscillation could be maintained even under the viscous loading conditions of an *in situ* experiment. Silver and copper concentrations were determined at sub ppb concentration levels at Pt coated Au EQCM electrodes. These results demonstrated the ability to perform electrochemical experiments and monitor simultaneously current and mass changes that occur at electrode surfaces as a function of various analyte/electrolyte systems. Since its inception, the EQCM has been used to study the underpotential deposition (UPD) and native oxide formation of various metals [32] including Au [33], Ti [34], Ag [35] and Cu [36]. It has been used also to study ion/solvent interactions with polymeric film coated EQCM electrodes [37-43]. Several excellent reviews on the EQCM and its applications are available [44-48].

EQCM Instrumentation

The EQCM apparatus (Figure 3A) is very similar to typical electrochemical apparatus except that the working electrode is one of the metallic films vapor-deposited onto the quartz wafer as seen in an expanded view in Figure 3B. The metallic film on the opposite side of the crystal contact is responsible for imposing the oscillating electric field to the crystal. The reference and counter electrodes are the same as in traditional electrochemical experiments. A schematic diagram of the EQCM circuitry is found in Appendix I Figure 2.

Figure 4 shows a diagram of the electrical circuit equivalent to the quartz crystal. C_0 is the capacitance of the quartz wafer. The surrounding media and internal friction produce a resistance (R) on the wafer. The energy stored during the crystal's oscillation corresponds to a capacitance (C) and is related to the elasticity of the crystal. The inertial energy produced as wafer mass is displaced during oscillation corresponds to an inductance (L). While it is possible to produce an oscillating circuit with conventional electronic components, using a quartz wafer as the oscillating element is more advantageous. The nature of quartz allows the wafers to maintain a very stable oscillation frequency. The measure of this stability is the "Q factor" which is proportional to the ratio of the energy stored per cycle to the energy dissipated per cycle. Effectively this is the ratio of L/R . With L and R values of 0.1H and 10 Ω , respectively in air, the value of Q for a quartz wafer is several orders of magnitude greater than for typical electronic circuits. The presence of a solution layer adjacent to the quartz surface

Figure 3. (A) Diagram of the EQCM cell and instrumentation. The side view shows how the crystal is attached to the port on the cell body. (B) An expanded view of the crystal showing the two Au films on the top and bottom surfaces of the quartz wafer. Crystal diameter is 2.54 cm. Large film area $\approx 1.21 \text{ cm}^2$. Small film area $= 0.28 \text{ cm}^2$. (C) An illustration of shear mode oscillations established with the quartz crystals.

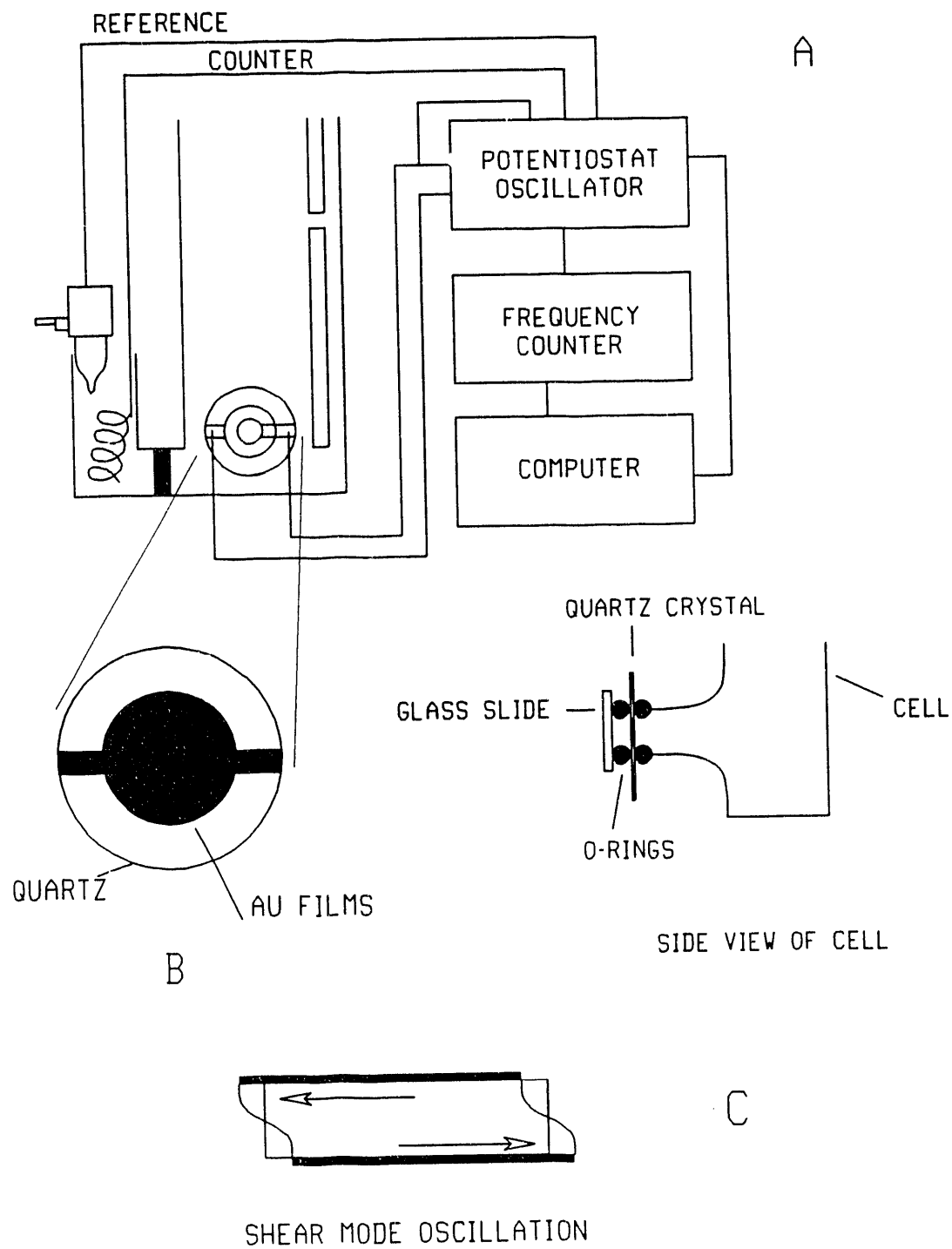
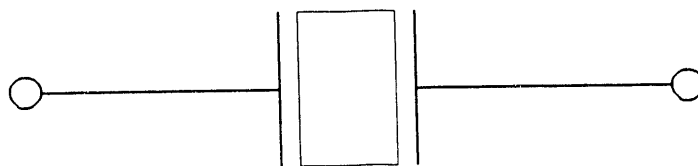
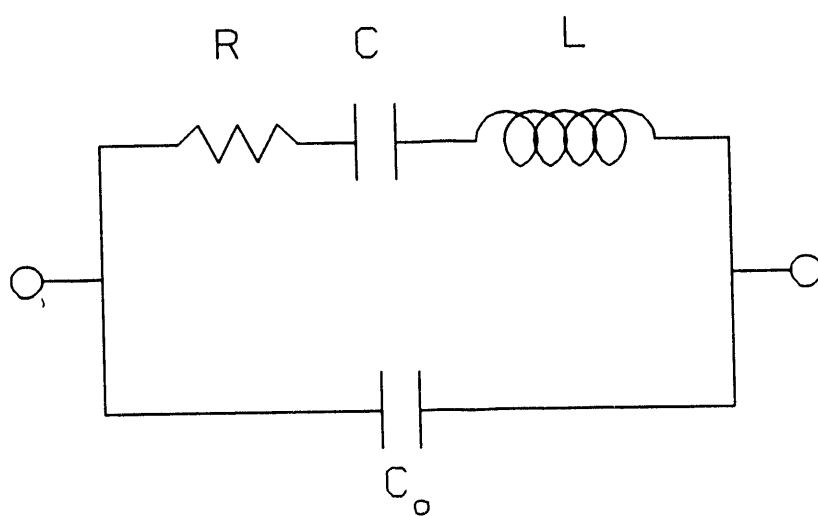


Figure 4. A diagram of the equivalent electrical circuit for a quartz crystal oscillator.



greatly increases R . However, with the proper circuitry, the effect of the solution is overcome to produce a Q value sufficient to maintain a stable oscillation frequency.

The oscillator circuitry signal is sent to a Phillips 6654C frequency counter that is able to resolve 1 Hz change in ca. 1 msec. In this work, the current and frequency values were read by a 286 XT computer interfaced to EQCM through a Data Translation 2800 series data acquisition. Data collection and initial manipulation was performed within the ASYST programming environment (Data Translations). The potential control for the electrochemical experiments was provided either with the analog linear-sweep waveform generator of a Pine Instruments RDE4 dual electrode potentiostat or digitally with the computer.

Au Film Preparation

Gold adheres very poorly to quartz surfaces. Therefore, it was necessary to determine a suitable means for anchoring the Au to the quartz. Two particular methods are emphasized in the literature: (1) the use of thin metal films including Si [44, 50], Cr [44, 51], and Ti [52]; or (2) the use of (3-mercaptopropyl)trimethoxysilane [53] to act as adhesive interlayers between the Au and quartz.

A thin film of Cr ($< 50\text{\AA}$) was the first adhesive interlayer tested. The Cr and Au were sequentially deposited onto the quartz disks in a resistive-heating vaporization chamber under low pressure conditions ($< 1 \times 10^{-6}$ torr). The useful potential window for Au electrodes is ca. -0.2V to 1.90V (vs. SCE) in acidic media. However, at potentials

$> 0.2\text{V}$, Cr was oxidized and solubilized from the electrode surface because of its ability to diffuse through the thin Au films. The Cr interlayer was dissolved completely within an hour as evidenced by the visible delamination of the Au films from the quartz surfaces. The Cr interlayer was tested also for its adhesive character in alkaline media in which the potential window is more negative ($-0.80\text{V} - +0.800\text{V}$ vs. SCE). As in acidic media, loss of Cr was still evident, albeit at a slower rate. The major problem with the Cr interlayer was its diffusion through the thin Au films. Deposition of thicker Au films was considered as a possible remedy for this problem. However, while effective for decreasing the diffusion of the Cr, it was a more expensive method of crystal preparation and was not pursued.

A second method proposed by Majda [53] used (3-Mercaptopropyl)trimethoxysilane (MPS) as the adhesive interlayer. The bare crystal wafers were cleaned in dilute chromic acid at 70°C followed by a 1:4 30% H_2O_2 : 90% H_2SO_4 solution to remove trace organic impurities. Once cleaned, the wafers were immersed for ca. seven minutes in a refluxing 2-propanol solution containing 2.5% MPS and 2.5% H_2O during which time the MPS bonded to the quartz surface. The wafers were dried for ten minutes at ca. 105°C . This process was repeated three times to ensure that the entire quartz surface was covered with MPS. The wafers were stored, typically, overnight but were stable after storage for a week prior to depositing the Au film. As before, vapor deposition of Au was used to produce Au films 2000 - 2500 Å thick.

The MPS interlayer was undesirable for two reasons. First, it was very difficult to clean the MPS sufficiently from the quartz wafers, especially if the MPS coating

procedure had been performed multiple times. The wafers were cleaned satisfactorily by immersion in an alcoholic-KOH solution. However, prolonged exposure to this alkaline media resulted in undesirable etching of the wafer surface. The second undesirable trait of the MPS interlayer was the inability to chemically clean the surface of the Au EQCM electrodes. It is often necessary to clean Au electrodes with a 1:4 30% H_2O_2 : glacial Acetic acid solution to remove PbO_2 films electrodeposited on the Au surface. This solution, while effective for removing the PbO_2 films, was also very effective in delaminating the Au films very quickly. The time required to produce a Au film made their use for only one experiment very inefficient. In addition, it was not possible to use these crystals in alkaline media. The Au films delaminated totally from the quartz surface after only a few minutes regardless of the applied potential.

Titanium was chosen as the most effective adhesive interlayer because it offers several advantages over the previous two methods. Even though Ti diffuses through the Au films, it does so at a much slower rate than Cr. Even when Ti diffuses through the Au and is exposed at the edge or surface of the Au electrodes, once oxidized the subsequent insoluble TiO_2 remains on the quartz surface electrochemically inactive. In addition, as with Cr, Ti and Au are deposited sequentially by thermal vaporization. Once the Au films are no longer useful, both the Au and Ti are removed easily to prepare the crystals for redeposition.

The use of the Ti interlayer has extended the accessible voltammetric range and pH range (0 - 13) of EQCM experiments, as well as the lifetime of the Au coated quartz crystal. Some crystals have been used for more than 14 consecutive days. In addition to

the other advantages, the Au/Ti/quartz system withstands a variety of cleaning methods including electrochemical, chemical, and even mild (very mild) abrasive polishing.

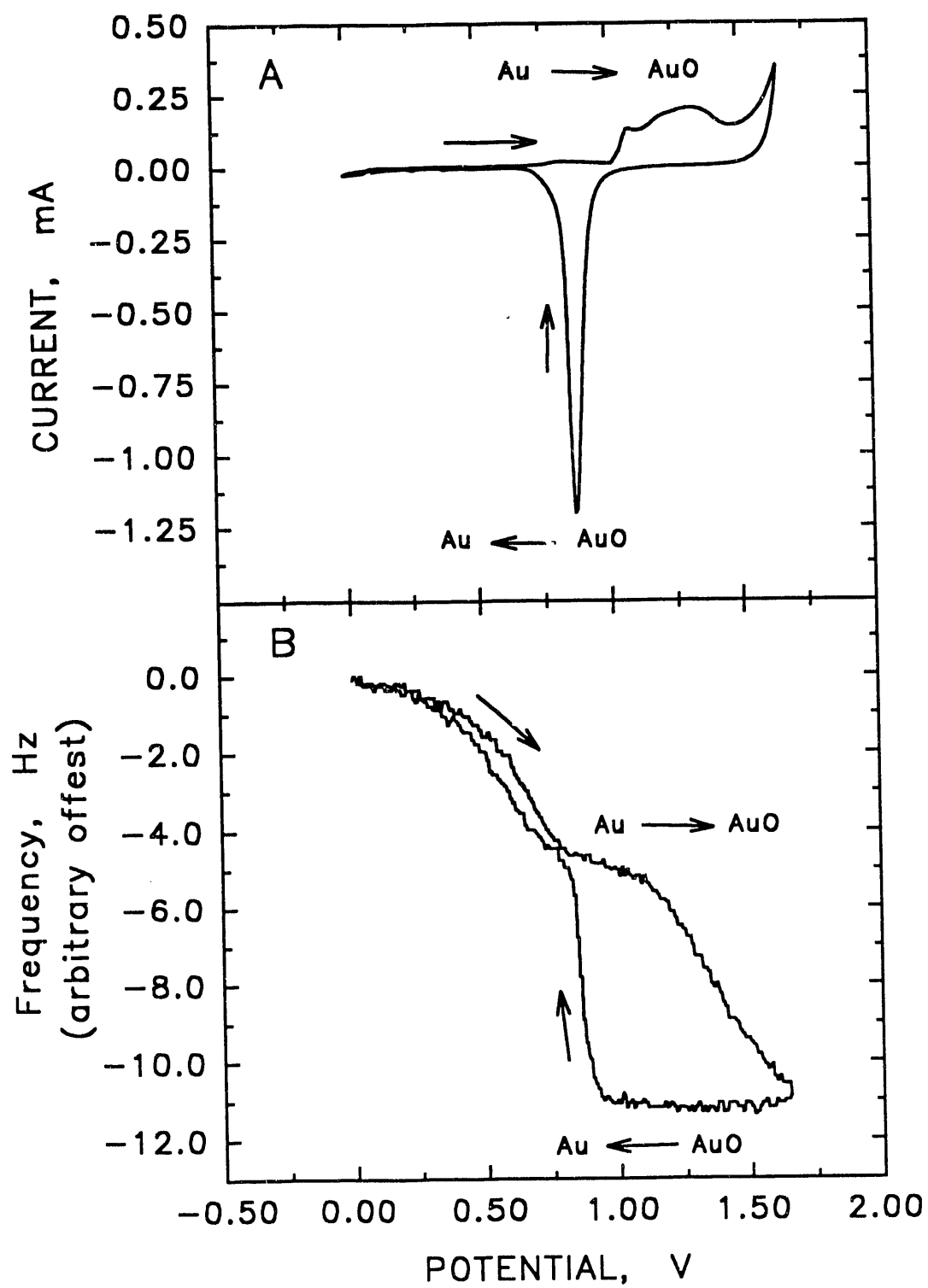
Diagnosis of Film Stability

The results from two methods were used as criteria to determine the stability of the Au films. Primarily, the results of cyclic voltammetric experiments were examined within the potential region of formation and reduction of Au oxide.

In performing a cyclic voltammetric experiment using the EQCM, the current and frequency values are recorded concomitantly as a function of an applied potential that is continuously cycled between some upper and lower potential limit. Several distinct qualitative characteristics can be observed in the plots of current vs. potential (i - E), and frequency vs. potential (f - E), Figures 5A and B respectively. In the i - E response, during the positive scan there is virtually no current until the formation of Au oxide at $E > 1.0\text{V}$. The general appearance of this anodic current response is maintained until water is discharged to evolve O_2 at $E > 1.6\text{V}$. As the potential is decreased, on the negative scan, the rapid decrease in current indicates no further formation of the Au oxide or O_2 evolution. The cathodic current having a peak potential (E_p) at *ca.* 0.8V indicates the reduction of the Au oxide to Au. The potential values quoted above will shift to more negative values, according to the Nernst equation, as the pH of the solution is increased.

In the f - E response, there are several important qualitative characteristics. On the forward scan, the frequency dramatically decreases at potentials $> 0.2\text{V}$ and 1.0V . As

Figure 5. Current (A) and frequency (B) vs. potential response for a cyclic potential scan on a Au EQCM electrode in 1.0M HClO_4 . Scan rate = 75 mV s^{-1} . No convective mixing.



the potential scan is reversed, the frequency is stable and constant until the oxide is reductively desorbed from the surface at potentials $< 0.8\text{V}$ where the frequency sharply rises and virtually retraces the forward scan. As in the i - E response, these characteristics are also pH dependent.

The i - E and f - E responses for Au EQCM electrodes will be considered in more detail in Chapter IV. However, for this discussion, only the general shape and magnitude of both the current and frequency responses are considered as evidence of acceptable behavior of the Au films. Typically, when a Au EQCM electrode is no longer useable, the f - E response contains fluctuations in frequency in the form of large sharp frequency changes or "spikes", a slow continuous drift in the frequency ($\pm 30\text{ Hz}$), or a combination of both. The i - E responses are seldom used to diagnose problems because they are less sensitive to the state of the EQCM's electrodes than the f - E responses.

The second method used in verifying the activity of a crystal is the examination of data obtained during its calibration.

Calibration of the EQCM Crystals

A major portion of this work involved the determination of mass-to-charge ratio ($\Delta m/\Delta q$) values for species electrodeposited or electrosorbed onto the electrode to facilitate their identification. Equation (8) shows the relationship between frequency and mass used to obtain $\Delta m/\Delta q$ values from the experimental data.

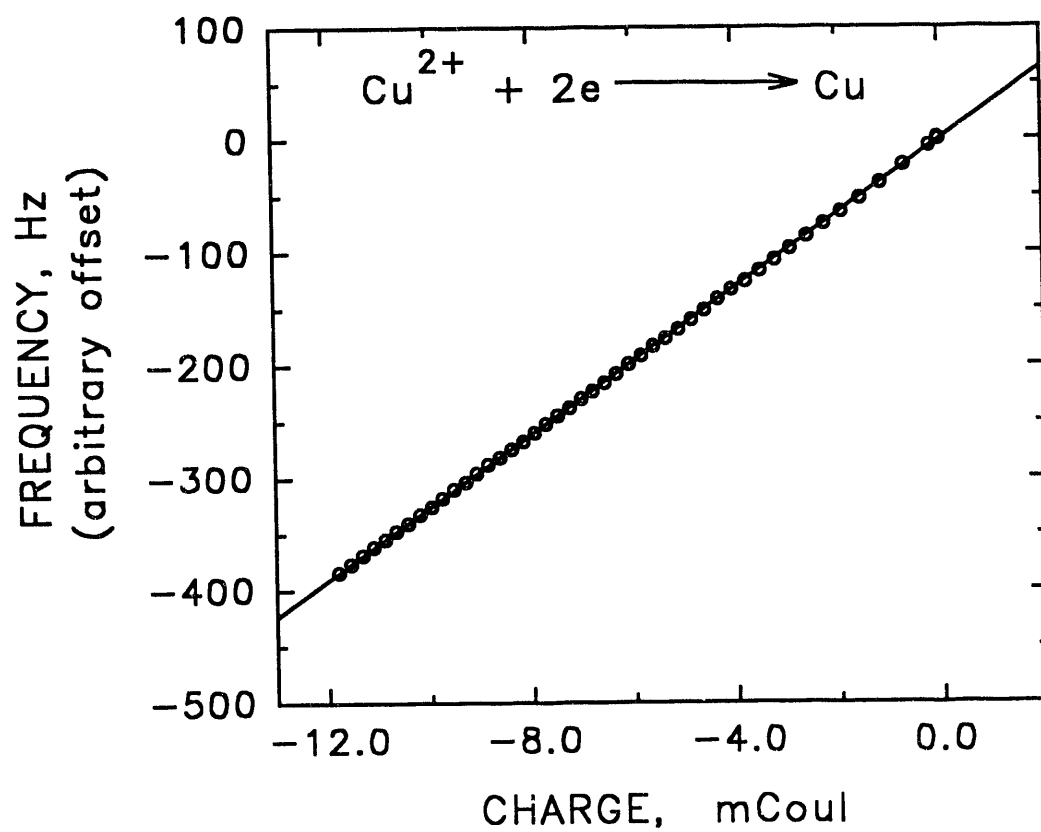
$$\Delta m/\Delta q = -(A_e/K)(df/dq) \quad (8)$$

In equation (8), df/dq is the slope of a plot of frequency vs. charge; K is Sauerbery's constant from equation (7); and A_e is the electrochemically active area.

The value of A_e/K , effectively a calibration constant, must be determined for each EQCM crystal because A_e varies slightly between crystals. A_e/K is obtained from the electrodeposition of Cu^0 . A chronoamperometric experiment is performed in which the electrode potential is stepped from 0.5V to -0.3V for 30-60 sec. The frequency and current are monitored simultaneously during the deposition period. The current is integrated to give electrical charge, and a plot of the frequency vs. charge (f - q) is made as illustrated in Figure 6. Again, the slope of this response is df/dq . Assuming that the Cu^{2+} is fully discharged at the electrode surface, i.e. $n = 2 \text{ eq mol}^{-1}$ [2], the value of $\Delta m/\Delta q$ for the deposition of Cu^0 is $0.329 \text{ mg coul}^{-1}$. Knowing the values of $\Delta m/\Delta q$ and df/dq , A_e/K is readily obtained. The value A_e/K , once established for a particular crystal, is used for subsequent $\Delta m/\Delta q$ determinations using that crystal.

The calibration procedure was used also in confirming the proper functioning of the crystal. In Figure 6, the f - q response for the electrodeposition of Cu on Au shows a linear correlation between the frequency and charge. The stability of the Au film is confirmed by this linearity. When the Au EQCM film is damaged, most often from delamination, the f - q response deviates from linearity. Deviations, referred to as "breaks", are seen as a positive deviations from linearity for charge values more positive than ca. -4 mcoul. When this result was obtained the crystal was recleaned using the acidic cleaning solutions mentioned above along with electrochemical cleaning. The Au and Ti films were removed from the crystal if the problem persisted.

Figure 6. Frequency vs. Charge response for the electrodeposition of Cu at a Au EQCM electrode. Conditions: $E_{\text{dep}} = -0.3\text{V}$ for 60 sec., 5mM CuSO_4 in 1.0M HClO_4 . No convective mixing.



PAPER I.

ELECTROCATALYSIS OF ANODIC OXYGEN-TRANSFER REACTIONS:
APPLICATION OF AN ELECTROCHEMICAL QUARTZ CRYSTAL
MICROBALANCE TO A STUDY OF PURE AND BISMUTH-DOPED
BETA-LEAD DIOXIDE FILM ELECTRODES

INTRODUCTION

A goal of research in this laboratory during recent years has been the development of electrode materials with enhanced activity for electrocatalysis of anodic oxygen-transfer reactions. Much success has been achieved using electrodeposited beta-PbO₂ films containing Group VA metal oxides [1-4]. It was shown by Yeo et al. [1, 2] that the apparent heterogeneous rate constant (k_{app}) for the electrooxidation of Mn(II) to MnO₄⁻ was greatly increased when Bi(III) was added to the deposition solution of Pb(II). Values of k_{app} increased for the Bi-doped PbO₂ films ("Bi-PbO₂") as the ratio Bi(III)/Pb(II) was increased to approximately unity. The films were mechanically unstable for higher levels of Bi(III). The rutile structure of pure beta-PbO₂ was retained in the Bi-PbO₂ films with a slight lattice expansion, as determined from X-ray diffraction data. The average oxidation state of Bi in the Bi-PbO₂ was concluded to be > 4.5, based on the unit cell volume calculated from the X-ray data and the results of exhaustive coulometric deposition from solutions of Pb(II) and Bi(III). Furthermore, the increase in k_{app} for Mn(II) oxidation was correlated with decreasing values for the O₂-evolution overpotential.

It was confirmed by LaCourse et al. [3] that k_{app} for anodic oxidation of several compounds was significantly larger at Bi-PbO₂ films as compared to PbO₂-film electrodes. However, the lifetimes of Bi-PbO₂ film electrodes for oxidation of Mn(II) to MnO₄⁻ were determined to be as low as ca. 30 min. under conditions of high Mn(II) flux. This loss of activity was concluded to result from surface fouling by the deposition of

MnO₂(s) produced by an insufficiently catalyzed reaction and/or from corrosion of the electrode surface with loss of Bi ions from the Bi-PbO₂ film. Recently, Chang and Johnson [4] have shown that the lifetime of Bi-PbO₂ for Mn(II) oxidation could be extended nearly 2-fold if a small amount (< 50 μ M) of Bi(III) was added to the solution containing Mn(II). Catalytic activity was also observed for PbO₂-film electrodes following exposure to Bi(III) solutions. It was speculated that Bi(III) was adsorbed at the PbO₂ surface and functioned as a heterogeneous mediator of the oxygen-transfer step by increasing the rate of anodic discharge of H₂O to produce adsorbed hydroxyl radicals (\cdot OH_{ads}). A singular value of half-wave potential ($E_{1/2} = 1.67 \pm 0.05$ V vs. SCE) was observed for the oxidation of a variety of compounds whose E° values varied over the range ca. -0.1 V to 1.45 V vs. SCE. The anodic discharge of H₂O at the catalytic electrodes was proposed as the rate-determining step in all of these reactions.

Here, we present direct evidence obtained with an electrochemical quartz crystal microbalance (EQCM) for the oxidation of Bi(III) during anodic deposition of Bi-PbO₂ films from solutions containing Pb(II) and Bi(III). Furthermore, evidence is presented for anodic adsorption of Bi(III) as Bi(V) onto PbO₂ surfaces in Pb(II)-free solutions containing Bi(III).

EXPERIMENTAL

Chemicals - All chemicals were reagent grade from Aldrich Chemical Company, Fisher Scientific, or Baker Chemicals. Solutions of Pb(II) and Bi(III) were prepared in HClO₄ or HNO₃ from PbO(s) and Bi(NO₃)₃(s). Distilled water was purified further in a Milli-Q system from Millipore (Bedford, MA). (3-Mercaptopropyl)trimethoxysilane was from Petrarch Systems (Bristol, PA). Gold (99.999% in purity) was obtained from the U.S. Department of Energy.

Instrumentation - A Au rotated disk electrode (RDE) (0.2 cm², Pine Instrument Company, Grove City, PA) was operated in a Model MSR rotator (Pine Instrument), and voltammetric control was by a Model RDE4 potentiostat/galvanostat (Pine Instrument). The instrumentation for the EQCM has been previously described [5-8]. Potentiostatic control, data acquisition and data analysis were achieved by interfacing the EQCM to an IBM-compatible PC/AT using a DT2801-A board (Data Translation, Marlboro, MA) which was driven from the ASYST programming environment (Data Translation, Marlboro, MA). Planar (2.5-cm dia.), overtone-polished, AT- cut quartz crystals (Valpey-Fisher, Hopkinton, MA) were operated at the fundamental frequency of 5 MHz. Gold film electrodes (ca. 200-nm thick, 0.38 cm² area) were evaporated onto both sides of the crystals using a Model E306A coating system (Edwards, West Sussex, England). The films were deposited in the "keyhole design" [9]. The piezoelectrical and electrochemical responses were calibrated for each crystal as described below. A coiled Pt wire (2.8 cm²) was the counter electrode. All potentials were recorded and are

reported vs. a Ag/AgCl reference.

Methods - The Au RDE was activated prior to each experiment as follows: after gentle polishing with 0.05-um alumina on microcloth, it was rinsed with deionized water and placed into the electrolysis cell; repeated cyclic potential sweeps between the potential limits for O₂ and H₂ evolution were applied for several minutes until no further changes were detected in the i-E curves. Conditions have been described for the electrodepositions of pure and Bi-doped PbO₂ films [1, 10], and the anodic adsorption of Bi(III) onto PbO₂ films [4].

Values of k_{app} and the effective number of electrons (n_{eff}) for the electrodeposition of PbO₂ and Bi-PbO₂ films on the Au RDE were calculated from the intercepts and slopes, respectively, of linear plots of $1/i$ vs. $1/\omega^{1/2}$, according to the Koutecky-Levich:

$$\frac{1}{i} = \frac{1}{n_{eff}FAk_{app}C^b} + \frac{1}{0.62n_{eff}FAD^{2/3}\nu^{-1/6}C^b}\left[\frac{1}{\omega^{1/2}}\right] \quad (1)$$

In equation (1), ω is the angular velocity of electrode rotation (s⁻¹), and other terms have their conventional electrochemical significance.

The quartz crystals were treated with mercaptopropylsilane to decrease surface hydrophilicity and enhance the adhesion of the Au films. The procedure was as follows: the crystals were cleaned by soaking in a chromic acid bath for 18 hrs. and then rinsed, in succession, with deionized water, ethanol and diethyl ether; the crystals were then transferred to a solution of 80% (v/v) ethanol, 5% (v/v) 0.1 M sodium acetate of pH 4.8,

and 15% (v/v) (3-mercaptopropyl)trimethoxysilane; the reaction was allowed to proceed for ca. 10 min. with gentle agitation by stirring; the treated crystals were dipped in ethanol and then cured by drying at room temperature in a desiccator for 18 hrs. The Au-coated crystals were electrochemically activated prior to all measurements by the application of repeated cyclic potential sweeps between the potential limits for O₂ evolution and reduction until no further changes were detected in the *i-E* curves.

For the EQCM, the relationship has been described [5-9] between the rate of change in the mechanical resonant frequency of the quartz crystal as a function of surface mass (df/dm , Hz mg⁻¹). The ratio of the net changes in mass and charge ($\Delta m/\Delta q$, mg coul⁻¹) for an electrosorbed or electrodeposited species is given by

$$\Delta m/\Delta q = -(A_e/K)(df/dq) \quad (2)$$

In equation (2), A_e is the electrochemically active area (cm²), K (cm² Hz mg⁻¹) is a proportionality constant dependent on the fundamental resonant frequency of the quartz crystal in the absence of the deposited mass, the shear modulus of quartz, and the density of quartz (5), and Δq (coul) is the total charge passed by the corresponding electrode reaction. Note that an increase in mass corresponds with a decrease in frequency. Values of A_e/K were determined experimentally for each crystal from df/dq for the stripping of electrochemically deposited Pb(0) using $\Delta m/\Delta q = 1.07$ mg coul⁻¹, corresponding to the process of $\text{Pb}(0) \rightarrow \text{Pb}^{+2} + 2e$. Lead(0) was electrodeposited at -0.5V from 0.1 M HClO₄ containing 5.0 mM Pb(II) and anodically stripped at 0.0 V. The deposition and stripping of Pb(0) was ideal for calibration of the Au electrodes. No

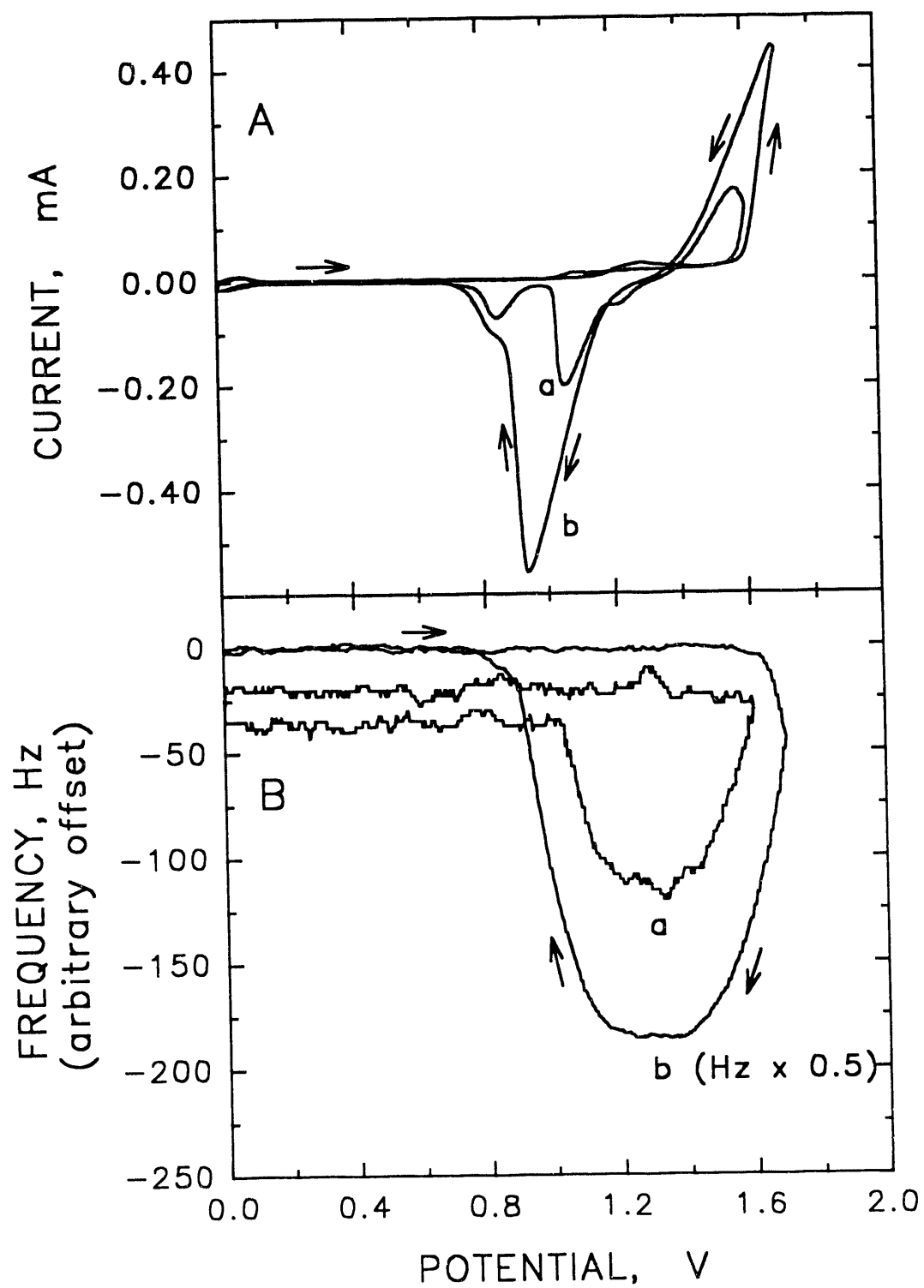
change was observed for the mass of the original Au film after several cycles of plating and stripping in the calibration process. Values of $\Delta m/\Delta q$ were calculated from values of df/dq for the electrodepositions of PbO_2 and Bi-PbO_2 films, and the anodic adsorption of Bi(III) on PbO_2 films.

RESULTS AND DISCUSSION

Deposition of PbO₂ and Bi-PbO₂ films - The EQCM was applied to the deposition of pure PbO₂ films, and typical current-potential (*i*-*E*) and frequency-potential (*f*-*E*) response curves are shown in Figure 1A and B, respectively. The two curves were obtained concurrently at a freshly prepared Au-film electrode in the EQCM during a cyclic potential scan in 0.1 M HClO₄ containing Pb(II). Curves a and b represent the first and fifth cyclic scans, respectively. As indicated by the curves, PbO₂ deposition commenced at ca. 1.60 V on the positive scans and continued to ca. 1.40 V on the succeeding negative scan. Stripping of PbO₂ during the negative scan produced a cathodic peak beginning at ca. 1.20 V and continuing to ca. 1.00 V (Curve a) and 0.80 V (Curve b). The small cathodic peak at ca. 0.80 V during the negative scans was produced by reduction of Au-oxide that formed at *E* > ca. 1.0 V during the preceding positive scans. As shown, the current and frequency responses were much smaller for Curve a.

The difference between the initial and final frequency values (Δf) in Figure 1B was ca. 20 Hz for Curve a which corresponded to a net mass increase (Δm) of ca. 180 ng during the first scan. There was no net mass increase for the fifth cyclic scan. It has been concluded [10] that bulk PbO₂ is not totally stripped during the first cyclic scan and the residue remaining was suggested to be a stable form of PbO. This PbO was reoxidized to PbO₂ during the subsequent positive scan [10] and appeared to function as a base for rapid nucleation of PbO₂ in the subsequent deposition process. On the basis of the mass increase of 180 ng (Figure 1B, Curve a), the equivalent of ca. 2.4 monolayers

Figure 1. Current (A) and frequency (B) responses obtained concurrently during a cyclic potential scan at the Au electrode of the EQCM for the anodic deposition and stripping of pure PbO_2 in 0.1 M HClO_4 . Conditions: 40 mV sec^{-1} , 5.0 mM Pb(II) , N_2 purged. Curves: (a) first scan, (b) fifth scan.



of PbO was estimated to remain adsorbed at the Au surface, assuming a roughness factor of 1.0. Figures 2A and B show typical i - E and f - E curves, respectively, that were obtained concurrently during a cyclic scan for the deposition and stripping of Bi-PbO₂ films from 0.1 M HClO₄ containing Pb(II) and Bi(III). The curves shown correspond to the fourth scan for a freshly prepared Au-film electrode in the EQCM. Underpotential deposition and stripping peaks were observed for the Bi(III)/Bi(0) couple at $E < 0.4$ V. Other significant differences observed for the Bi-PbO₂ film (Figure 2), as compared to the pure PbO₂ film (Figure 1), were as follows: (i) anodic deposition occurred over a smaller potential range, i.e., from ca. 1.65 V on the positive scan to ca. 1.50 V on the negative scan; (ii) cathodic stripping of the oxide occurred at more negative potential values, i.e., from ca. 1.0 V to 0.6 V on the negative scan; (iii) a substantial amount of the deposited mass (ca. 360 ng) remained on the Au surface following cathodic stripping; and (iv) a small increase in residual surface mass was observed for each cyclic scan. This last observation is indicative of the accumulation of an ad-layer of a mixed metal oxide (Bi-PbO and/or Bi-PbO₂) whose thickness increased with each successive scan. This ad-layer was not stripped even for potential values as low as 0.0 V and became visible to the eye after ca. 5 cyclic scans. The ad-layer was removed by immersion of the electrode into a mixture containing 50% (v/v) glacial acetic acid, 15% (v/v) hydrogen peroxide and 35% (v/v) H₂O.

Typical plots of frequency shift as a function of coulombic charge are shown in Figure 3 for the deposition of PbO₂ (Curve a) and Bi-PbO₂ (Curve b) at constant potential. Deposition was performed in triplicate. The values of A_e/K were

Figure 2. Current (A) and frequency (B) responses obtained concurrently during a cyclic potential scan at the Au electrode of the EQCM for deposition and stripping of Bi-doped PbO_2 in 0.1 M HClO_4 . Conditions: 50 mV sec^{-1} , 5.0 mM Pb(II) and 0.2 mM Bi(III) , N_2 purged, 4th cyclic scan shown.

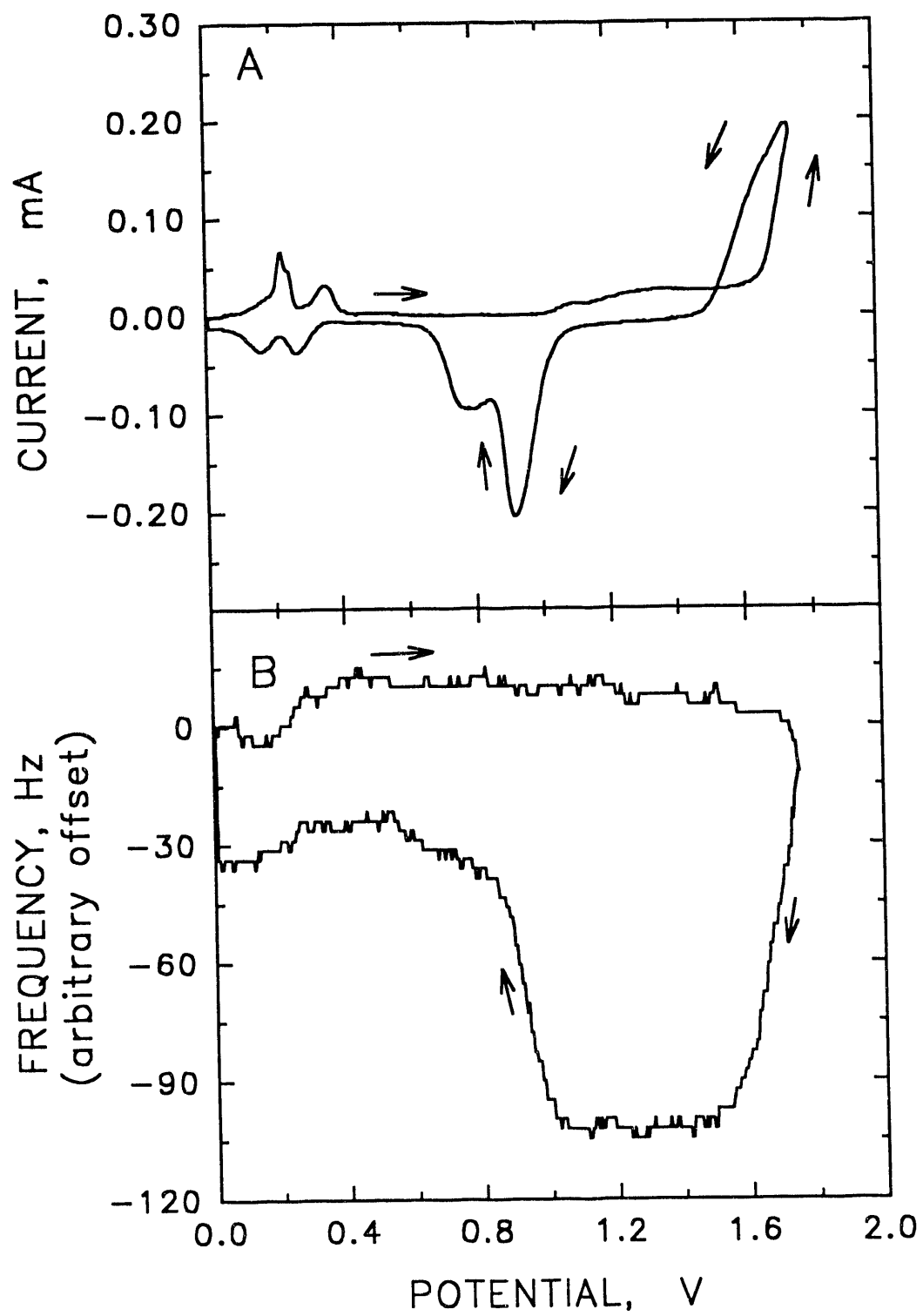
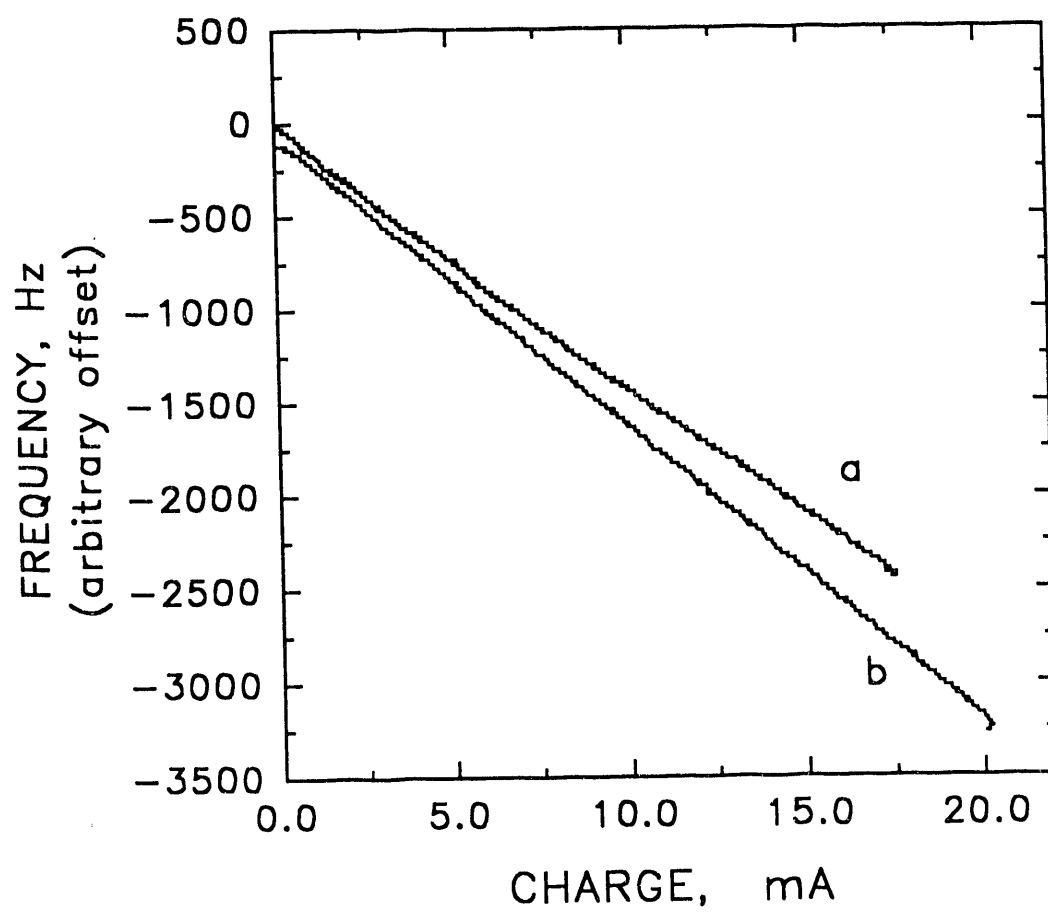


Figure 3. Plot of frequency shift versus total charge for the electrodepositions of PbO_2 (a) and Bi-doped PbO_2 (b) in 0.1 M HClO_4 . Conditions: (a) 5.0 mM Pb(II) , (b) 5.0 mM Pb(II) and 0.5 mM Bi(III) . Deposition potentials: (a) 1.6 V, (b) 1.7 V.



$0.94 \times 10^{-5} \text{ mg Hz}^{-1}$ and $0.85 \times 10^{-5} \text{ mg Hz}^{-1}$ for the crystals used to obtain Curves a and b, respectively. Equation (2) is valid for calculating $\Delta m/\Delta q$ values only when the deposited film is uniform, rigid, thin, and elastic, and when the solution component of the signal remains constant during the measurement [5]. The linearity displayed by f-q plots for deposition of both films shown in Figure 3 was considered evidence that these conditions were met.

A value of $\Delta m/\Delta q = 1.26 \pm 0.04 \text{ mg coul}^{-1}$ was calculated for PbO_2 films (Figure 3, Curve a) using equation (2); the confidence interval represents one standard deviation. The total frequency shift shown in Curve a corresponded to deposition of the equivalent of approximately 60 monolayers of PbO_2 . The theoretical value of $\Delta m/\Delta q$ is $1.24 \text{ mg coul}^{-1}$ for the deposition of PbO_2 according to equation (3) which is in excellent agreement with experiment ($1.26 \text{ mg coul}^{-1}$). This agreement indicates that H_2O and HClO_4 were not extensively incorporated into the PbO_2 film, assuming $n = 2 \text{ eq mol}^{-1}$.



A value $\Delta m/\Delta q = 1.32 \pm 0.03 \text{ mg coul}^{-1}$ was obtained for Bi- PbO_2 films (Figure 3, Curve b). The deposition of Bi- PbO_2 was repeated using the conditions described in Figure 3 but with HNO_3 as the supporting electrolyte and the value of $\Delta m/\Delta q$ was $1.27 \pm 0.03 \text{ mg coul}^{-1}$. The larger value of $\Delta m/\Delta q$ for Bi- PbO_2 in 0.1 M HClO_4 as compared to 1.0 M HNO_3 could be the result of incorporation of ClO_4^- or H_2O into the film. Nielson et al. [12] recently reported that results of depth profiling studies using Auger spectroscopy indicated that Cl was present in Bi- PbO_2 films deposited from HClO_4 solutions. They speculated that the Cl might have originated from Cl^- impurity in the

HClO₄ [12]. Some evidence has been reported [13,14] that Bi(III) might exist in HClO₄ solutions as the ion pair Bi(OH)₂ClO₄ [13, 14] and we suspect that ClO₄⁻ and not Cl⁻ was the source of the Cl found by Nielson et al. [12]. Nielson et al. [12] found some Cl in PbO₂ films deposited from HClO₄ solutions, but only in the outer layers.

The observation that $\Delta m/\Delta q$ values obtained in HNO₃ solutions were virtually identical for PbO₂ (1.26 mg coul⁻¹) and Bi-PbO₂ (1.27 mg coul⁻¹) is consistent with the fact that Bi and Pb have nearly equivalent atomic weights, and the evidence from x-ray diffraction patterns for the intact thin films that new phases did not form when Bi was introduced into PbO₂.

Oxidation state of Bi in Bi-PbO₂ films - Exhaustive electrolysis at constant potential was applied for the determination of n (eq mol⁻¹) for the deposition of Pb(II) as PbO₂. The average of five determinations was $n = 1.96 \pm 0.05$ equiv mol⁻¹. The value of n for oxidation of Bi(III) during deposition of Bi-PbO₂ was estimated from amperometric data obtained with the Au RDE by comparison of the slopes of plots of $1/i$ vs. $1/\omega^{1/2}$ according to equation (1). Linear regression statistics for that data are shown in Table 1 for PbO₂ and Bi-PbO₂ films. The existence of non-zero intercepts in the $1/i-1/\omega^{1/2}$ plots indicated that the electrodeposition reactions were under mixed kinetic-transport control. As seen in Table 1, the quality of the linear fits were quite good and use of equation (1) was considered appropriate for characterization of the electrode processes. In the calculation of n for the oxidation of Bi(III) during deposition of Bi-PbO₂, it was necessary to assume that $n = 2.0$ equiv mol⁻¹ for Pb(II) and that the diffusion coefficients

Table 1. Linear regression parameters obtained from results of current versus rotation velocity studies for the deposition of pure and Bi-doped PbO_2 films in 0.1 M HClO_4 ^{a,b}.

$$1/i = m^{-1/2} + b$$

[Pb(II)] (mM)	[Bi(III)] (mM)	m (s ^{-1/2} mA ⁻¹)	b (mA ⁻¹)	Std. Error (mA ⁻¹)	Correlation coefficient (r)
2.1	0.0	20.52 ± 1.08	0.33 ± 0.10	0.3161	0.9992
2.0	0.1	20.00 ± 1.00	0.36 ± 0.14	0.3222	0.9995

^a Conditions: E = 1.7 V, $\omega = 20.9 - 261.7 \text{ rad s}^{-1}$ (N = 8).

^b Average of four depositions for each film.

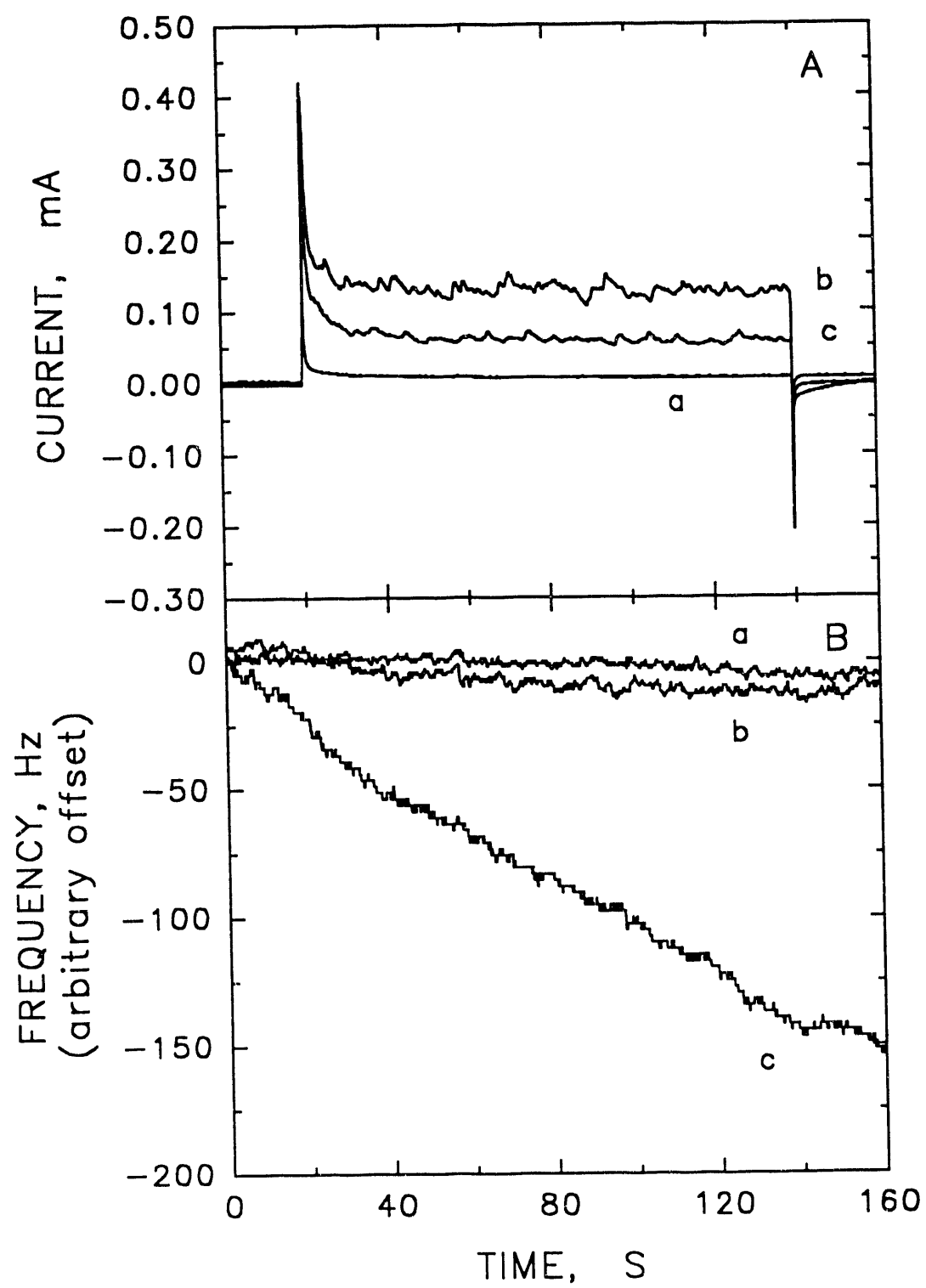
of Pb(II) and Bi(III) were equivalent. The average oxidation state for Bi in Bi-PbO₂ films was calculated to be 5.01 ± 0.10 from the ratio of the slopes shown in Table 1.

Loss of activity of Bi-PbO₂ films during Mn(II) oxidation - LaCourse et al. [3]

observed a rapid loss of activity for some Bi-PbO₂ film electrodes during the oxidation of Mn(II) to MnO₄⁻. They speculated that the surface might be fouled by deposition of MnO₂(s) or by corrosive losses of active Bi-sites in the electrode surface. The EQCM is perfectly suited for establishing which of these explanations is most probable because fouling leads to the increase of surface mass and corrosion to mass decrease.

Simultaneous i-t and f-t curves are shown in Figure 4A and B, respectively, for a Bi-PbO₂ film in the EQCM following a potential step from 1.4 V to 1.7 V in the presence and absence of Mn(II). The potential was stepped to 1.7 V at 20 sec. and back to 1.4 V

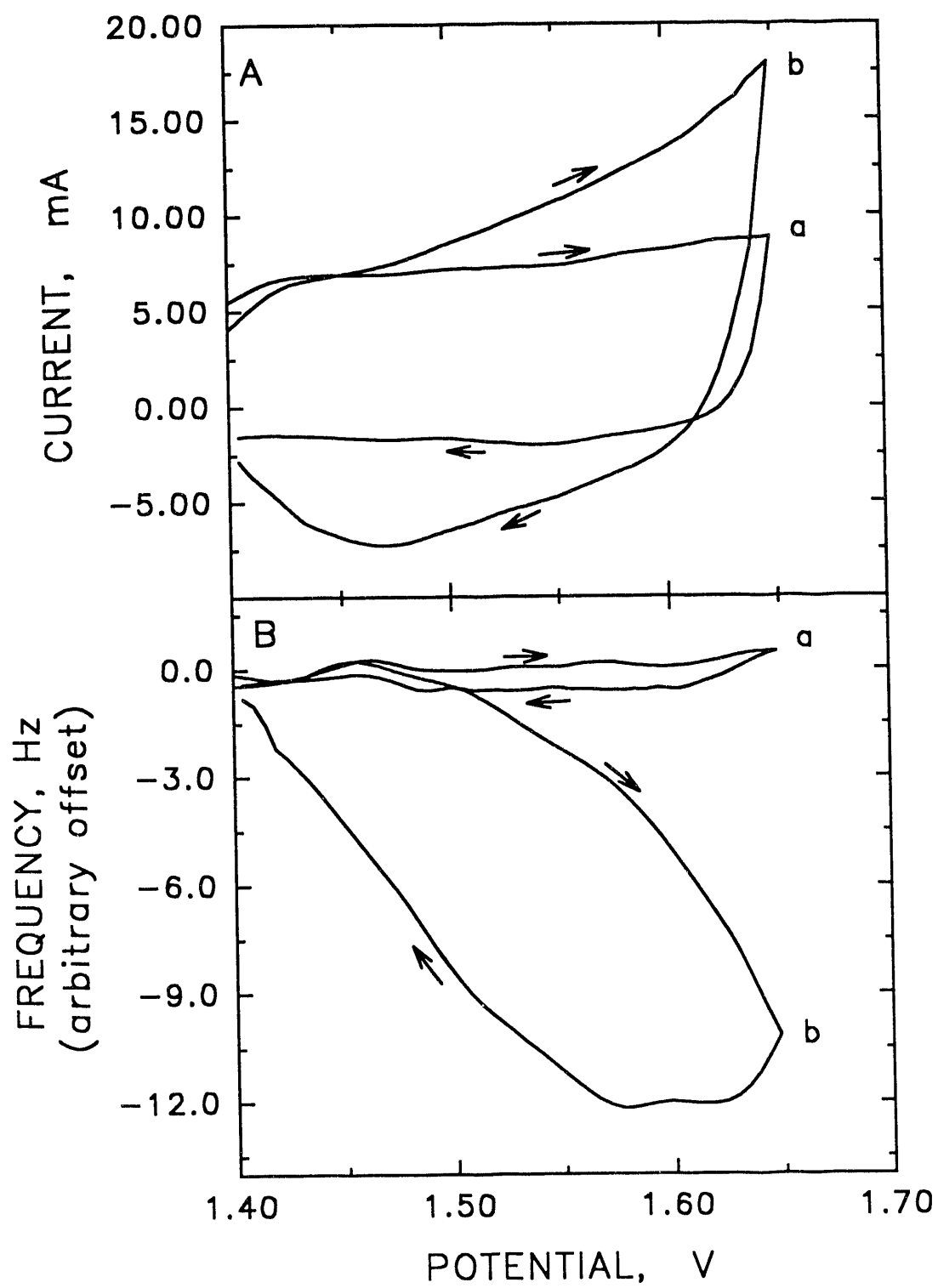
Figure 4. Current (A) and frequency (B) responses obtained concurrently as a function of time at a Bi-doped PbO_2 film on the Au electrode of the EQCM for the oxidation of Mn(II) in 1.0 M HClO_4 . Conditions: convectively mixed by N_2 purge. Potential: 1.4 V at $t = 0.0$ sec; step to 1.7 V at $t = 20.0$ sec; return to 1.4 V at $t = 140$ sec. Curves: (a) residual response, (b) 1.0 mM Mn(II) added, first experiment, (c) same as (b) but fifth experiment.



at 140 sec. Curve a corresponds to the residual response in the absence of Mn(II). The first and fifth experiments performed in the presence of Mn(II) are shown by Curves b and c, respectively. It is significant that the current was largest and the mass gain smallest for Curve b. The current was decreased by ca. 2X and the mass gain increased by ca. 15X for Curve c. These data are consistent with the diagnosis that loss of catalytic activity resulted from surface fouling, probably by the insoluble product $\text{MnO}_2(\text{s})$ [3].

Anodic adsorption of Bi(III) on PbO_2 -film electrodes - The EQCM was applied to obtain direct evidence that Bi(III) is anodically adsorbed on PbO_2 surfaces in Pb(II)-free solutions containing Bi(III). Figures 5A and B show typical i-E and f-E curves, respectively, obtained concurrently during a cyclic scan of potential at the PbO_2 -film electrode in Pb(II)-free 0.1 M HClO_4 . The PbO_2 film had been deposited on the Au-film in the EQCM from a HClO_4 solution of Pb(II). Curves a and b correspond to the absence and presence, respectively, of Bi(III). We suggest that these data indicate that Bi(III) was anodically adsorbed during the positive scan for $E > \text{ca. } 1.45 \text{ V}$ (Curve b) and cathodically desorbed for $E < \text{ca. } 1.57 \text{ V}$ during the subsequent negative scan. Curve b (Figure 5B) shows that the mass of the PbO_2 film returned to its original value with the conclusion of the cyclic scan at 1.4 V. Hence, all Bi(III) adsorbed during the positive scan was quantitatively stripped as Bi(III) during the negative scan under these conditions. For much faster scan rates ($> > 5 \text{ mV s}^{-1}$), the mass returned to the original value only after several seconds passed following termination of the negative scan at 1.40 V. That

Figure 5. Current (A) and frequency (B) responses obtained concurrently during a cyclic potential scan at a pure PbO_2 film on the Au electrode of the EQCM for the anodic adsorption of Bi(III) in 1.0 M HClO_4 . Conditions: 5.0 mV sec^{-1} , no convective mixing. Curves: (a) residual response, (b) 5.0 mM Bi(III) added.



observation undoubtedly resulted from slow desorption kinetics.

Values of total charge for anodic adsorption of Bi(III) (Δq) were determined by integration of the net current corresponding to the difference between Curves a and b in Figure 5A. Net values of Δf were taken from f - E plots. The average value of $\Delta m/\Delta q$ for four determinations was $1.72 \pm 0.02 \text{ mg coul}^{-1}$. The experiment was repeated with 1.0 M HNO_3 , using a PbO_2 -film electrode deposited from HNO_3 , and the average of four determinations was $\Delta m/\Delta q = 1.30 \pm 0.03 \text{ mg coul}^{-1}$. Exact interpretation of the $\Delta m/\Delta q$ data requires more detailed information than is available for the identity of the adsorbed species. Bismuth(III) in aqueous solutions has been reported to exist in various polymeric forms [15] and this polymeric nature might be reflected in the adsorbed species. The complexity is increased by the fact that PbO_2 is a basic oxide and, hence, adsorption of an anionic species could involve ion-exchange with surface OH^- . Furthermore, evidence has been reported that Bi(III) might form ion-paired complexes with ClO_4^- [14,15] and this anion could be co-adsorbed.

The anodic adsorption of Bi(III) was assumed to give Bi(V), i.e., $n = 2 \text{ equiv mol}^{-1}$. This was justified by the evidence that Bi(V) was produced during deposition of Bi- PbO_2 . Predicted values of $\Delta m/\Delta q$ are given in Table 2 corresponding to several possible adsorption reactions involving only monomeric forms of Bi(V). In Table 2 Case I corresponds to Bi(V) adsorbed as neutral species and Case II corresponds to anionic Bi(V) adsorbed by displacement of surface OH^- . As seen by comparison of predicted values of $\Delta m/\Delta q$ for Cases I.A and II.A, it is virtually impossible to distinguish between adsorption of Bi(V) as a neutral species and as an anionic species adsorbed with ion

Table 2. Theoretical values of $\Delta m/\Delta q$ (mg coul⁻¹) for several possible products of the anodic adsorption of Bi(III) on PbO₂ films. Experimental results:

$$\Delta m/\Delta q = 1.72 \pm 0.02 \text{ mg coul}^{-1} \text{ (0.1 M HClO}_4\text{)}$$

$$= 1.30 \pm 0.03 \text{ mg coul}^{-1} \text{ (0.1 M HNO}_3\text{)}$$

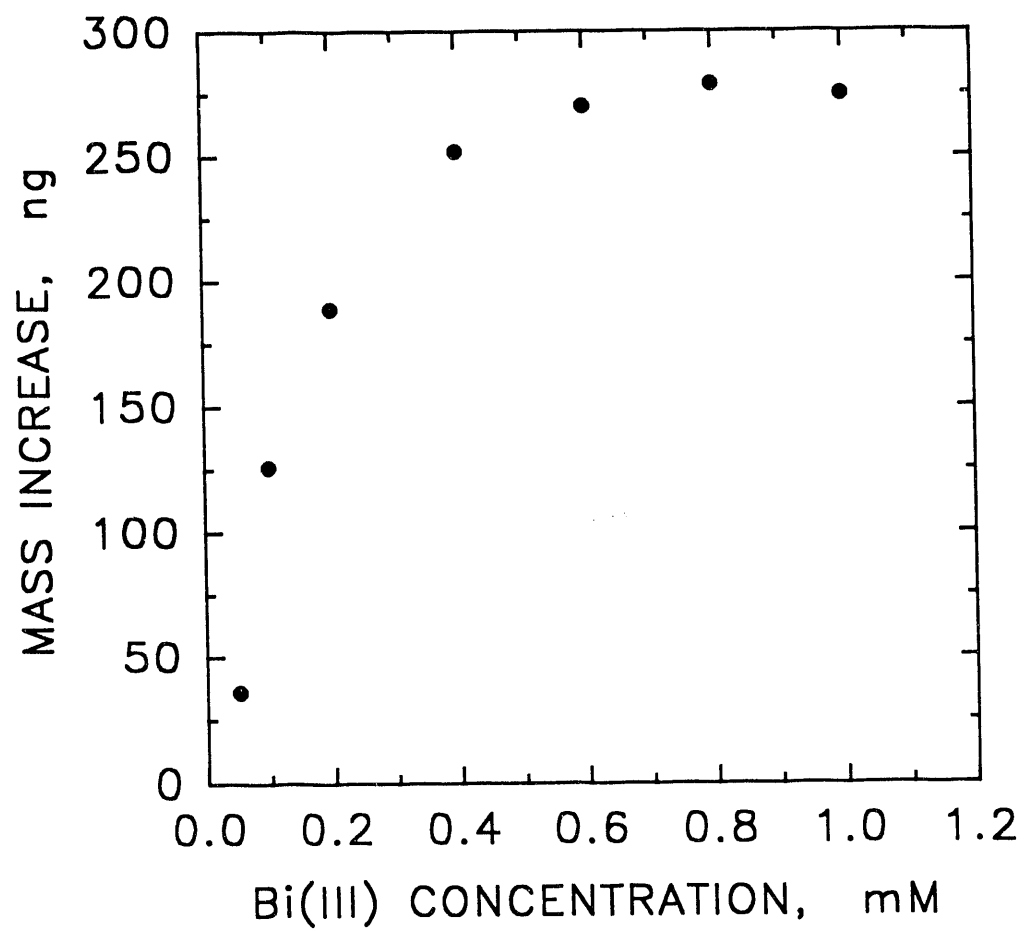
Reaction		$\Delta m/\Delta q$ theory (mg C ⁻¹)
I. Without ion exchange		
A. No ion pairing		
1. PbO ₂ + Bi(III)	→ PbO ₂ [BiO(OH) ₃]	1.43
2.	→ PbO ₂ [BiO ₂ (OH)]	1.34
B. Ion pairing		
1. PbO ₂ + Bi(III)	→ PbO ₂ [BiO ₂ ClO ₄]	1.76
2.	→ PbO ₂ [BiO(OH) ₂ ClO ₄]	1.86
3.	→ PbO ₂ [BiO ₂ NO ₃]	1.57
4.	→ PbO ₂ [BiO(OH) ₂ NO ₃]	1.66
II. With Ion exchange		
A. No ion pairing		
1. PbO(OH) ₂ + Bi(III)	→ PbO(OH)[BiO ₂ (OH) ₂]	1.34
2.	→ PbO[BiO ₂ (OH) ₃]	1.34
B. With ion pairing		
1. PbO(OH) ₂ + Bi(III)	→ PbO[BiO ₂ (OH) ₂ ClO ₄]	1.76
2.	→ PbO(OH)[BiO(OH) ₃ ClO ₄]	1.86
3.	→ PbO[BiO ₂ (OH) ₂ NO ₃]	1.57
4.	→ PbO(OH)[BiO(OH) ₃ NO ₃]	1.66

exchange. For those reactions offered in Table 2, the experimental data from 0.1 M HClO_4 corresponded most closely with cases where ClO_4^- was paired with the adsorbed Bi(V) (Rxns. I.B.1 and II.B.1). Data for 1.0 M HNO_3 correspond most closely with cases where adsorbed Bi(V) was not paired with NO_3^- (Rxns. I.A.2 & II.A.1-2).

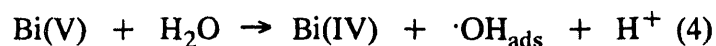
A significant application of the EQCM is foreseen for determinations of adsorption isotherms. The feasibility of that application is illustrated in Figure 6 showing the increased surface mass as a function of Bi(III) concentration in 1.0 M HClO_4 after a 40 sec. adsorption period at 1.7 V ($A_e/K = 9.0 \text{ ng Hz}^{-1}$). The curve shown has the general appearance of an adsorption isotherm; however, we hasten to note that the mass continued to increase, albeit slowly, after 40 sec. and the equilibrium surface coverage by Bi(V) was not attained for the concentration values shown here. The largest net mass increase shown in Figure 6 (i.e. 275 ng) corresponded to a surface coverage equivalent to 0.6 monolayer when calculated for adsorbed BiO_2ClO_4 . As expected, the quantity of Bi(V) anodically adsorbed during the 40 sec. period was influenced by convection, as determined using dispersed N_2 . No further attempt was made to determine the exact form of the isotherm because of the difficulty of controlling convection in this cell. A new cell is under construction according to the "wall-jet" design which allows reproducible control of convection for characterization of the adsorption isotherm.

Mechanism of anodic adsorption of Bi(III) - Bismuth(V) is a powerful oxidizing agent with estimates of E° value for the $\text{Bi(V)}-\text{Bi(III)}$ couple in the range 1.4 V (16) to 1.8 V [15] vs. Ag/AgCl . In aqueous solutions, Bi(V) oxide ions can oxidize Mn^{2+} to

Figure 6. Increase in electrode mass from anodic adsorption of Bi(III) on a pure PbO_2 film of the Au electrode of the EQCM as a function of Bi(III) concentration in 1.0 HClO_4 . Conditions: 1.7 V, 40 sec accumulation time, no convective mixing.



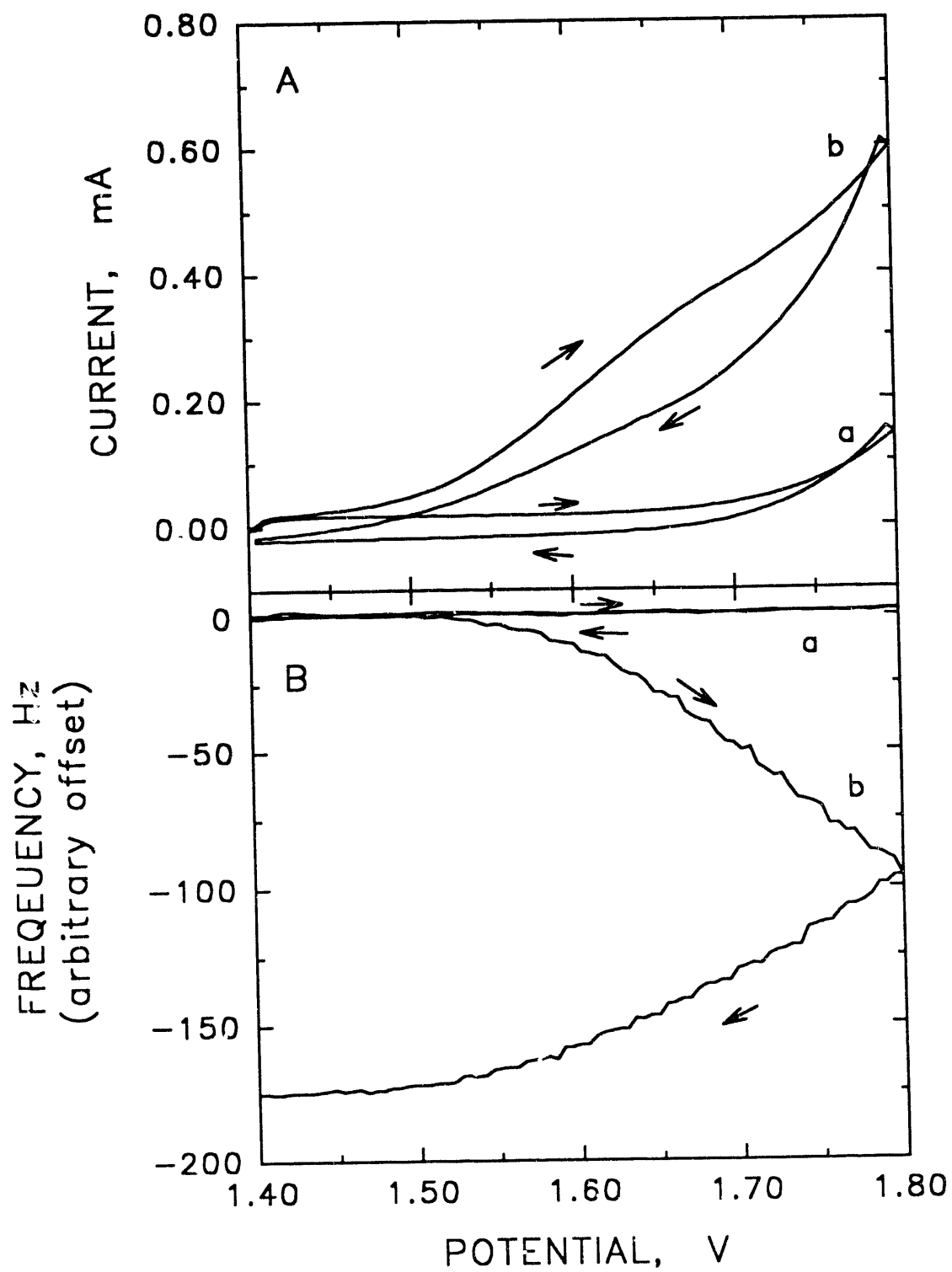
MnO_4^- [17] and can decompose H_2O , with the initial step reported to be that given by equation (4) [18].



No oxidation of Bi(III) was observed at Au, Pt and C electrodes. Hence, the oxidation of Bi(III) to Bi(V) during deposition of Bi-PbO₂ and during anodic adsorption at PbO₂ surfaces apparently benefited from a stabilizing interaction of the Bi(V) within the oxide surface lattice.

Regardless of the exact chemical formulas of Bi(III) in solution and Bi(V) adsorbed on PbO₂-film electrodes, it is suspected that the anodic adsorption reaction occurred with surface-catalyzed transfer of oxygen from H₂O to the Bi(V). Hence, it was suspected that the potential dependency for the anodic adsorption reaction might be similar to that for anodic deposition of Pb(II) onto PbO₂-film electrodes which also requires transfer of oxygen from H₂O. Typical *i-E* and *f-E* response curves are shown in Figure 7A and 7B, respectively, for a cyclic potential scan at a pure PbO₂-film electrode without (Curves a) and with (Curves b) Pb(II) in the solution. As indicated by the increase in anodic current and the decrease of frequency (i.e., increased surface mass), anodic deposition of PbO₂ occurred for $E > \text{ca. } 1.45 \text{ V}$ during both positive and negative scans. This onset potential is well above the formal potential of ca. 1.2 V vs. Ag/AgCl for the PbO₂/Pb(II) couple in 0.1 M HClO₄. Chang and Johnson [10] reported evidence that initiation of the anodic deposition of Pb(II) as PbO₂ at clean Pt, Au and carbon electrodes was correlated with the overpotential for O₂ evolution at the substrate material. This correlation was interpreted as evidence that the deposition process is facilitated by the generation of

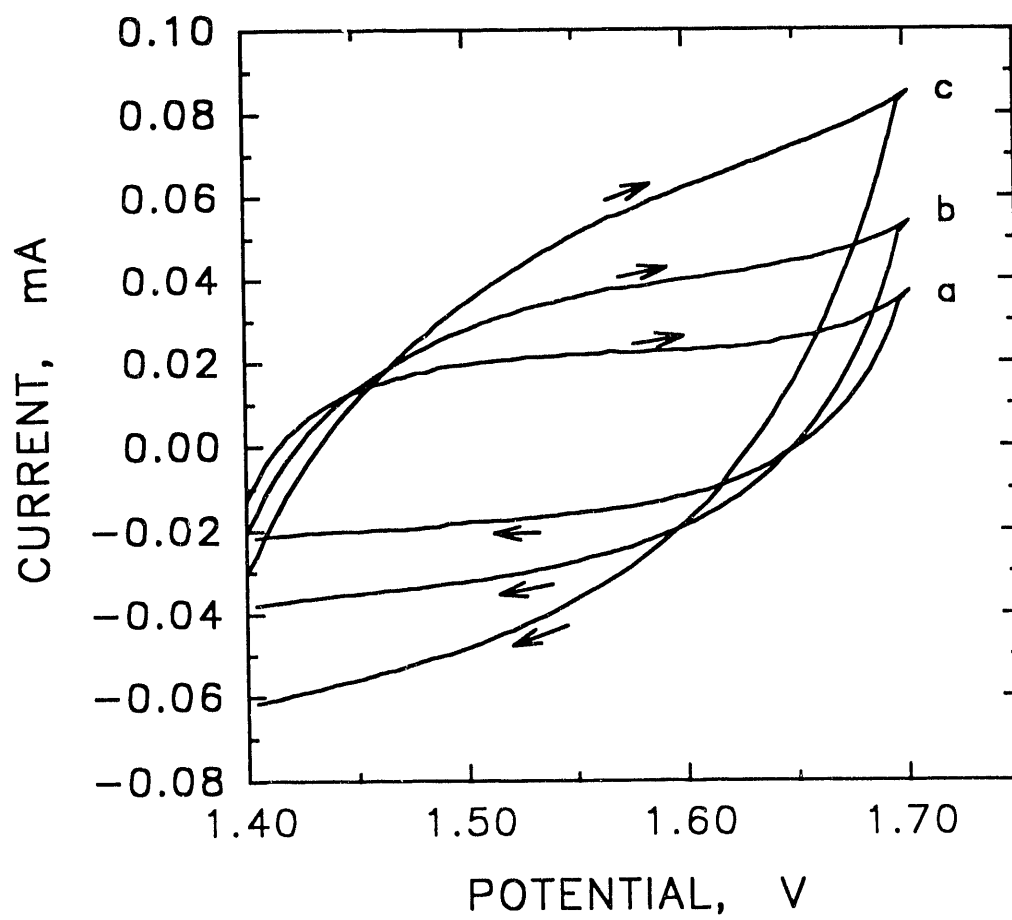
Figure 7. Current (A) and frequency (B) responses obtained concurrently during a cyclic potential scan at a pure PbO_2 film on a Au RDE for the anodic adsorption of PbO_2 in 1.0 M HClO_4 . Conditions: 100 mV sec^{-1} , convectively mixed by N_2 purge. Curves: (a) residual response, (b) 2.0 mM Pb(II) added.



$\cdot\text{OH}_{\text{ads}}$ as the intermediate product of O_2 evolution [19, 20]. Accordingly, continued deposition of PbO_2 on a PbO_2 electrode can be expected to correlate with the overpotential for O_2 evolution at that PbO_2 surface. It would seem to be more than coincidence that the potential for onset of PbO_2 deposition (Figure 7) and anodic adsorption of Bi(III) (Figure 5) were virtually identical on PbO_2 -film electrodes. This is considered to be evidence supporting the conclusion that a common electrochemical step controls the rates of both processes, i.e., the anodic discharge of H_2O to produce adsorbed $\cdot\text{OH}$.

Residual i-E curves for a PbO_2 -film electrode are shown in Figure 8 for cyclic scans at three scan rates within the potential limits 1.4 V and 1.7 V. Possible sources of the small anodic current during the positive scan for $E > 1.45$ V include double-layer charging, faradaic transformation of the film, and anodic discharge of H_2O to produce an adsorbed product. The reaction $2\text{H}_2\text{O} \rightarrow \text{O}_2 + 4\text{H}^+ + 4\text{e}$ is not expected to be sensitive to changes in scan rate. The cathodic current observed during the negative scan can originate from discharge of the double layer and from the reverse faradaic transformation of the surface. Reduction of O_2 would not occur in the potential range shown. We expect that double-layer charging and discharging accounts for the majority of the currents observed. However, because the rate of H_2O discharge to produce $\text{O}_2(\text{g})$ increased dramatically for $E > 1.7$ V and because that process has an exponential dependence on potential, we suggest also that discharge of H_2O contributes an anodic component to the total current observed for all values $E > \text{ca. } 1.45$ V. The fact that the deposition of Pb(II) (Figure 7) and anodic adsorption of Bi(III) (Figure 5) both

Figure 8. Voltammetric response of a pure PbO_2 film on a stationary Au RDE as a function of potential scan rate in 1.0 M HClO_4 . Conditions: 0.0 rad sec^{-1} . Scan rate (mV sec^{-1}): (a) 25, (b) 50, (c) 100.

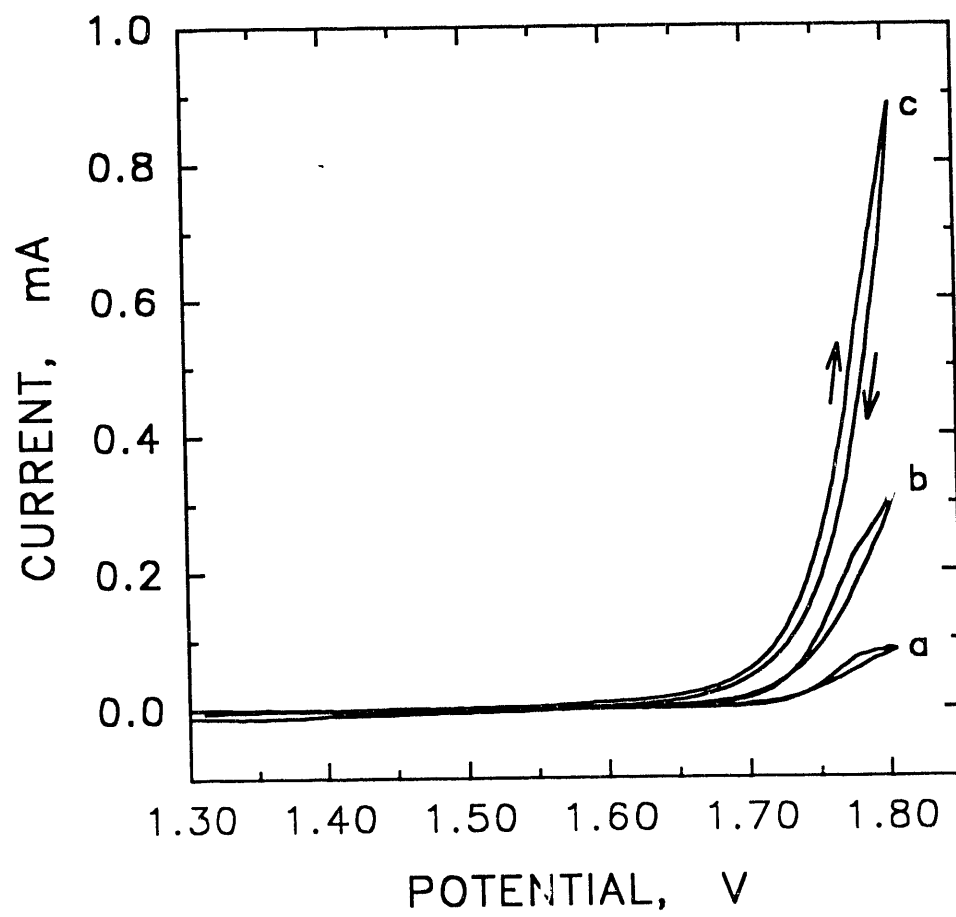


commenced at 1.45 V during the positive scan are interpreted as indicating that the requirement for both reactions is the anodic discharge of H_2O , probably to the product $\cdot\text{OH}_{\text{ads}}$. It is commonly agreed that $\cdot\text{OH}_{\text{ads}}$ is an intermediate product in O_2 evolution [19-20].

Electrocatalytic role of adsorbed Bi(V) - In a previous publication from this laboratory, Yeo et al. [2] reported for Bi-PbO₂ film electrodes that the net overpotential for O_2 -evolution decreased as the Bi/Pb ratio was increased. Furthermore, this trend correlated with the increased rate of the anodic O-transfer reaction for Mn(II). That correlation was interpreted as supporting the tentative conclusion that $\cdot\text{OH}_{\text{ads}}$ produced by H_2O discharge at the Bi-sites is consumed in the anodic oxygen-transfer mechanism by which Mn(II) is oxidized to produce MnO_4^- .

Figure 9 contains voltammetric evidence that the overpotential for O_2 evolution at PbO₂-film electrodes also was decreased as a result of adsorbed Bi(V). The magnitude of the anodic current was visibly increased in the region $E > 1.6$ V with addition of small quantities of Bi(III) to the supporting electrolyte. We reject the possibility that the increased current resulted from continuous oxidation of Bi(III) to produce a soluble Bi(V) species or a multi-layered deposit of insoluble Bi(V) at the PbO₂ surface. Evidence includes the following: 1) the anodic current observed was much larger than could be justified on the basis of oxidation of Bi(III) at these low concentrations, 2) the i - E curves were independent of the rotation speed of the electrode, and 3) the current measured at a constant potential in the range 1.6 V to 1.8 V remained virtually unchanged when the electrode was transferred from the solution containing Bi(III) to a Bi(III)-free solution. In

Figure 9. Voltammetric response of a pure PbO_2 film on a Au RDE in 1.0 M HClO_4 containing Bi(III). Conditions: 20 mV sec^{-1} , 167 rad sec^{-1} . $C^{\text{b}}_{\text{Bi(III)}} \text{ (uM)}$: (a) 3.0, (b) 6.0, (c) 52.

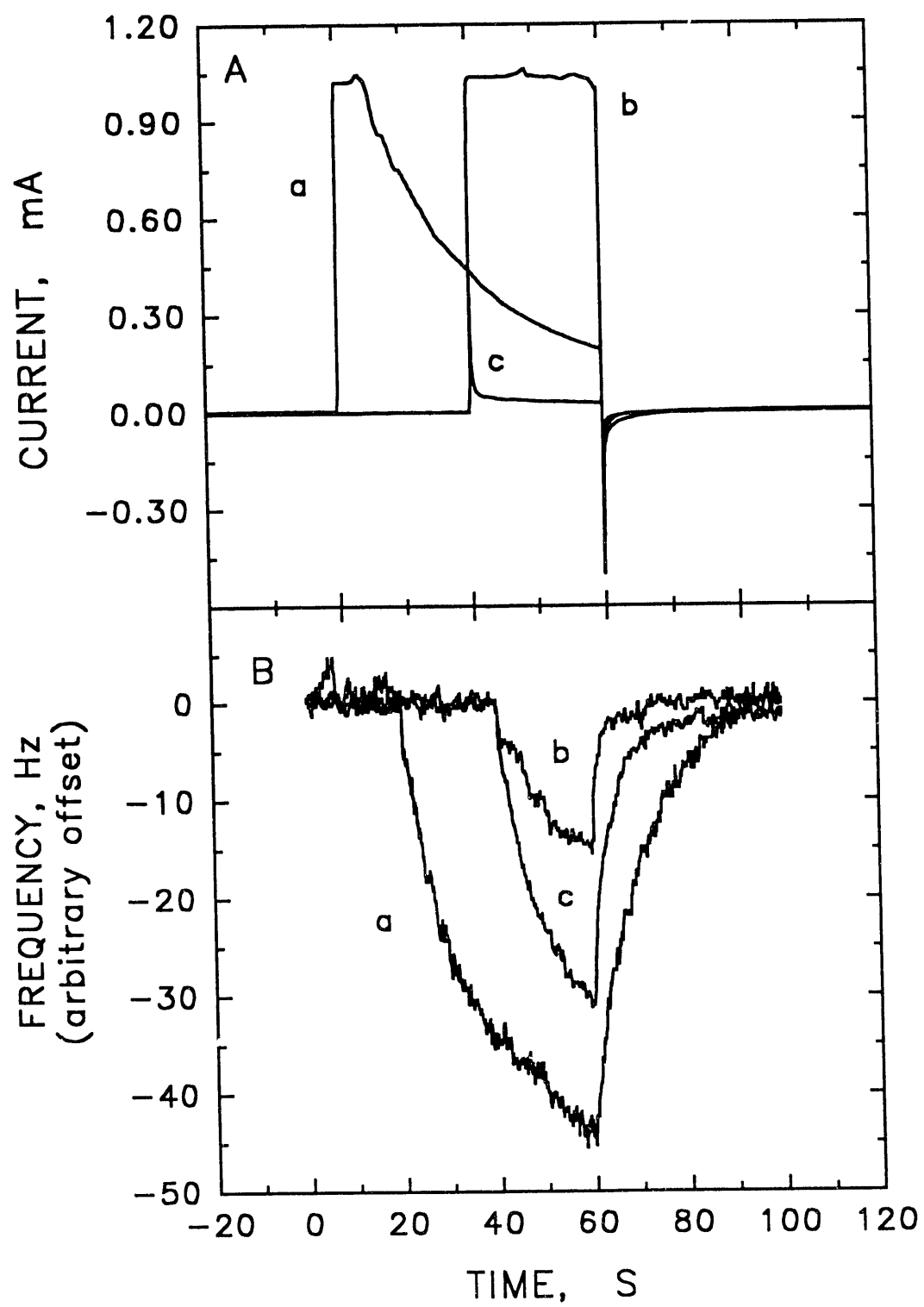


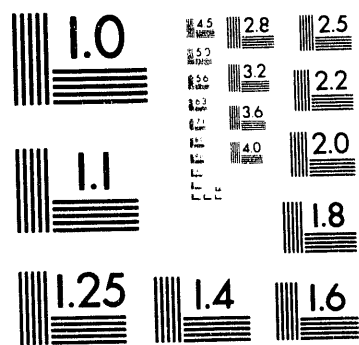
the later experiment, the i - E response in the region $E > 1.6$ V always returned to that for a pure PbO_2 -film electrode following a scan to 1.4 V in the Bi(III) solution. That undoubtedly was the consequence of cathodic desorption of Bi(V) .

Voltammetric results for DMSO have already been reported to illustrate the catalytic benefit of adsorbed Bi(V) on PbO_2 -film electrodes [4]. The EQCM was applied to determine if the presence of DMSO resulted in modification of the rate of accumulation of adsorbed Bi(V) . The i - t and f - t response curves are shown in Figures 10A and B, respectively, for solutions containing 14 mM DMSO with 5.0 mM Bi(III) (Curve a) and 0.5 mM Bi(III) (Curve b), and 0.5 mM Bi(III) without DMSO (Curve c). The potential was stepped from 1.4 V to 1.8 V at 20 sec. for Curve a and at 40 sec. for Curves b and c, and then back to 1.4 V at 60 sec. The anodic current remained at its transport-limited anodic value (ca. 1.0 mA) with increasing time for the smallest Bi(III) concentration (0.5 mM, Curve b). However, for 5.0 mM Bi(III) (Curve a), the current decreased from its initial value with increasing time. As indicated by the frequency response obtained concomitantly (Figure 10B), the quantity of adsorbed Bi(V) was decreased ca. 2X by the presence of DMSO.

These phenomena were further examined by cyclic voltammetry at a pure PbO_2 film on a Au RDE. Figure 11 gives values of the anodic current for DMSO oxidation measured at 1.8 V and plotted vs. log of Bi(III) concentration. Starting from zero current, as observed for 0 mM Bi(III) , the current increased for increasing values of Bi(III) concentration (ca. 2 - 20 μM). However, for $\text{Bi(III)} > \text{ca. } 50 \mu\text{M}$, the DMSO current decreased from its transport limited value [4].

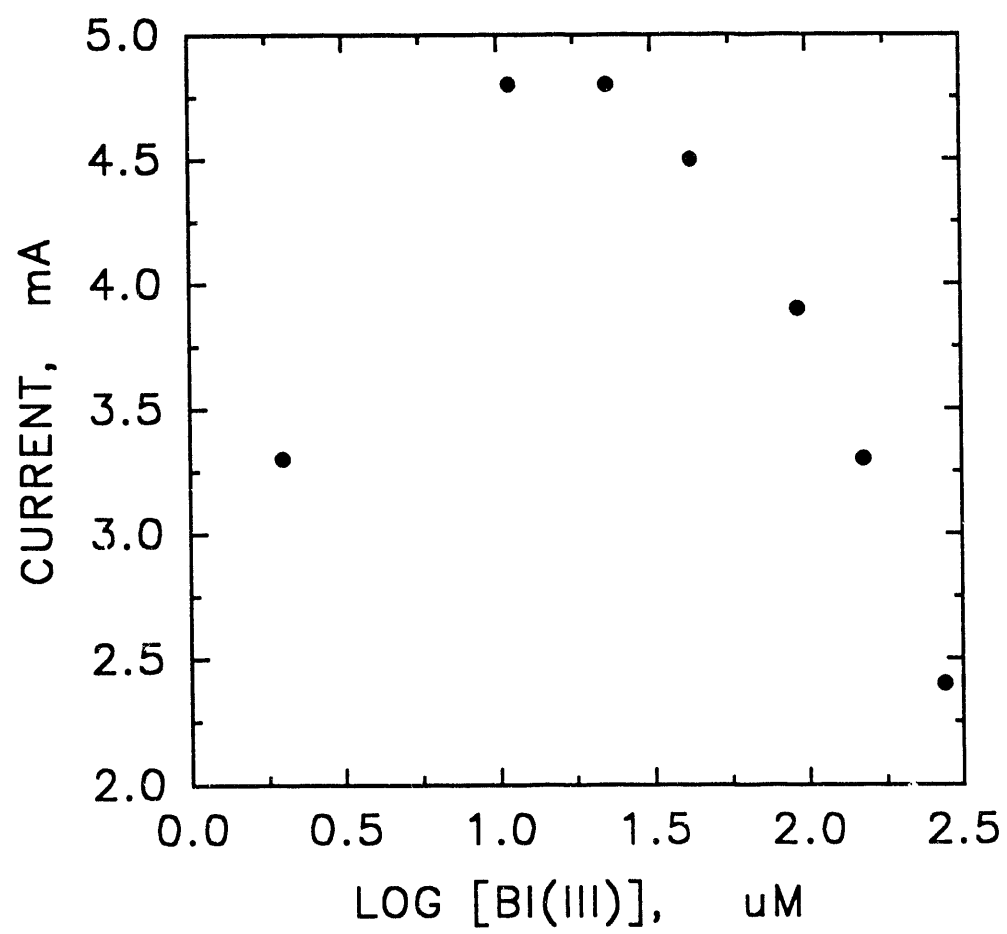
Figure 10. Current (A) and frequency (B) responses obtained concurrently at a PbO_2 film on the Au electrode of the EQCM as a function of time for the oxidation of DMSO in the presence of Bi(III) in 1.0 M HClO_4 . Conditions: convective mixing by N_2 purge. Potential: 1.4 V at $t = 0.0$ sec (a, b and c); step to 1.8 V at $t = 20$ sec (a), or $t = 40$ sec, (b and c); return to 1.4 V at $t = 60$ sec (a, b and c). Curves: (a) 14 mM DMSO with 5.0 mM Bi(III), (b) 14 mM DMSO with 0.5 mM Bi(III), (c) 14 mM DMSO but without Bi(III).





2 of 3

Figure 11. Anodic current response for 10 mM DMSO at a pure PbO_2 film on the Au RDE as a function of Bi(III) concentration in 1.0 M HClO_4 . Conditions: $E = 1.8 \text{ V}$, 262 rad sec^{-1} .



CONCLUSIONS

The production of $\cdot\text{OH}_{\text{ads}}$ by anodic discharge of H_2O has been tentatively concluded to be the prerequisite for numerous anodic oxygen-transfer reactions including the electrodeposition of Pb(II) as PbO_2 (1-4,10). Based on result reported here, it is also proposed that production of $\cdot\text{OH}_{\text{ads}}$ is a prerequisite for the anodic adsorption of Bi(III) as Bi(V) at PbO_2 -film electrodes. As a result, the voltammetric response for anodic adsorption of Bi(V) is dictated by the overpotential for the H_2O discharge process.

The exact identity of adsorbed Bi(V) species cannot be discerned from the EQCM data because the molecular or ionic form of the species is unknown. Experimental values of $\Delta m/\Delta q$ obtained for Bi(III) in HClO_4 solutions were consistent with Bi(V) adsorbed both as neutral species (e.g., BiO_2ClO_4 and $\text{BiO(OH)}_2\text{ClO}_4$) as well as anionic species (e.g., $\text{BiO(OH)}_3\text{ClO}_4^-$ and $\text{BiO}_2(\text{OH})_2\text{ClO}_4^{2-}$). Adsorption of the anionic forms at basic surface sites might involve ion-exchange with surface OH^- . Values of $\Delta m/\Delta q$ measured in HNO_3 were consistent with adsorbed neutral species (e.g., BiO(OH)_3 or $\text{BiO}_2(\text{OH})$), as well as anionic species (e.g., $\text{BiO}_2(\text{OH})_2^-$ and $\text{BiO}_2(\text{OH})_3^{2-}$).

Bismuth(V) oxides ions are not observed to have high stability in aqueous solutions because of slow oxidative decomposition of H_2O [16]. However, Bi(V) in Bi-doped PbO_2 films was not dissolved into acidic solutions even at open circuit potential. Hence, it is apparent that the Bi(V) in the Bi-PbO_2 is stabilized significantly by interaction with the PbO_2 matrix. As a result, the oxidizing power of Bi(V) in solid Bi-PbO_2 must be assumed to be significantly lower than that of soluble Bi(V) oxide ions. Conversely,

Bi(V) adsorbed on PbO₂-film surfaces was desorbed under open-circuit conditions because the potential tended to drift to ca. 1.4 V vs. Ag/AgCl.

The EQCM is concluded to offer significant advantages for the study of electrochemical deposition and stripping, and adsorption and desorption processes. Future work will include application of SIMS to estimate the empirical formulas of the adsorbed Bi(V) species. Future work will also include determination of the adsorption isotherms as a function of applied potential using the EQCM in a flow-through cell.

REFERENCES

1. Yeo, I.; Johnson, D. C., *J. Electrochem. Soc.*, **134**, 1973 (1987).
2. Yeo, I.; Kim, S.; Jacobson, R.; Johnson, D. C., *J. Electrochem. Soc.*, **136**, 1395 (1989).
3. LaCourse, W. R.; Hsiao, Y-L.; Weber, W. H.; Johnson, D. C., *J. Electrochem. Soc.*, **136**, 3714 (1989).
4. Chang, H.; Johnson, D. C., *J. Electrochem. Soc.*, submitted.
5. Ostrom, G. S.; Buttry, D. A., *J. Electroanal. Chem.*, **256**, 411 (1988).
6. Varineau, P. T.; Buttry, D. A., *J. Phys. Chem.*, **91**, 1292 (1987).
7. Orata, D.; Buttry, D. A., *J. Am. Chem. Soc.*, **109**, 3574 (1987).
8. Melroy, O.; Kanazawa, K.; Gordon, J. G.; Buttry, D. A., *Langmuir*, **2**, 697 (1986).
9. Bruckenstein, S.; Shay, M., *Electrochim. Acta*, **30**, 1295 (1985).
10. Chang, H.; Johnson, D.C., *J. Electrochem. Soc.*, **136**, 17 (1989).
11. Levich, V. G., in "Physicochemical Hydrodynamics," p. 75, Prentice Hall, Englewood Cliffs, NJ (1962).
12. Nielsen, B. S.; Davis, J. L.; Thiel, P.A., *J. Electrochem. Soc.*, **137**, 1017 (1990).
13. Holmberg, W. R.; Kraus, K. A.; Johnson, J. S., *J. Am. Chem. Soc.*, **78**, 5506 (1956).
14. Hunt, J. P., in "Metal Ions in Aqueous Solution," W. A. Benjamin, Inc., New York (1963).
15. Cotton, F. A.; Wilkinson, G., in "Advanced Inorganic Chemistry", 5th ed., pp. 420-

- 30, John Wiley & Sons: New York (1988).
16. Latimer, W. M., in "Oxidation Potentials," 2nd edition, p. 125, Prentice-Hall, Englewood Cliffs, New Jersey (1952).
17. Sharpe, A. G., in "Inorganic Chemistry," Longman Inc., New York (1981).
18. Ford-Smith, M. H.; Habeeb, J. J., *Chem. Comm.*, 1445 (1969).
19. Trasatti, S.; Lodi, G., in "Electrodes of Conductive Metallic Oxides," Part B, S. Trasatti, Ed., p. 521, Elsevier Pub. Co., New York (1981).
20. Anderson, B. A., *J. Electrochem. Soc.*, **136**, 158 (1989).

PAPER II.

APPLICATION OF AN ELECTROCHEMICAL QUARTZ CRYSTAL
MICROBALANCE TO A STUDY OF THE DEPOSITION
OF PbO_2 AND Bi-PbO_2 FILMS ON GOLD ELECTRODES

INTRODUCTION

Environmental concern over the fate of toxic chemical wastes has prompted research in our laboratories directed to the development of electrolytic technologies for anodic degradations of these toxins. This work focuses on the evaluation of anode materials for their electrocatalytic activity in support of both direct and indirect oxidative degradation reactions for various organic compounds. All reactions of interest involve the transfer of oxygen from H_2O in the solvent phase to the oxidation products and, therefore, we refer to these electrolytic technologies as *electrochemical incineration*.

Our desire to understand the mechanistic origin(s) of the electrocatalytic activity of so-called "Bi-PbO₂" electrodes has led to various efforts to understand the structure and composition of these electrode materials. Yeo *et al.* [1] demonstrated that x-ray diffraction (XRD) spectra of thick films ($> 1000 \text{ \AA}$) of PbO₂ and Bi-PbO₂ electrodeposited from acidic media are virtually identical, and are consistent with that of the rutile structure of pure β -PbO₂. Furthermore, they observed slightly greater lattice parameters for Bi-PbO₂ in comparison to PbO₂ and concluded that the average oxidation state of bismuth in Bi-PbO₂ films is *ca.* +4.6. However, Larew *et al.* [2], using an Electrochemical Quartz-Crystal Microbalance (EQCM), concluded for PbO₂ electrodes in acidic solutions of Bi^{3+} , that bismuth is electrosorbed as a Bi^{+5} species corresponding to BiO_2ClO_4 in 0.1 M HClO_4 and to BiO_2OH in 0.1 M HNO_3 .

Here the EQCM has been applied to the electrodeposition of so-called "PbO₂" and "Bi-PbO₂" films from acidic media. Empirical formulas for the films are inferred from

the net change in surface mass as a function of faradaic charge ($\Delta m/\Delta q$) calculated from the slope of plots of frequency vs. charge (df/dq) [3-6]. The theoretical value of $\Delta m/\Delta q$ for PbO_2 is $1.24 \text{ mg coul}^{-1}$. However, previous workers have reported that films believed to be $\beta\text{-PbO}_2$ that are electrodeposited from acidic solutions of Pb^{2+} are actually nonstoichiometric oxides with variable composition corresponding to the empirical formula $\text{PbO}_{1.80-1.98}(\text{OH})_{0.11-0.26}$ [7]. This suggests the possibility that Pb^{+2} and OH^- (and/or H_2O) can exist within the PbO_2 films. Naegele and Plieth [8], using electron spectroscopy, detected Pb^{+2} in PbO_2 films electrodeposited on Au substrates and reported that the ratio $\text{Pb}^{+2}/\text{Pb}^{+4}$ steadily decreases with increasing film thickness. Kim *et al.* [9], using x-ray photoelectron spectroscopy, detected H_2O confined near the surfaces of PbO_2 films. Thiel *et al.* [10], using Auger spectroscopy, identified Cl throughout Bi- PbO_2 films deposited from HClO_4 . In research reported here, we anticipated that EQCM data might contribute to a greater understanding of the composition of electrodeposited PbO_2 and Bi- PbO_2 films.

EXPERIMENTAL

Chemicals - All chemicals were reagent grade (Fisher Scientific) and were used as received. The PbO_2 films were prepared from stock solution of Pb^{+2} in HClO_4 and HNO_3 . Stock solutions of Bi^{+3} were prepared from $\text{Bi}(\text{NO}_3)_3$ in HClO_4 and HNO_3 . Deionized water was produced from a NANO-pure II system (SYBRON/Barnstead). Gold (99.999%) and titanium (99.7%) (Johnson Matthey) were used to make EQCM electrodes.

Methods - All experimental data was collected by interfacing the EQCM to an 286 IBM-compatible PC/AT computer via a DT2801-A board (Data Translation, Marlboro, MA) operated within the ASYST programming environment. Overtone-polished, AT-cut, 5-MHz quartz crystals were used in the experiments. The gold films (ca. 200 nm) were prepared by thermal evaporation of Au using a Model E306A coating system (Edwards, West Sussex, England). A thin film of Ti (ca. 20 nm) was used as an adhesive interlayer between the quartz and Au [11].

All X-ray diffraction spectra were collected with a Scintag diffractometer using $\text{Cu K}\alpha$ radiation. The 2θ (two-theta) angles ranged from 10 to 70° with a step size of 0.03° . The scanning electron micrographs (SEMs) were obtained with a Jeol Model JSM-840A microscope. A Au rotated disk electrode (RDE) (0.2 cm^2 , Pine Instrument Company, Grove City, PA) governed by a Model MSR rotator (Pine Instruments) was used for the RDE voltammetry. Voltammetric control was provided by a Model RDE4 Potentiostat/Galvanostat (Pine Instruments). All potentials are reported with reference to a saturated

calomel electrode (SCE). A Pt wire was used as the auxiliary electrode.

The net change in mass (Δm) as a function of charge (Δq) for an electrosorbed or electrodeposited species at an EQCM electrode is given by

$$\Delta m / \Delta q = -(A_e / K)(df/dq) \quad (1)$$

where A_e is the electrochemically active area (cm^2); K is a fundamental constant for the quartz crystal ($\text{cm}^2 \text{ Hz mg}^{-1}$); and df/dq is the slope of a plot of frequency vs. charge. Values for the proportionality constant, A_e/K , were determined experimentally for each crystal from deposition of Cu as described in the General Introduction.

Bi-PbO₂ films were electrodeposited onto a Au RDE to study the electrocatalytic activity of these films toward anodic oxygen-transfer reactions. By controlling the rotation rate of the RDE, a precise hydrodynamic transport of material is accomplished to the electrode surface. Under these conditions, the Koutecky-Levich equation can be used to determine various reaction parameters. The Koutecky-Levich equation is given in Equation 2:

$$\frac{1}{i} = \frac{1}{0.62nFAD^{2/3}\nu^{-1/6}\omega^{1/2}C^b} + \frac{1}{nFAk_{app}C^b} \quad (2)$$

where n is the number of electrons transferred; A is the electrode area; F is Faraday's constant; D is the diffusion coefficient; ν is the kinematic viscosity; ω is the rotation rate; C^b is the bulk concentration of the analyte; and k_{app} is the apparent rate constant for the electrode reaction. From the slope and intercept of a plot of $1/i$ vs. $1/\omega^{1/2}$ (Koutecky-Levich plot), a number of variables can be obtained including, for our purposes, k_{app} .

RESULTS AND DISCUSSION

Electrodeposition of PbO₂ film electrodes - Figures 1A and B, respectively, show typical *i-E* and *f-E* responses for the oxidation of Pb²⁺ to PbO₂ in 0.1M HClO₄. Formation of surface oxide (AuO) occurs during the positive potential scan at *ca.* 1.0V. A small concomitant decrease in frequency is seen in the *f-E* response corresponding to the contribution of Au oxide to the electrode's mass. The anodic deposition of PbO₂ occurs at *E* > 1.5V. The frequency rapidly decreases in response to the formation of the PbO₂ on the electrode surface. The frequency continues to decrease on the negative potential scan until *ca.* 1.3V. The cathodic current at *E* < 1.2V results from the reduction of the PbO₂ film. Reduction of the electrode oxide films continues as evidenced by a rise in the frequency until both the PbO₂ and Au oxide have been reductively desorbed from the electrode surface at *E* < 1.2 and 0.9V, respectively. The reduction of both oxides is observed in the *i-E* response at *E_p* = 0.90V and 0.70V for PbO₂ and Au oxide, respectively. Note that the original value of the frequency is obtained at the end of the cycle. Subsequent potential scans show identical *i-E* and *f-E* responses.

Figure 2 shows the *f-E* response for a chronoamperometric anodic deposition and cathodic reduction of a PbO₂ film on a Au EQCM electrode. As in the cyclic voltammetric results, all of the PbO₂ deposited was cathodically desorbed from the electrode surface.

Relatively thick films (> 1000 Å) of PbO₂ were deposited at constant potentials. The

Figure 1. Current (A) and frequency (B) vs. potential response for a cyclic potential scan at a Au EQCM electrode for oxidative deposition and reductive desorption of a PbO_2 film onto a Au EQCM electrode from 0.1M HClO_4 . Conditions: 70 mV s^{-1} , 6.0mM $\text{Pb}(\text{NO}_3)_2$.

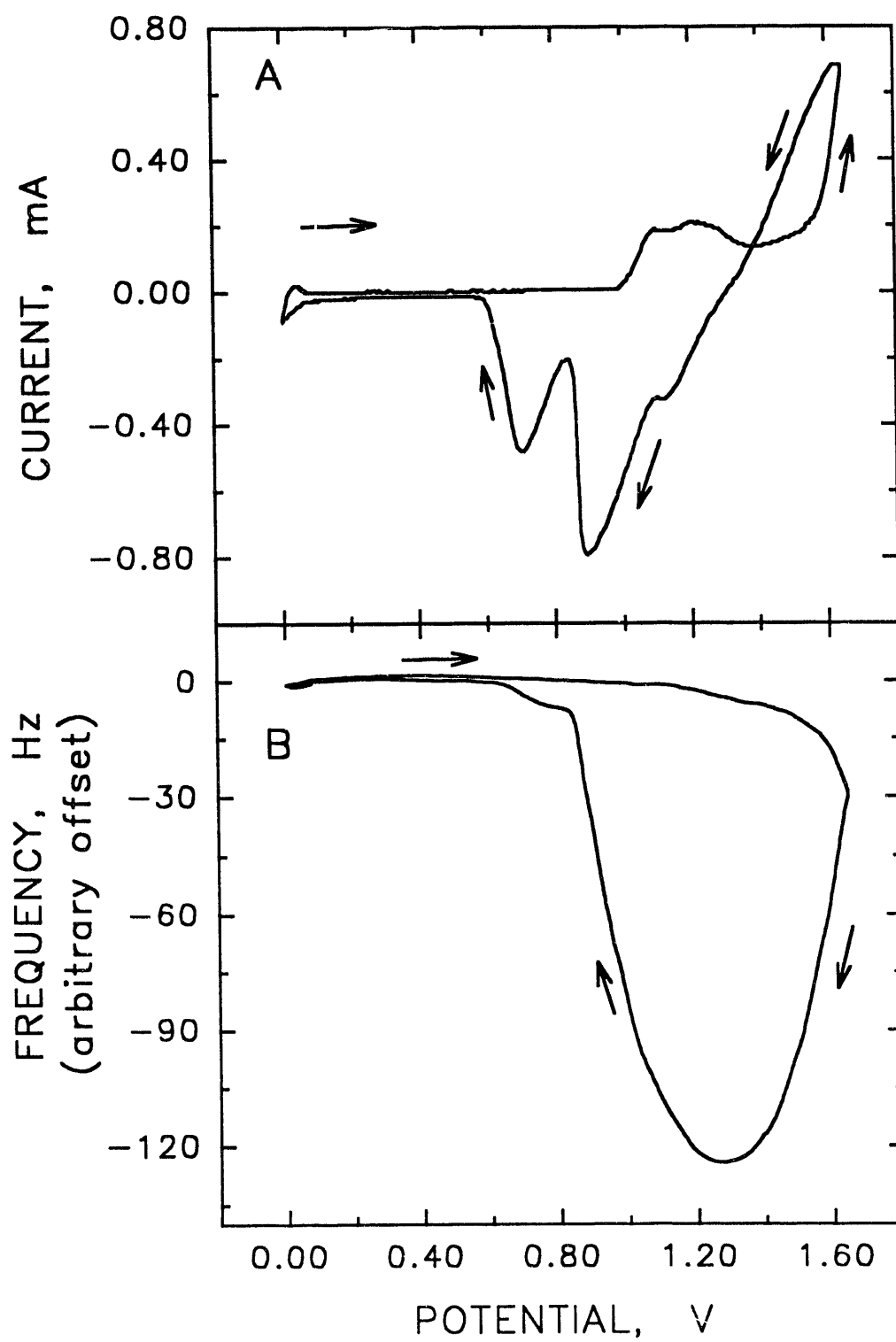
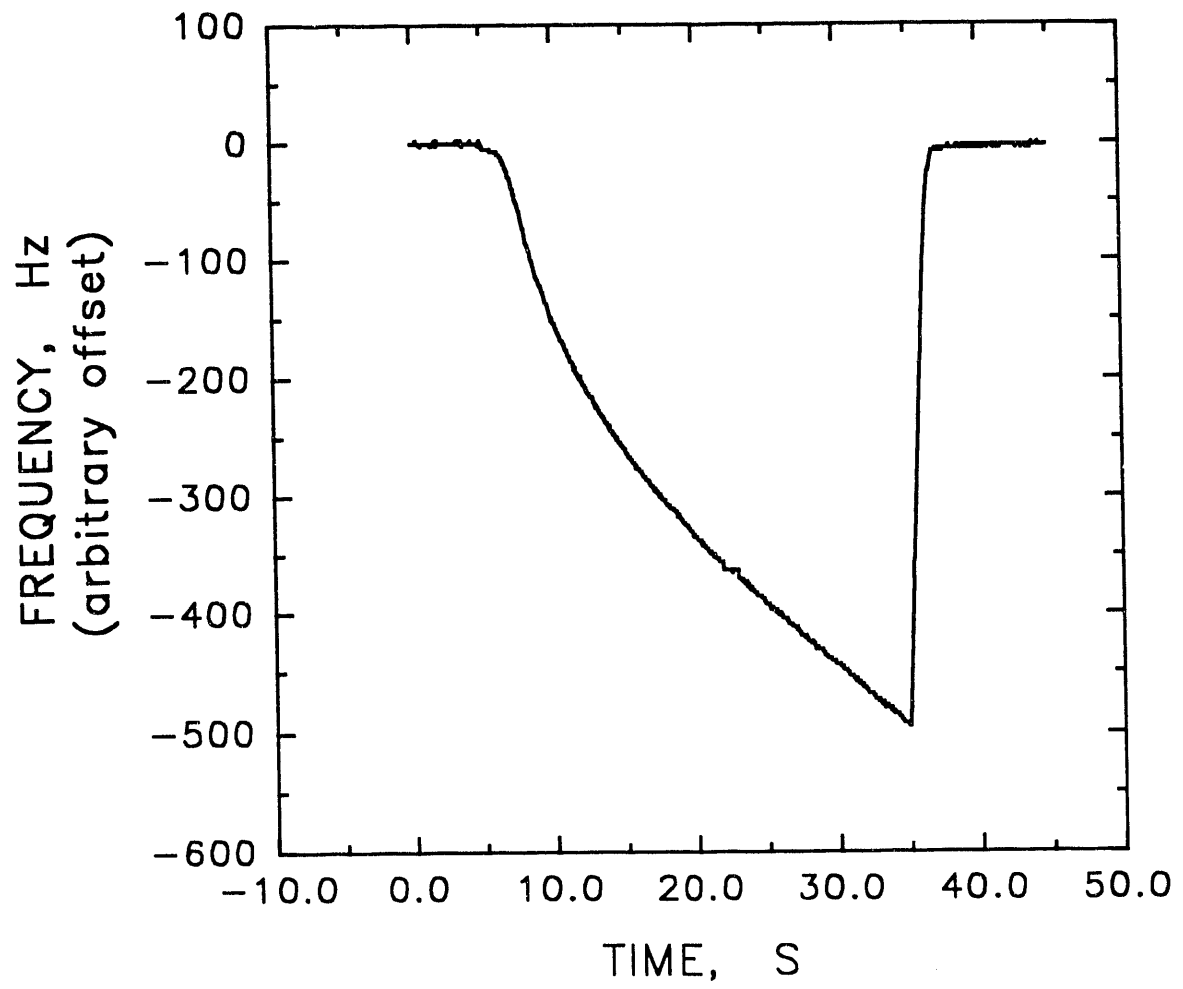


Figure 2. Frequency vs. time response for the electrodeposition and reduction of a PbO₂ film on a Au EQCM electrode. Potential steps: 0.70V to 1.60V (30 sec.), 1.60V to 0.70V (10 sec.). Conditions: 5mM Pb²⁺ in 0.1M HClO₄.



value of $\Delta m/\Delta q$ for the electrodeposition of the PbO_2 was determined from the resulting plots of frequency vs. charge ($f-q$). In these experiments, the potential of the electrode was poised at 1.60V for the oxidation of Pb^{+2} to PbO_2 for 20-30 sec. The oxide was reductively desorbed by stepping the potential to 0.3V. Plots of $f-q$ deviate from linearity. This deviation, or "break", produces two linear segments in the $f-q$ response shown in Figure 3 for deposition of PbO_2 from 0.1M HClO_4 . The values of $\Delta m/\Delta q$ for these two segments were calculated from Equation 1 using $A_e/K = 0.88 \times 10^{-5} \text{ mg Hz}^{-1}$ for the electrode. For $q \leq 2.0 \text{ mCoul}$, the initial value of $\Delta m/\Delta q = 1.44 \pm 0.05 \text{ mg Coul}^{-1}$. For $q \geq 2.0 \text{ mCoul}$, the limiting value of $\Delta m/\Delta q = 1.20 \pm 0.02 \text{ mg Coul}^{-1}$, which is very close to the theoretical value of $1.24 \text{ mg Coul}^{-1}$. In Figure 4, $f-q$ responses are given for the electrodeposition of PbO_2 from 5mM Pb^{+2} in 0.1M HClO_4 and 0.1M HNO_3 , (A) and (B) respectively. Table 1 consists of $\Delta m/\Delta q$ values for pure and various doped PbO_2 films. From Figure 4 and Table 1, it is seen that both $f-q$ responses yield the same $\Delta m/\Delta q$ values for the two linear segments and occur at ca. 240 Hz which corresponds to a total mass change of about $4.2 \mu\text{g cm}^{-2}$. For clarity (B) was offset from (A) by an arbitrary amount.

The reductive desorption of the PbO_2 films was studied using linear sweep voltammetry. The potential of the electrode was stepped to 1.60V to deposit PbO_2 and poised at that potential for 20-30 sec. After deposition, the potential was scanned back to 0.10V, well past the peak potential for film reduction. A residual potential scan, recorded in the absence of Pb^{+2} , was used to background correct the data to avoid inclusion of the charge and mass from the dissolution of Au oxide. In Figure 5, the $f-q$

Table 1. Experimental $\Delta m/\Delta q$ values for electrodeposition of PbO_2 and Bi-PbO_2 films in various media.

Film	$\frac{[\text{Bi}^{+3}]}{[\text{Pb}^{+2}]}$	$\Delta m/\Delta q$ (mg coul ⁻¹) ($\pm = 1\sigma$)			
		0.1 M HClO_4		0.1 M HNO_3	
		initial value	limiting value	initial value	limiting value
PbO_2	0.00	1.44 ± 0.05	1.23 ± 0.02	1.42 ± 0.02	1.22 ± 0.02
Bi-PbO_2	0.10	1.44 ± 0.03	1.44 ± 0.03	1.43 ± 0.04	1.43 ± 0.04
Bi-PbO_2	0.25	1.56 ± 0.03	1.44 ± 0.06	1.54 ± 0.07	1.39 ± 0.06
Bi-PbO_2	0.50	1.69 ± 0.03	1.50 ± 0.05	1.62 ± 0.03	1.43 ± 0.02

Figure 3. Frequency vs. charge response for the electrodeposition of PbO_2 . Conditions: $E_{\text{dep}} = 1.60\text{V}$, $t_{\text{dep}} = 30 \text{ sec.}$, 5.0mM Pb^{+2} in 0.1M HClO_4 .

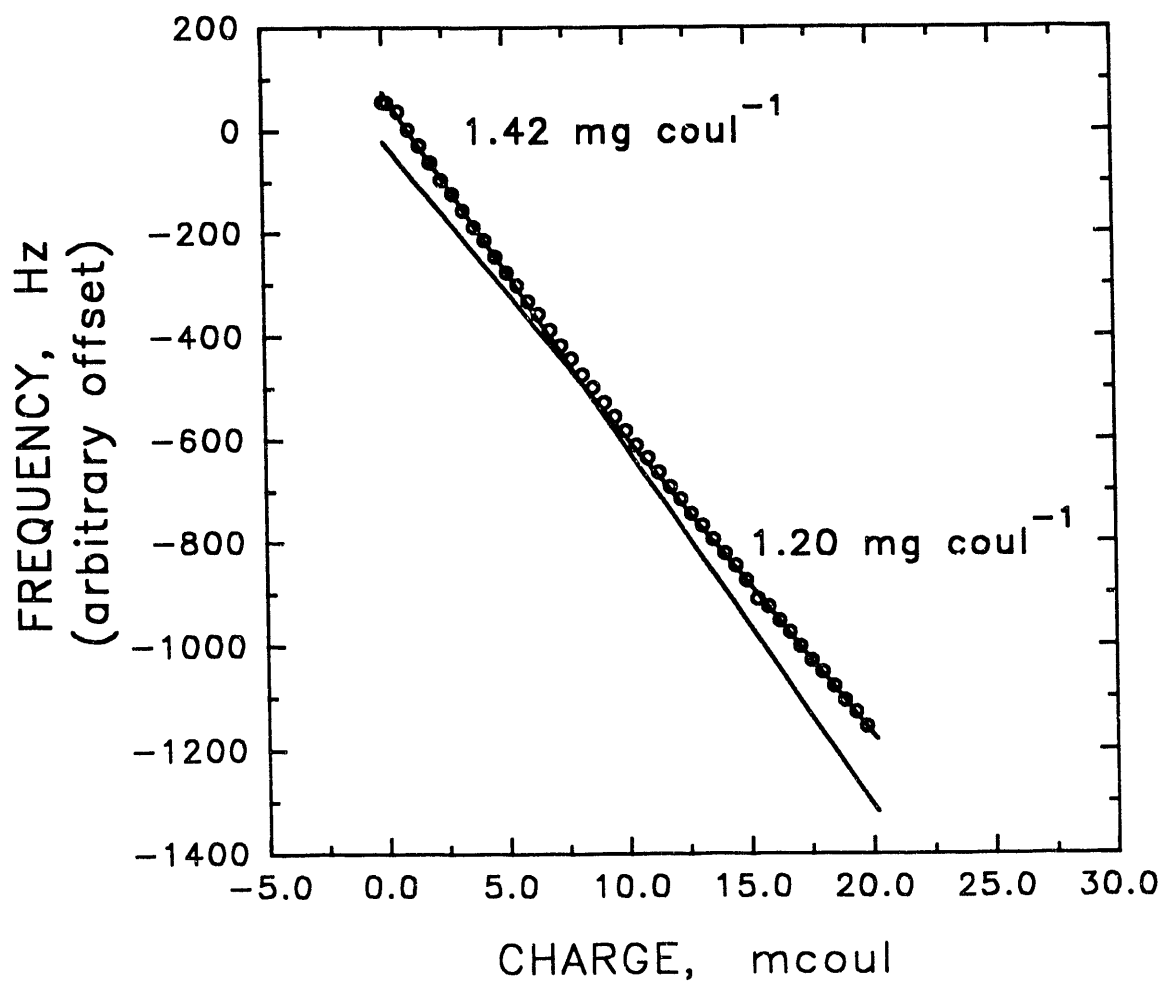


Figure 4. Frequency vs. Charge response for the electrodeposition of PbO_2 from 5mM Pb^{+2} in (A) 0.1M HNO_3 and (B) 0.1M HClO_4 . Conditions: $E_{\text{dep}} = 1.60\text{V}$, $t_{\text{dep}} = 20 \text{ sec}$.

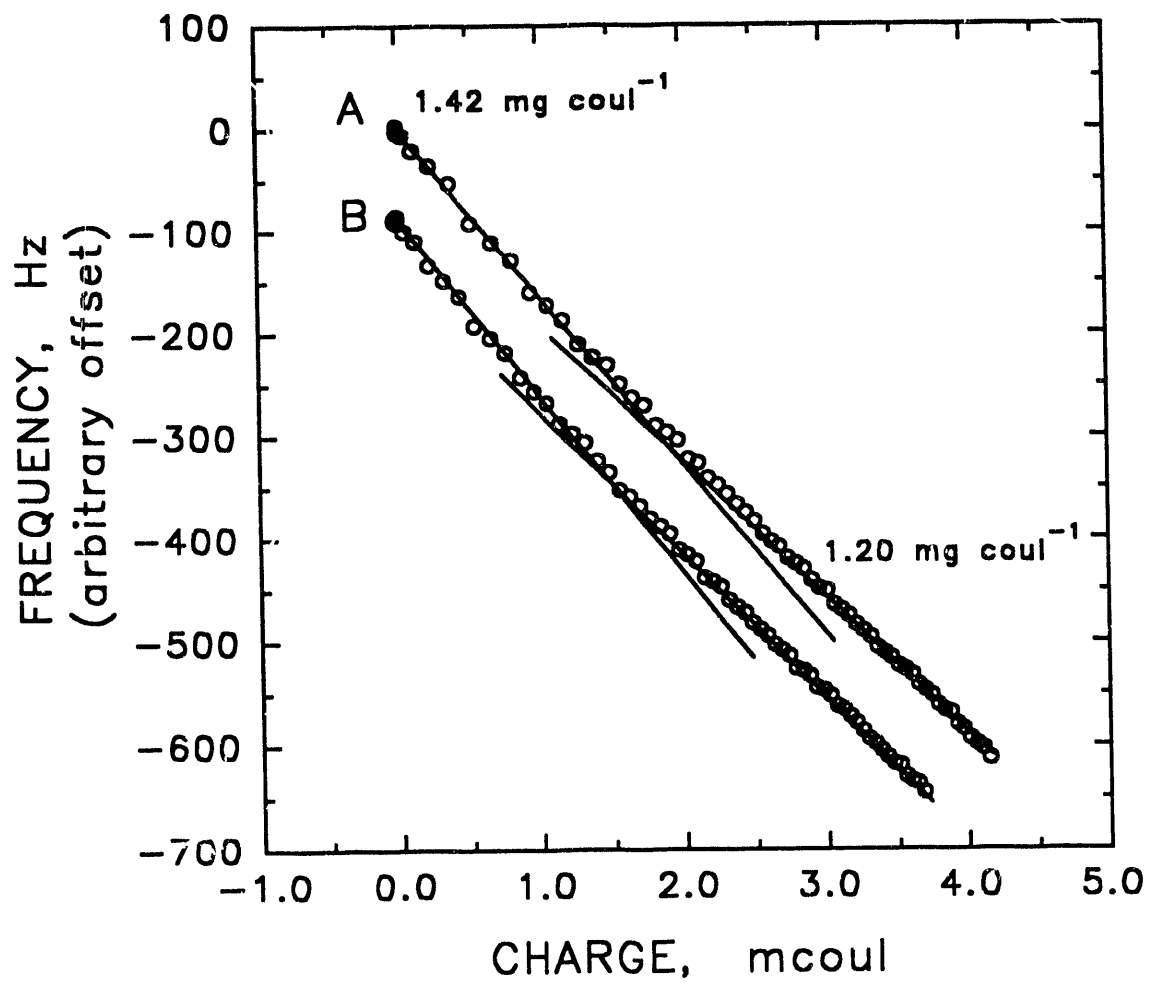
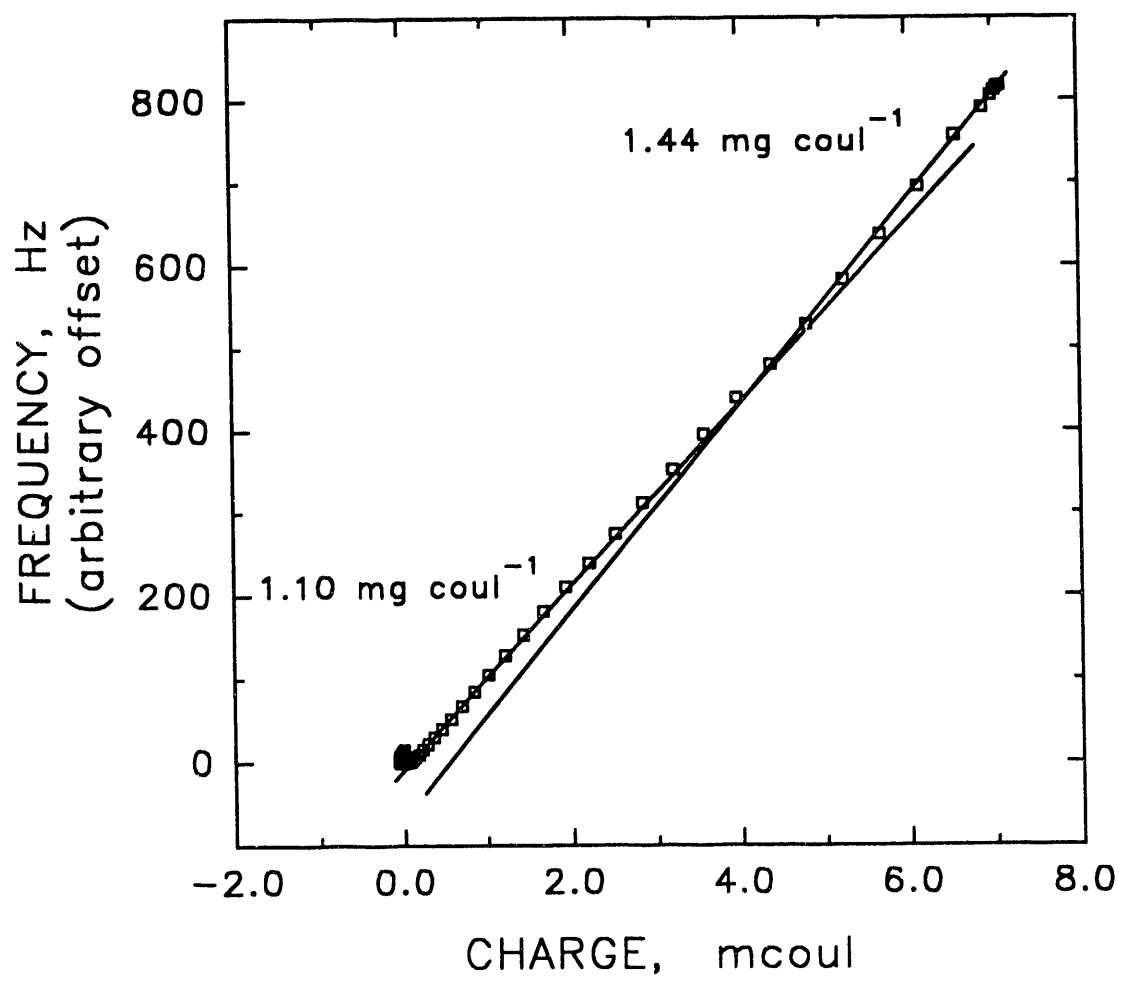


Figure 5. Frequency vs. charge response for the reductive desorption of a PbO_2 film in 0.1M HNO_3 . Conditions: scan rate 100 mV s^{-1} after deposition at 1.6V for 20 sec.



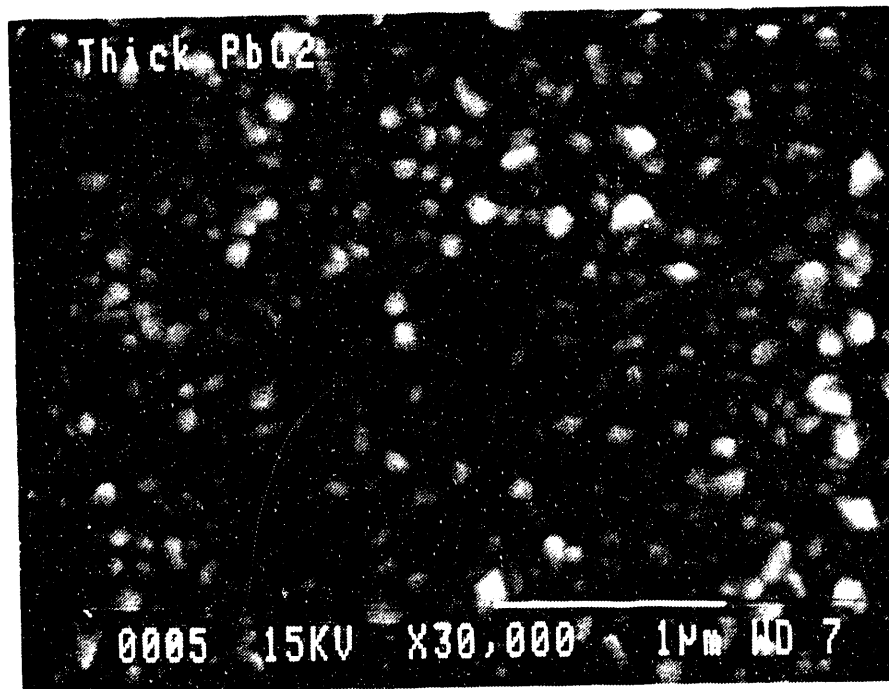
response is given for a voltammetric scan at 100 mV s^{-1} . The f - q response was independent of scan rate from $10 - 200 \text{ mV s}^{-1}$. The two linear segments in the f - q response are similar to those observed for electrodeposition. As the reductive desorption is completed ($q > 5 \text{ mcoul}$), the value of $\Delta m/\Delta q$ is $1.44 \text{ mg coul}^{-1}$. This value agrees very well with the initial value of $\Delta m/\Delta q$ for the deposition process where a relatively thin film exists on the electrode surface. During the reduction of the bulk PbO_2 ($q < 5 \text{ mcoul}$), the value of $\Delta m/\Delta q$ is $1.10 \text{ mg coul}^{-1}$, slightly lower than the theoretical value. The break in the f - q response occurs at *ca.* 520 Hz which when subtracted from the total frequency change corresponds to $4.9 \mu\text{g cm}^{-2}$ remaining on the electrode surface. This corresponds well to the $4.2 \mu\text{g cm}^{-2}$ deposited on the electrode surface at the point of the break in the plot of f - q for the anodic deposition.

Scanning electron micrographs were taken of both thick (*ca.* 1000\AA) and thin ($< 200\text{\AA}$) films of the PbO_2 electrodeposited on Au and are shown in Figures 6A and B, respectively. At a magnification of $30,000\times$, well developed crystallites of PbO_2 are seen for the thick film. The thin film was deposited to a thickness slightly greater than that indicated by the transition (break) region of the f - q response. Under the same magnification, this surface has a uniform distribution of very small crystallites covering the electrode surface.

Thin-film x-ray diffractometry (XRD) was used study these films further. In Figure 7A, the XRD spectrum is shown for a PbO_2 film electrodeposited for 5 min at 1.60V . All the peaks are assigned to either Au, β - PbO_2 , or the quartz substrate. The XRD spectrum is shown in Figure 7B for a PbO_2 film deposited for only a short time (< 15

Figure 6. Scanning electron micrographs of a (A) thick (ca. 1000Å) and (B) thin(<200Å) film of PbO₂. Conditions: E_{dep} = 1.60V; t_{dep} = 5 min (A) and 15 sec. (B); 5.0mM Pb⁺² in 0.1M HClO₄.

A



B

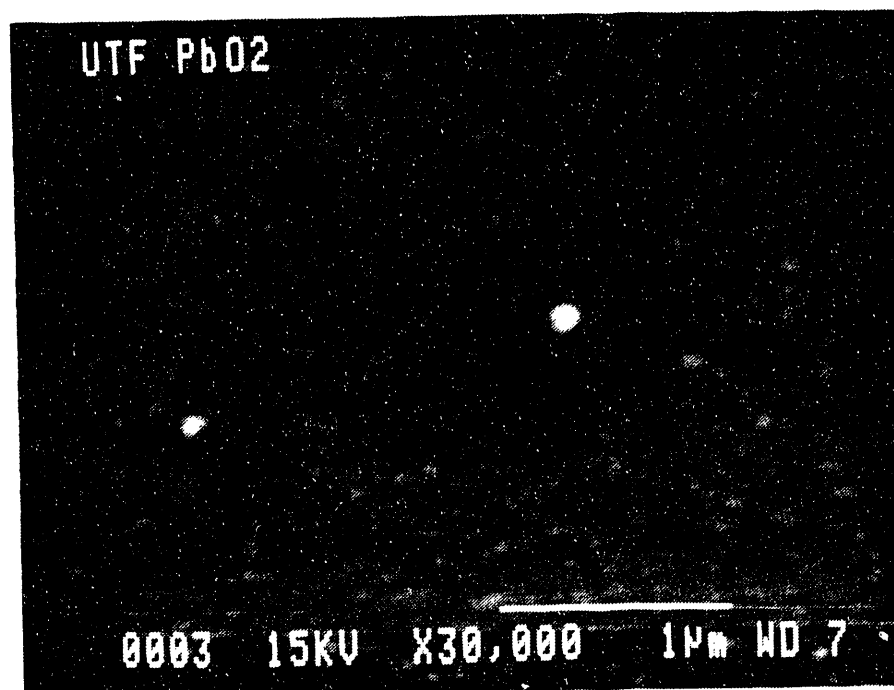
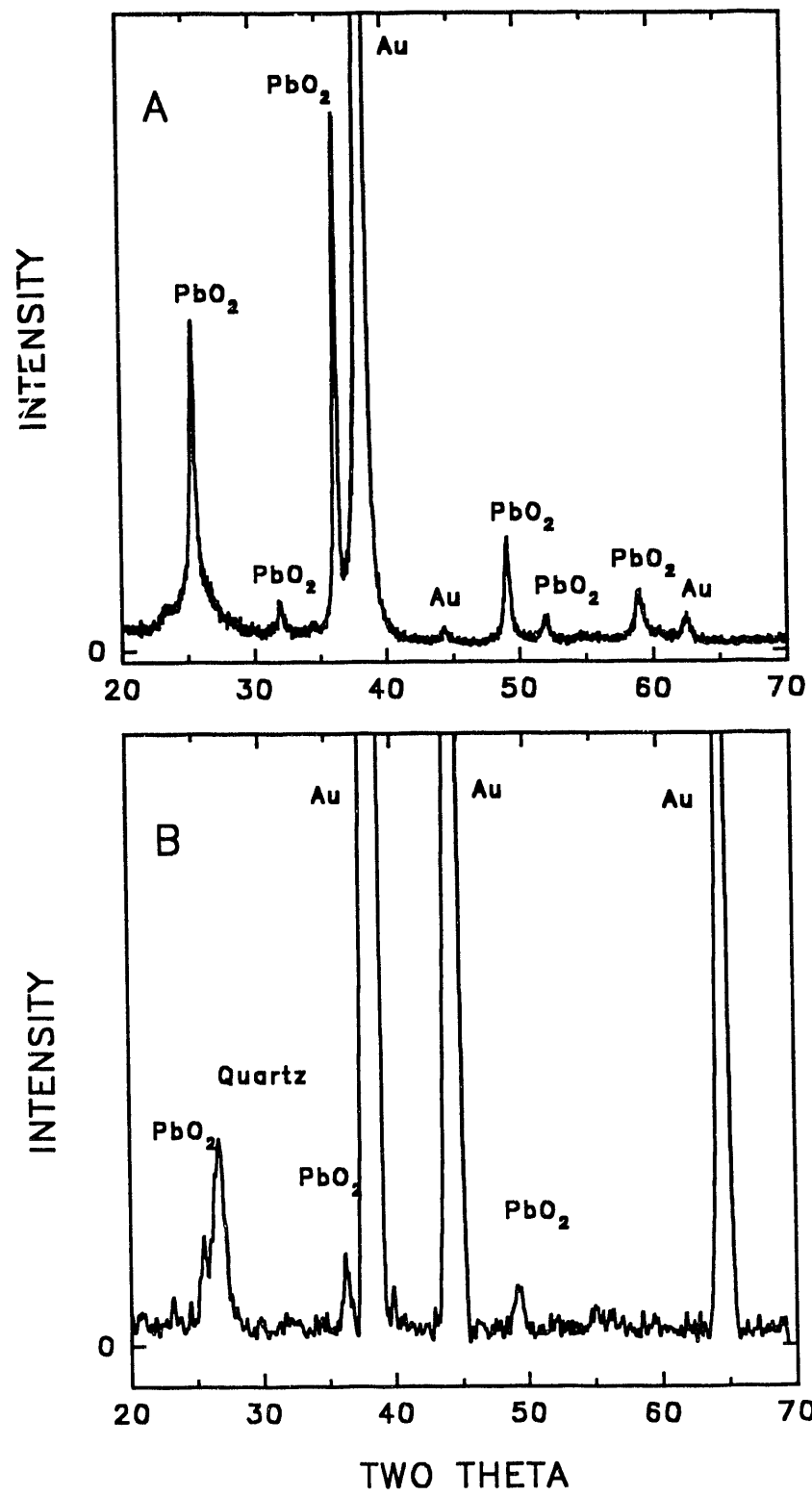


Figure 7. XRD spectra for (A) thick and (B) thin PbO₂ films. Conditions:

$E_{\text{dep}} = 1.60\text{V}$, $t_{\text{dep}} = 5 \text{ min. (A), 15 sec. (B)}$. 5mM Pb^{+2} in

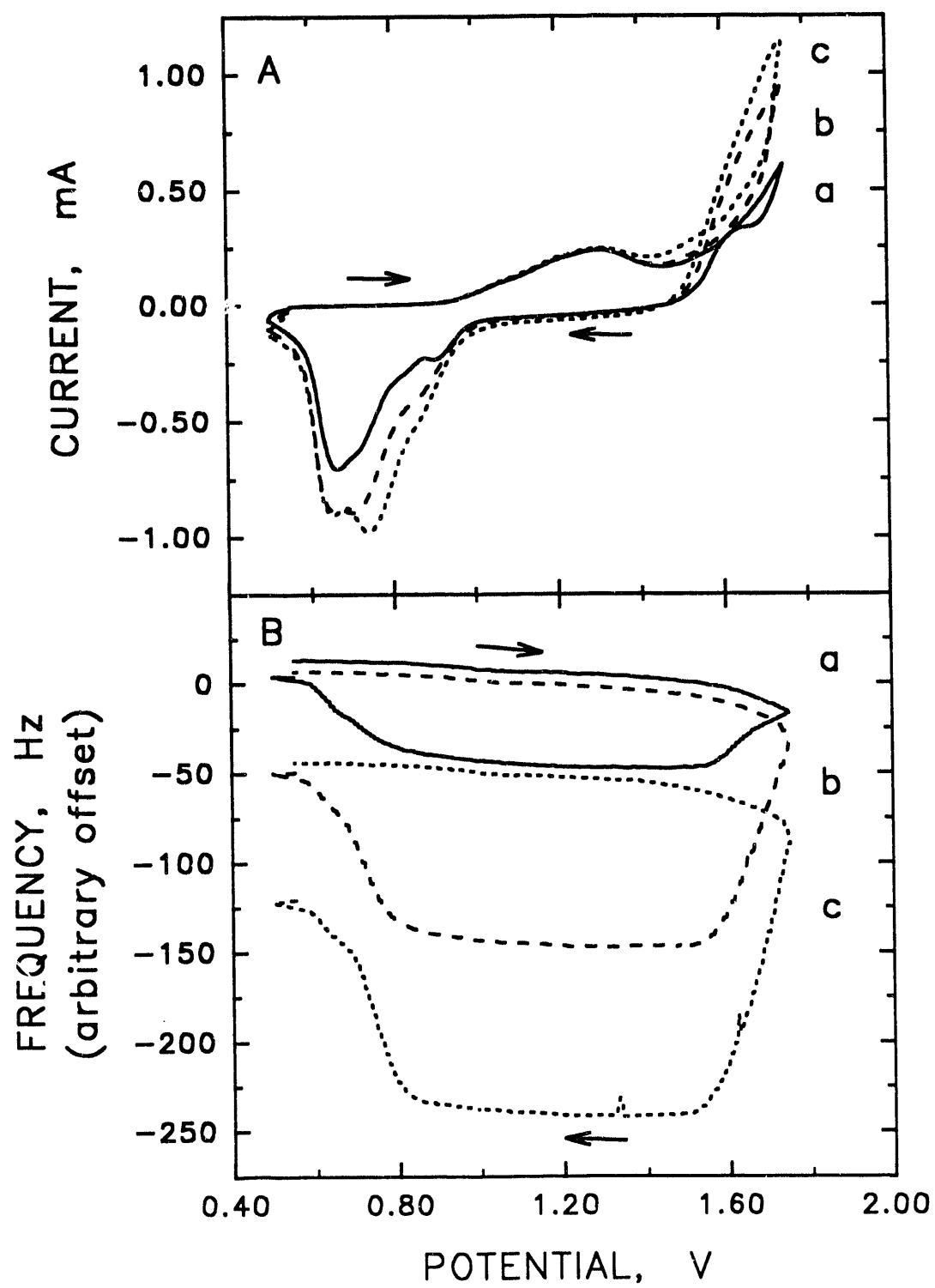
0.1M HClO_4 . Two theta = $10\text{-}70^\circ$, Cu K α radiation.



sec. at 1.60V). As with the thicker film, the only peaks in the spectrum corresponded to Au, α -PbO₂ and quartz. Because the film was only *ca.* 200Å thick, the spectrum was collected over a period of 7 hrs by stepping 0.03° and collecting diffracted x-rays for 15 sec. at each step. The spectrum was background corrected also to help distinguish the film's diffraction pattern.

Electrodeposition of Bi-PbO₂ film electrodes - The *i-E* and *f-E* responses are given in Figures 8A and B, respectively, for a series of sequential cyclic voltammograms showing the electrodeposition of Bi-PbO₂ films on a Au EQCM electrode from a 0.1M HClO₄ solution with [Bi⁺³]/[Pb⁺²] = 0.1. From Figure 8A, the formation of Au oxide occurs at *ca.* 1.0V during the positive potential scan of the first cycle (a). The anodic deposition of the PbO₂ film occurs at $E > 1.7V$ as evidenced by the increase in current. Previous work has shown that this film is doped with Bi [11]. During the negative potential scan, the hysteresis in the current from the positive scan indicates the continued deposition of Bi-PbO₂. At $E < 1.4V$, the current decays indicating no further film formation. The cathodic current, E_p *ca.* 0.9V, results from the reduction of the Au oxide to Au. The large cathodic current, E_p *ca.* 0.65V, results from reduction of doped-PbO₂. The current decreases to zero, following the reduction of both oxide films. During the second (b) and third (c) consecutive scans, the onset of film deposition shifts slightly to more negative potentials and increases in magnitude with each cycle. The Bi-PbO₂ cathodic desorption current increases in magnitude indicating that a thicker film is deposited on each successive cycle. Also, the reduction of the film commences at increasingly more

Figure 8. Current (A) and frequency (B) vs. potential responses for successive cyclic potential scans at a Au EQCM electrode for the oxidative deposition and partial reductive desorption of a Bi-PbO₂ film. Scan number: (a) 1, (b) 2, and (c) 3. Conditions: 70 mV s⁻¹, 8mM Pb⁺² and 0.8mM Bi⁺³ in 0.1M HClO₄.

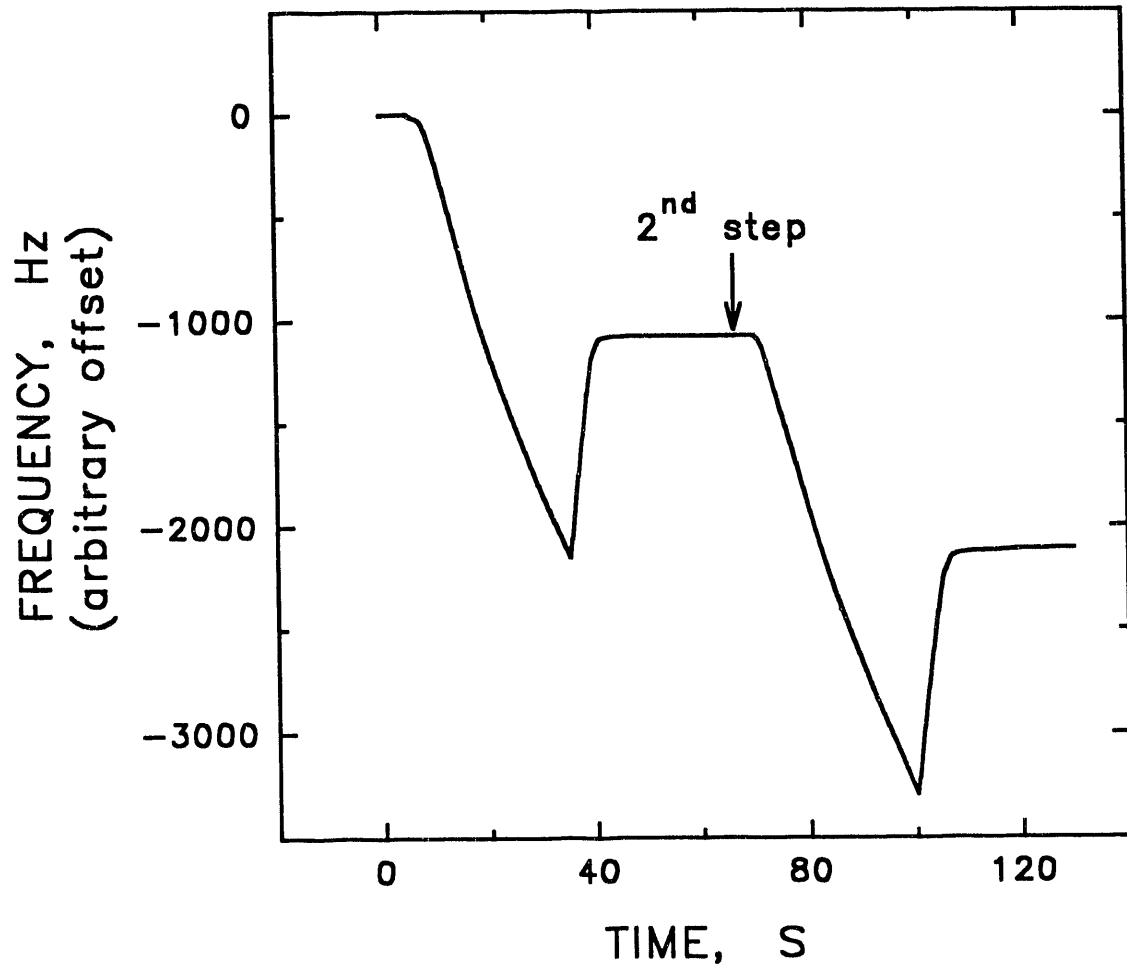


positive potentials as a new convoluted cathodic reduction current, $E_p = 0.75V$, becomes more apparent with cycle number. It is interesting to note that with the addition of Bi^{+3} , the order for cathodic dissolution of the Au oxide and $Bi-PbO_2$ is reversed from the order observed in the dissolution of PbO_2 (Figure 1A).

The f - E response for the first cycle is shown in curve a of Figure 8B. On the positive scan, the frequency slightly decreases at $E > 1.0V$ from the formation of the Au oxide. There is no change until ca. 1.70V where the frequency again decreases evidencing the deposition of the $Bi-PbO_2$. The frequency decrease continues on the negative scan until $E < 1.50V$. The frequency remains constant until $E < 0.8V$ when the Au oxide and PbO_2 films are reductively desorbed from the electrode surface. Unlike the PbO_2 films, the frequency changes for the cathodic dissolution of the Au oxide and $Bi-PbO_2$ are convoluted. A striking feature is that the value of the frequency at the end of the cycle is less than at the beginning. With subsequent cycles (b) and (c), the frequency difference between the beginning and ending of a particular cycle increases from the previous cycle. In addition, the total difference between the beginning value of the frequency of the first cycle and the ending frequency value for each cycle becomes increasingly larger indicating that a successively thicker film is deposited onto the electrode surface.

The f - t response from potential step experiments verify the formation of a film remaining on the electrode surface and give an indication of its stability. In Figure 9, the f - t response is shown for two sequential potential steps depositing a $Bi-PbO_2$ film from a $[Bi^{+3}]/[Pb^{+2}] = 0.1$ solution. A frequency decrease of ca. 2000 Hz is observed upon

Figure 9. Frequency vs. time responses for successive chronoamperometric experiments for the electrodeposition of a Bi-PbO₂ film at a Au EQCM electrode. Conditions: E_{dep} = 1.65V, 8.0mM Pb⁺² and 0.8mM Bi⁺³ in 0.1M HClO₄.

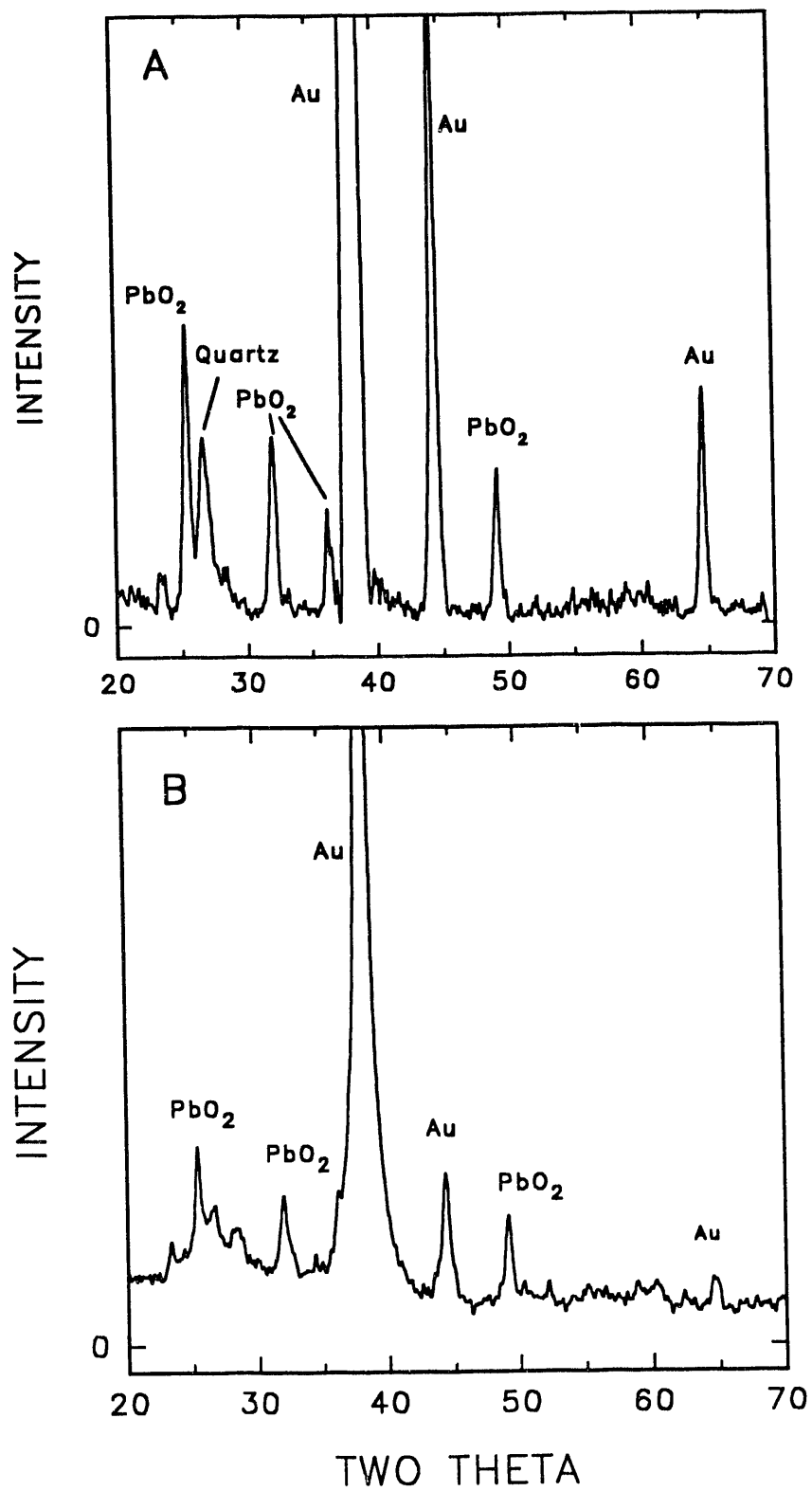


making the first potential step. When the value of the potential is returned to 0.5V at 35 sec., the frequency increases ca. 1000 Hz. However, it does not return to its starting value, indicating that a portion of the film was not reductively desorbed from the electrode surface. During the time preceding the second potential step (ca. 30 sec.), there is no further film dissolution. Upon making a second potential step, the $f-t$ response indicates an additional frequency decrease of ca. 2000 Hz, and upon returning the potential value to 0.5V, the frequency rapidly increases but does not return to its starting value. Subsequent potential steps produce an increasingly thicker film on the electrode surface.

A XRD spectrum obtained for thin films of Bi-PbO₂ deposited from continuous cyclic voltammetric experiments is shown in Figure 10A. XRD spectra taken of these films are virtually identical to that for PbO₂ (Figure 6), showing peaks corresponding to PbO₂, Au and the quartz substrate.

Chronoamperometry was used also to deposit the Bi-PbO₂ films from solutions with $[\text{Bi}^{+3}]/[\text{Pb}^{+2}] = 0.1, 0.25$ and 0.5 . Thicker films ($> 1000 \text{ \AA}$) were produced using this approach over cyclic voltammetry. Typically, the potential was stepped from ca. 1.2V to 1.65V to deposit the Bi-doped films. This procedure was performed several times in pure electrolyte to establish the Au oxide onto which all of these films were deposited. XRD spectra obtained for films prepared in this manner were identical to those prepared from cyclic voltammetric experiments except for being more intense (Figure 10B). XPS data indicate that the $[\text{Bi}^{+3}]/[\text{Pb}^{+2}]$ in the films was identical to that in the deposition solutions.

Figure 10. X-ray diffraction spectrum for a (A) thin Bi-PbO₂ film electrodeposited via cyclic voltammetry and (B) thick Bi-PbO₂ electrodeposited via constant potential on a Au EQCM electrode. Conditions: 8.0mM Pb⁺² and 0.8mM Bi⁺³ in 0.1M HClO₄, , Two Theta range = 10 - 70°, Cu Kα radiation, step size = 0.03°. The signal was integrated for 15 sec. at each step.

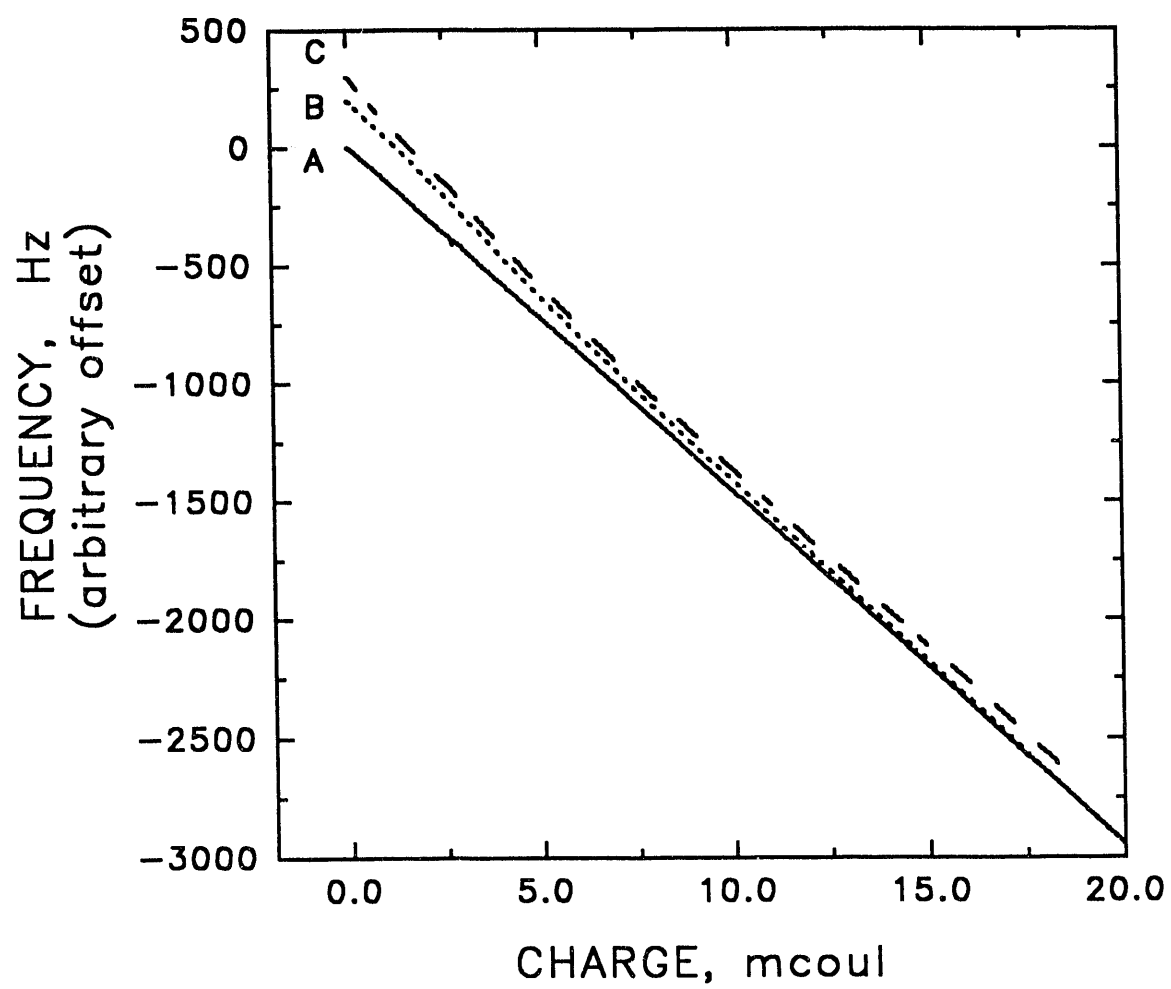


The f - q response obtained from a chronoamperometric experiment is given in Figure 11A for a film deposited from a solution of $[\text{Bi}^{+3}]/[\text{Pb}^{+2}] = 0.1$ in 0.1M HClO_4 . There are two distinguishing differences between the f - q response for the deposition of these Bi- PbO_2 films and PbO_2 films. First, the value of $\Delta m/\Delta q$ is substantially higher than that determined for PbO_2 . From Table 1, the value of $\Delta m/\Delta q = 1.44 \pm 0.03 \text{ mg coul}^{-1}$ for deposition from 0.1M HClO_4 . The experiments were repeated using 0.1M HNO_3 as supporting electrolyte. The value of $\Delta m/\Delta q = 1.43 \pm 0.04 \text{ mg coul}^{-1}$ in this electrolyte. The value of $\Delta m/\Delta q$ is the same upon performing a second potential step, creating a thicker film on top of the original film. Second, there is no break. Throughout the entire deposition process, only a single $\Delta m/\Delta q$ value is obtained.

Films were deposited from solutions with $[\text{Bi}^{+3}]/[\text{Pb}^{+2}] = 0.25$. Figure 11B shows a f - q response for a Bi- PbO_2 film deposited from such a solution. A break, similar to that for the deposition of PbO_2 , appears in the f - q responses for deposition of Bi- PbO_2 . From Table 1, the limiting values of $\Delta m/\Delta q = 1.44 \pm 0.06$ and 1.39 ± 0.06 for deposition of the bulk film from 0.1M HClO_4 and 0.1M HNO_3 solutions, respectively. These limiting values are very similar to those obtained for the $[\text{Bi}^{+3}]/[\text{Pb}^{+2}] = 0.1$ films.

Lastly, films were deposited from solutions with $[\text{Bi}^{+3}]/[\text{Pb}^{+2}] = 0.5$. The f - q response is seen in Figure 11C. As with the $[\text{Bi}^{+3}]/[\text{Pb}^{+2}] = 0.25$ films, a break appears in the f - q response. The limiting values of $\Delta m/\Delta q = 1.50 \pm 0.05$ and 1.43 ± 0.02 for deposition from 0.1M HClO_4 and HNO_3 solutions (Table 1). In Figures 11B and C, little difference is observed between the f - q response for solution with,

Figure 11. Frequency vs. charge responses for electrodeposition of Bi-PbO₂ films at constant potential on a Au EQCM electrode. Conditions: E_{dep} = 1.65V, 0.1M HClO₄. Concentration of Pb²⁺ = 8mM. [Bi³⁺]/[Pb²⁺] = (A) 0.1, (B) 0.25, and (C) 0.5



$[\text{Bi}^{+3}]/[\text{Pb}^{+2}] = 0.5$ and 0.25 . The f - q responses in Figure 11 indicate that the limiting values of $\Delta m/\Delta q$ for films deposited from the three different solutions are very similar.

Koutecky-Levich data for oxidation of DMSO at Bi-PbO₂ film electrodes - Bi-PbO₂

films were electrodeposited onto a Au rotated disk electrode (RDE) from the various solutions of $[\text{Bi}^{+3}]/[\text{Pb}^{+2}] = 0.1, 0.25$ and 0.5 . The films were deposited from quiescent solutions to mimic the EQCM conditions as closely as possible. Their activities were examined toward the oxidation of DMSO which is an example of the simplest anodic oxygen-transfer reactions as described in the General Introduction. Figure 12 shows typical i - E responses for the oxidation of DMSO for a film electrode prepared from a solution of $[\text{Bi}^{+3}]/[\text{Pb}^{+2}] = 0.5$. The rotation rate dependence of the anodic current indicates a degree of transport-limited oxidation of DMSO, i.e., oxidation limited by the flux of the reactant to the electrode surface. The small intercept of the Koutecky-Levich plot (insert Figure 12) evidences the very fast oxidation kinetics (Equation 2). Figure 13 contains typical i - E responses for the various electrodes at $\omega = 3600$ rpm. The $E_{1/2}$ s shift negatively upon increasing the ratio of Bi in the deposition solution. The value of k_{app} for each electrode indicates that the rate of the oxidation also increases with the ratio of Bi in the depositing solution:

$$[\text{Bi}^{+3}]/[\text{Pb}^{+2}] = 0.1, \quad k_{\text{app}} = 0.009 \text{ cm s}^{-1}$$

$$[\text{Bi}^{+3}]/[\text{Pb}^{+2}] = 0.25, \quad k_{\text{app}} = 0.037 \text{ cm s}^{-1}$$

$$[\text{Bi}^{+3}]/[\text{Pb}^{+2}] = 0.5, \quad k_{\text{app}} = 0.113 \text{ cm s}^{-1}$$

Figure 12. Current vs. potential response for the oxidation of 5mM DMSO at Bi-PbO₂ film electrodeposited onto a Au rotated disk electrode from quiescent solutions. Conditions: $E_{\text{dep}} = 1.65\text{V}$, $[\text{Bi}^{+3}]/[\text{Pb}^{+2}] = 0.5$ in 0.1M HClO₄. (a) residual in 1.0M HClO₄, $\omega = 500$ RPM (b) same as (a) with 5mM DMSO, $\omega = 100$ RPM, (c) 200 RPM, (d) 500 RPM, (e) 700 RPM, (f) 1200 RPM, (g) 2500 RPM, and (h) 3600 rpm. The insert is the Koutecky-Levich plot of $1/i$ vs. $1/\omega^{1/2}$ from the i-E response measured at 1.80V. Scan rate = 30 mV S⁻¹.

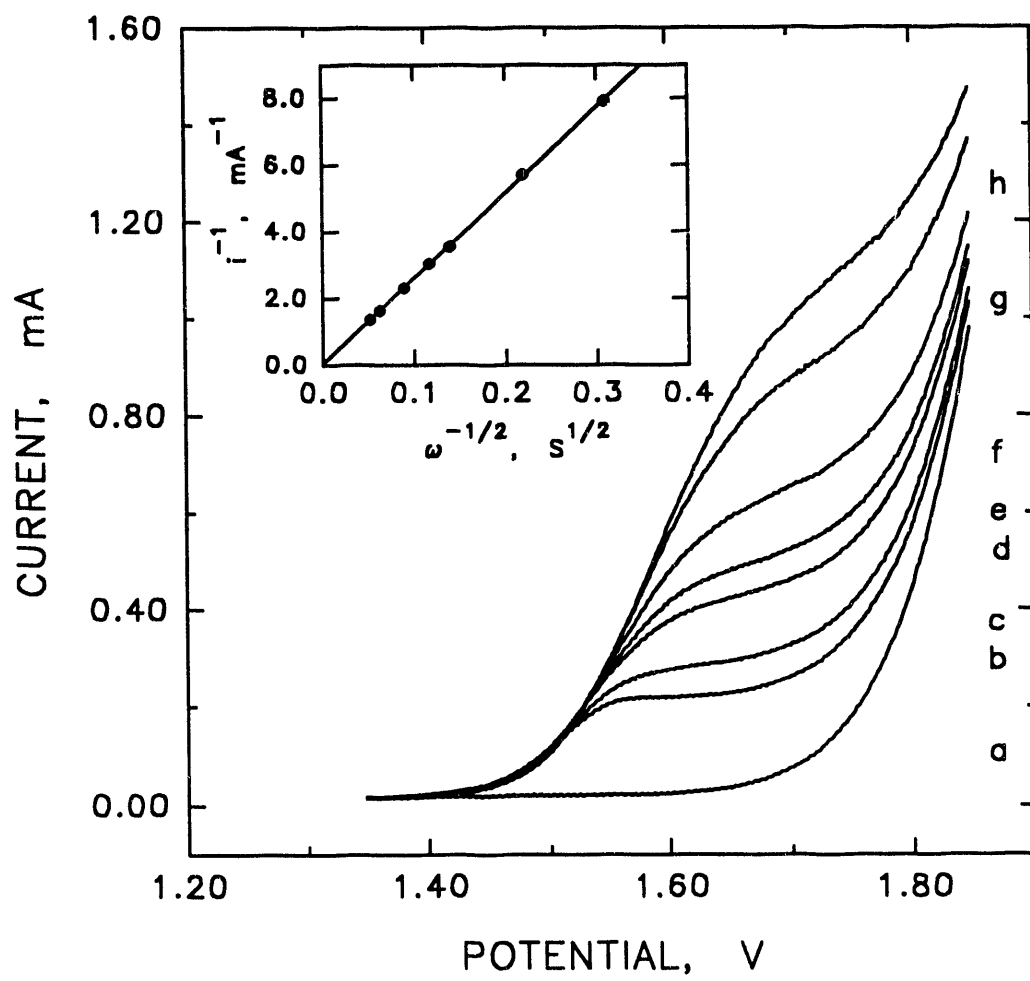
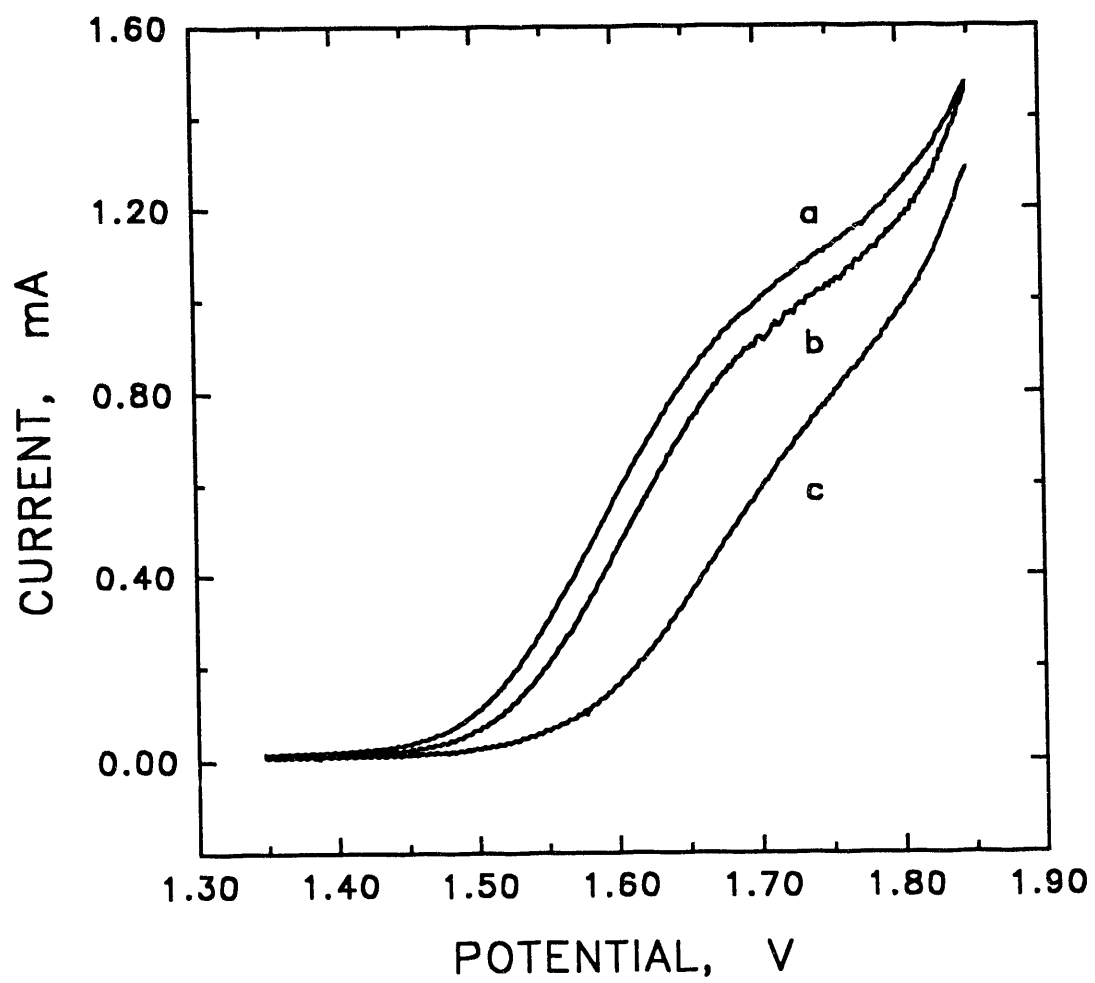


Figure 13. Current vs. potential response for the oxidation of 5mM DMSO at Bi-PbO₂ film electrodes deposited from solutions of [Bi⁺³]/[Pb⁺²] = (a) 0.5, (b) 0.25 and (c) 0.1. Conditions: 1.0M HClO₄, 30 mV S⁻¹, ω = 3600 RPM.



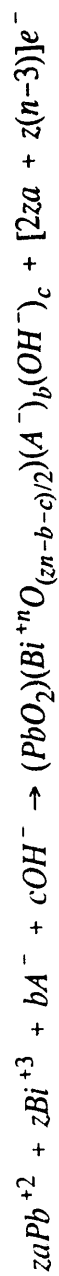
CONCLUSIONS

Based on the XPS results that ratio of Bi:Pb in the films was the same as in the deposition solutions, Tables 2, 3 and 4 were constructed which contain the values of $\Delta m/\Delta q$ of possible Bi species electrodeposited into the film from solution of various $[\text{Bi}^{+3}]/[\text{Pb}^{+2}]$ in 0.1M HNO_3 and HClO_4 solutions. The $\Delta m/\Delta q$ values are grouped into Tables 2, 3, and 4 according to Bi species in the +3, +4 and +5 oxidation state, respectively.

For $[\text{Bi}^{+3}]/[\text{Pb}^{+2}] = 0.1$, Bi comprises such a small portion of the film that changes in its speciation produce a relatively small spread in the calculated values of $\Delta m/\Delta q$. Bi species representing all three oxidation states (Table 2 D-F; Table 3 D-F; and Table 4 L-M) correspond well (within two standard deviations, 2σ) to the experimentally observed values for both NO_3^- and ClO_4^- .

With $[\text{Bi}^{+3}]/[\text{Pb}^{+2}] = 0.25$, the Bi species constitutes a larger portion of the film and produces a larger difference in the values of $\Delta m/\Delta q$ as the speciation of the Bi is varied. The corresponding $\Delta m/\Delta q$ values in Tables 2, 3 and 4 indicate that the Bi^{+3} species have $\Delta m/\Delta q$ values that are much larger than that experimentally observed. The possible Bi species with the closest values of $\Delta m/\Delta q$ are those in which the Bi is in the +4 or +5 oxidation state (Table 3 A, B, C, and Table 4 D, F-J). The largest spread in calculated $\Delta m/\Delta q$ is obtained with $[\text{Bi}^{+3}]/[\text{Pb}^{+2}] = 0.5$. The values of $\Delta m/\Delta q$ in Table 2, 3 and 4 closest to those experimentally observed fall exclusively within the possibilities in which Bi is in the +5 oxidation state (Tab. 4 G-H). Once the ratio of Bi:Pb is this large, there

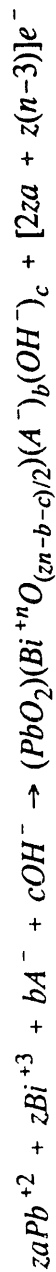
Table 2. Values of $\Delta m/\Delta q$ calculated from the indicated equation for possible Bi^{+3} species incorporated into the Bi-PbO₂ films.



(shaded areas contain values $> 2\sigma$ of the experimental values)

Film Composition	z	b	c	n	$\Delta m/\Delta q$ A = NO ₃ ⁻ z/a = 0.1	$\Delta m/\Delta q$ A = ClO ₄ ⁻ z/a = 0.1	$\Delta m/\Delta q$ A = NO ₃ ⁻ z/a = 0.25	$\Delta m/\Delta q$ A = ClO ₄ ⁻ z/a = 0.25	$\Delta m/\Delta q$ A = NO ₃ ⁻ z/a = 0.5	$\Delta m/\Delta q$ A = ClO ₄ ⁻ z/a = 0.5
I. A. (PbO ₂) _{za} (BiO)(OH ⁻)	1	0	1	3	1.36	1.36	1.55	1.55	1.87	1.87
B. (PbO ₂) _{za} (Bi ₂ O ₃)	2	0	0	3	1.36	1.36	1.54	1.54	1.84	1.84
C. (PbO ₂) _{za} (Bi ₂ (OH ⁻) ₃)	1	0	3	3	1.37	1.37	1.58	1.58	1.91	1.91
D. (PbO ₂) _{za} (BiO)(A ⁻)	1	1	0	3	1.39	1.41	1.61	1.66	1.98	2.08
E. (PbO ₂) _{za} (Bi ₂ (A ⁻)(OH ⁻) ₂)	1	1	2	3	1.40	1.42	1.63	1.68	2.03	2.13
F. (PbO ₂) _{za} (Bi ₂ (A ⁻) ₂ (OH ⁻))	1	2	1	3	1.42	1.46	1.69	1.79	2.15	2.34
G. (PbO ₂) _{za} (Bi ₂ (A ⁻) ₃)	1	3	0	3	1.44	1.50	1.75	1.89	2.26	2.55

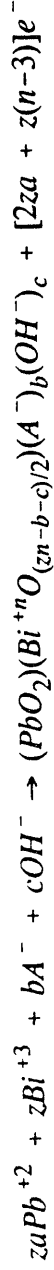
Table 3. Values of $\Delta m/\Delta q$ calculated from the indicated equation for possible Bi^{+4} species incorporated into the Bi-PbO₂ films.



(shaded areas contain values $> 2\sigma$ of the experimental values)

Film Composition	z	b	c	n	$\Delta m/\Delta q$ A = NO ₃ ⁻ z/a = 0.1	$\Delta m/\Delta q$ A = ClO ₄ ⁻ z/a = 0.1	$\Delta m/\Delta q$ A = NO ₃ ⁻ z/a = 0.25	$\Delta m/\Delta q$ A = ClO ₄ ⁻ z/a = 0.25	$\Delta m/\Delta q$ A = NO ₃ ⁻ z/a = 0.5	$\Delta m/\Delta q$ A = ClO ₄ ⁻ z/a = 0.5
II. A. (PbO ₂) _{za} (Bi _z O ₂)	1	0	0	4	1.30	1.30	1.38	1.38	1.49	1.49
B. (PbO ₂) _{za} (Bi _z (OH) ⁻) ₄	1	0	4	4	1.32	1.32	1.42	1.42	1.56	1.56
C. (PbO ₂) _{za} (Bi _z (A ⁻)(OH) ₃)	1	1	3	4	1.34	1.36	1.47	1.51	1.56	1.73
D. (PbO ₂) _{za} (Bi _z (A ⁻) ₂ (OH) ₂)	1	2	2	4	1.36	1.40	1.52	1.61	1.75	1.90
E. (PbO ₂) _{za} (Bi _z (A ⁻) ₃ (OH))	1	3	1	4	1.38	1.44	1.58	1.70	1.84	2.07
F. (PbO ₂) _{za} (Bi _z (A ⁻) ₄)	1	4	0	4	1.41	1.48	1.63	1.80	1.94	2.24

Table 4. Values of $\Delta m/\Delta q$ calculated from the indicated equation for possible Bi^{+5} species incorporated into the Bi-PbO₂ films.



(shaded areas contain values $> 2\sigma$ of the experimental values)

Film Composition	z	b	c	n	$\Delta m/\Delta q$ A = NO ₃ ⁻ z/a = 0.1	$\Delta m/\Delta q$ A = ClO ₄ ⁻ z/a = 0.1	$\Delta m/\Delta q$ A = NO ₃ ⁻ z/a = 0.25	$\Delta m/\Delta q$ A = ClO ₄ ⁻ z/a = 0.25	$\Delta m/\Delta q$ A = NO ₃ ⁻ z/a = 0.5	$\Delta m/\Delta q$ A = ClO ₄ ⁻ z/a = 0.5
III. A. (PbO ₂) _{za} (Bi _z O ₅)	2	0	0	5	1.24	1.24	1.25	1.25	1.26	1.26
B. (PbO ₂) _{za} (Bi _z O)(OH ⁻) ₃	1	0	3	5	1.26	1.26	1.28	1.28	1.30	1.30
C. (PbO ₂) _{za} (Bi _z) ₅ (OH ⁻) ₅	1	0	5	5	1.26	1.26	1.30	1.30	1.33	1.33
D. (PbO ₂) _{za} (Bi _z O ₂)(A ⁻)	1	1	0	5	1.27	1.29	1.30	1.34	1.35	1.41
E. (PbO ₂) _{za} (Bi _z O ₂)(OH ⁻)	1	0	1	5	1.27	1.27	1.27	1.27	1.27	1.27
F. (PbO ₂) _{za} (Bi _z O)(A ⁻)(OH ⁻) ₂	1	1	2	5	1.28	1.29	1.32	1.32	1.38	1.44
G. (PbO ₂) _{za} (Bi _z)(A ⁻)(OH) ₄	1	1	4	5	1.29	1.30	1.34	1.38	1.41	1.48
H. (PbO ₂) _{za} (Bi _z O)(A ⁻) ₂ (OH ⁻)	1	2	1	5	1.30	1.33	1.37	1.45	1.46	1.59
I. (PbO ₂) _{za} (Bi _z)(A ⁻) ₂ (OH) ₃	1	2	3	5	1.31	1.34	1.39	1.47	1.49	1.62
J. (PbO ₂) _{za} (Bi _z O)(A ⁻) ₃	1	3	0	5	1.32	1.37	1.42	1.53	1.54	1.73
K. (PbO ₂) _{za} (Bi _z)(A ⁻) ₃ (OH) ₂	1	3	2	5	1.33	1.38	1.44	1.55	1.57	1.76
L. (PbO ₂) _{za} (Bi _z)(A ⁻) ₄ (OH)	1	4	1	5	1.35	1.42	1.48	1.64	1.57	1.76
M. (PbO ₂) _{za} (Bi _z)(A ⁻) ₅	1	5	0	5	1.37	1.46	1.53	1.72	1.72	2.04

are very few entries in the table which correlate well with the observed $\Delta m/\Delta q$ for both NO_3^- and ClO_4^- .

The calculated $\Delta m/\Delta q$ values in Tables 2, 3 and 4 indicate that a variety of different Bi species could exist within the film. However, using this and previous data, we speculate on a narrower range of possibilities. Previous x-ray diffraction [13] and electrochemical [14] results indicate that the Bi is incorporated into the films in primarily the +5 oxidation state. This decreases the likelihood that the Bi^{+3} and Bi^{+4} possibilities from Tables 2 and 3 are dominant within the film. In addition, the calculated values of $\Delta m/\Delta q$ for the Bi^{+3} and Bi^{+4} species at the highest ratio of Bi:Pb are much greater than those experimentally observed. These species are suspect also because the observed value $\Delta m/\Delta q$ will set the upper limit of reasonable calculated values.

Bismuth is seldom observed in its purely cationic form of Bi^{+3} , and especially not in the Bi^{+5} form [15]. It has been isolated in the +3 oxidation state as a cationic oxide BiO^+ [15]. The literature on aqueous Bi^{+5} is limited because of its instability being a strong oxidizing agent. However, we speculate that the most likely form of Bi^{+5} is $\text{BiO}_2(\text{A}^-)$, similar to the Bi^{+3} species, because very little lattice expansion is observed upon the incorporation of Bi into PbO_2 films [1]. This excludes the possibilities (Table 4 G-H) of Bi^{+5} being charge balanced with multiple anionic species except for OH^- , perhaps, which appears very unlikely under the acidic conditions of this work. However, some incorporation of electrolyte anions is likely from XPS data [10], which indicated the presence of Cl throughout the bulk of Bi- PbO_2 films that was concluded to originate from the ClO_4^- in the deposition solution.

It is suggested that the most likely Bi species deposited into the films is the $\text{BiO}_2(\text{A}^-)$. From Table 4, if $\text{BiO}_2(\text{A}^-)$ were the depositing species, there should be a broader range in the $\Delta m/\Delta q$ values as the ratio of Bi:Pb is increased. Experimentally, however, these values are seen to be almost identical. The calculated values for the case of $[\text{Bi}^{+3}]/[\text{Pb}^{+2}] = 0.1$ are too low, while the values from $[\text{Bi}^{+3}]/[\text{Pb}^{+2}] = 0.25$ and 0.5 are closer to the experimental values. To account for this, the possibility of the Bi existing in a mixed oxidation state was also considered. Yeo reported that at least 75% of the Bi was in the +5 oxidation state [1]. Given the above arguments for the preferred composition of the Bi species in the film, Table 5 was constructed to show the $\Delta m/\Delta q$ values obtained for various ratios of $\text{Bi}^{+3}:\text{Bi}^{+5}$ in the form of $\text{BiO}(\text{A}^-):\text{BiO}_2(\text{A}^-)$. The values of $\Delta m/\Delta q$ for films of at most 25% Bi^{+3} are the closest to those that are experimentally observed (within 2σ).

From previous work, it has been shown also that the Bi-doped films are more porous than the PbO_2 films [1]. This could lead to trapping of water within the films as the films deposit, yielding a higher than expected values of $\Delta m/\Delta q$.

Therefore, it is concluded that the values of $\Delta m/\Delta q$ are most consistent with Bi- PbO_2 films composed of PbO_2 and Bi in the predominantly +5 oxidation state, most probably in the form of $\text{BiO}_2(\text{A}^-)$, with the possibility that Bi^{+3} coexists to a lesser extent as $\text{BiO}(\text{A}^-)$. The similarity in the experimentally observed $\Delta m/\Delta q$ for the various ratios of Bi:Pb is considered to be a result of either Bi species existing in different oxidation states within the film, the entrapment of water as a result of the porosity of these films, and/or a combination of both. Since the highest ratios of Bi:Pb yield the greatest variation in the

Table 5. Values of $\Delta m/\Delta q$ calculated for films containing various ratios of $\text{Bi}^{+3}:\text{Bi}^{+5}$

$\text{BiO}(\text{A}^-)/\text{BiO}_2(\text{A}^-)$ % film composition	$\Delta m/\Delta q$ $\text{A}^- = \text{NO}_3$ $z/a = 0.1$	$\Delta m/\Delta q$ $\text{A}^- = \text{ClO}_4$ $z/a = 0.1$	$\Delta m/\Delta q$ $\text{A}^- = \text{NO}_3$ $z/a = 0.25$	$\Delta m/\Delta q$ $\text{A}^- = \text{ClO}_4$ $z/a = 0.25$	$\Delta m/\Delta q$ $\text{A}^- = \text{NO}_3$ $z/a = 0.5$	$\Delta m/\Delta q$ $\text{A}^- = \text{ClO}_4$ $z/a = 0.5$
10/90	1.28	1.30	1.33	1.37	1.41	1.48
20/80	1.29	1.31	1.36	1.40	1.48	1.54
25/75	1.30	1.32	1.38	1.42	1.51	1.58
50/50	1.33	1.35	1.46	1.50	1.67	1.75
75/25	1.36	1.38	1.53	1.58	1.82	1.91
80/20	1.37	1.39	1.55	1.60	1.85	1.95
90/10	1.38	1.40	1.58	1.63	1.92	2.07

calculated $\Delta m/\Delta q$ values, it is suggested that further work be done on increasingly higher Bi:Pb ratios, perhaps to determine more precisely the Bi speciation within these films.

The cause of the initial break in the f - q response was also considered. The deposition of PbO_2 films from solutions with HClO_4 and HNO_3 as the electrolyte indicate that the same $\Delta m/\Delta q$ is obtained under either condition (Figure 4). This would be unlikely if simple electrolyte anion incorporation were the cause of the break in f - q because of the difference in formula weight in ClO_4^- and NO_3^- . In addition, previous XPS data do not support the incorporation of ClO_4^- into electrodeposited PbO_2 [10]. A second possibility is the incorporation of oxygen-deficient oxides initially into the film because of the initial oxygen-deficient environment. The incorporation of Pb^{+2} into the Pb^{+4} matrix would produce a high value of $\Delta m/\Delta q$. However, XRD and XPS data do not indicate the presence of varying oxides within the films.

It is speculated that the break seen in the f - q responses for the electrodeposition of PbO_2 films is a result of the difference in surface hydration of the Au oxide substrate and the depositing film. The particular values of $\Delta m/\Delta q$ indicate that two additional water molecules are hydrating the surface per PbO_2 surface site than on the Au oxide surface. The deposition of PbO_2 indicates that this water is bound only at the surface because once there is a surface coverage of the PbO_2 and the surface hydration becomes constant, the value of $\Delta m/\Delta q$ approaches the theoretical value. This conclusion is consistent with the observation that the larger value of $\Delta m/\Delta q$ is observed regardless of whether the film is being oxidatively deposited (Figure 3) or reductively desorbed from the electrode surface (Figure 5). The break in the f - q response for the deposition of the Bi- PbO_2 is

considered to be caused by the same difference in hydration.

The XPS data indicate that the ratio of Bi:Pb in the deposition solution was reflected in the films. The increase in the ratio of the Bi in the film electrodes decreases the intersite distance of the active sites, thus increasing the activity of the electrodes toward anodic oxygen-transfer redox reactions as described in the General Introduction.

REFERENCES

1. Yeo, I-H., Ph.D. Dissertation, Iowa State University, 1987.
2. Larew L. A.; Gordon, J. S.; Hsiao, Y-L; Johnson, D. C.; Buttry, D. A., *J. Electrochem. Soc.*, **137**, 3071 (1990).
3. Deakin, M. R.; Melroy, O., *J. Electroanal. Chem.*, **239**, 321 (1988).
4. Bruckestein, S.; Shay, M., *J. Electroanal. Chem.*, **188**, 131 (1985).
5. Deakin, M. R.; Buttry, D. A., *Anal. Chem.*, **61**, 1147A (1989).
6. Deakin, M. R.; Li, T. T.; Melroy, O., *J. Electroanal. Chem.*, **243**, 343 (1988).
7. Ellis, S. R.; Hampton, N. A.; Ball, M. C.; Wilkinson, F., *J. Applied Electrochem.*, **16**, 159 (1986).
8. Naegele, K. D.; Plieth, W. P., *Electrochimica Acta*, **25**, 241-246 (1980).
9. Kim, K. S.; O'Leary, T. J.; Winograd, N., *Anal. Chem.*, **45**, 2214-2218 (1973).
10. Nielsen, B. S.; Davis, J. L.; Thiel, P. A., *J. Electrochem. Soc.*, **137**, 1017 (1990).
11. Gordon, J. S., Ph.D. Dissertation, Iowa State University, 1993.
12. Chang, H.; Ph.D. Dissertation; Iowa State University, 1989.
13. Yeo, I.; Kim, S.; Jacobson, R.; Johnson, D. C., *J. Electrochem. Soc.*, **136**, 1390 (1989).
14. Wels, B.; Johnson, D. C.; unpublished
15. Heslop, R. R.; in "Inorganic Chemistry", Elsevier, 3rd ed., New York, 1967, p. 468.

PAPER III.

APPLICATION OF AN ELECTROCHEMICAL QUARTZ CRYSTAL
MICROBALANCE TO A STUDY OF WATER ADSORPTION
AT GOLD SURFACES IN ACIDIC MEDIA

INTRODUCTION

Since its inception in 1980 [1], the electrochemical quartz-crystal microbalance (EQCM) has been used to study a variety of electrochemical processes including underpotential deposition of metal films [2], electrodeposition of metal oxide films [3], ionic interactions with surface films [4], transport of ions into polymeric films [5], and formation and reduction of native oxides on electrode surfaces [6].

In applications of the EQCM, the change in surface mass (Δm) is calculated from the change in resonant frequency (Δf) after an equation by Sauerbrey [7]:

$$\Delta m = \frac{-\Delta f}{(K/A_p)} \quad (1)$$

In Equation 1, K is a fundamental constant predicted to be $56.6 \times 10^3 \text{ Hz cm}^2 \text{ mg}^{-1}$ for quartz crystals having a resonant frequency of *ca.* 5 MHz, and A_p is the piezoelectrically active area of the quartz crystal covered by the Au film. It is significant that a decrease in frequency corresponds to an increase in surface mass.

Our research has focused on the study of thin films of electrodeposited PbO_2 that are modified by incorporation of various cationic and anionic species. These studies are relevant to our interest in the activation of thin PbO_2 -film electrodes for anodic reactions in which oxygen is transferred from H_2O in the solvent phase to the oxidation product(s) [8]. Previously, the EQCM was successfully applied to a study of the activation of pure PbO_2 -film electrodes by the electrosorption of Bi(III) as Bi(V) [3]. During a recent investigation of the electrodeposition of pure PbO_2 films on AuO substrates, a higher than expected mass-to-charge ratio ($\Delta m/\Delta q$) was encountered during the nucleation phase of

deposition [9]. Consideration of various plausible explanations has led to the tentative conclusion that the anomalously large $\Delta m/\Delta q$ is caused by differences in the hydration for the AuO and PbO₂ surfaces. This speculation prompted a study of possible changes in surface hydration that might occur at Au electrodes during anodic formation of surface oxide (AuO).

Bruckenstein and Shay [10] were the first to apply the EQCM for a study of the voltammetric formation and dissolution of surface oxide on Au electrodes in acidic media. In HClO₄ media, a distinct frequency decrease (mass increase) was observed during the positive potential scan starting *ca.* 0.5 V negative of the potential for onset of AuO formation. In subsequent discussions, we will refer to this potential region as the "preoxide region". Bruckenstein and Shay attributed this negative Δf to the specific adsorption of ClO₄⁻ [10].

Shumacher and Stockel [11] also applied the EQCM in a similar study and reported that the frequency increased only in the voltammetric region corresponding to AuO formation. However, in a subsequent study [12], Schumacher and Stockel used a high current sensitivity to record the *i-E* response, and they observed a small anodic wave in the preoxide region which developed concomitantly with a decrease in frequency. They concluded, in agreement with Bruckenstein and Shay [10], that specific adsorption of anions is responsible for the small anodic wave as well as the increase in surface mass. Schumacher and Stockel also concluded [12], on the basis of capacitance and voltammetric data, that Cl⁻, Br⁻ and I⁻ are adsorbed reversibly in the preoxide region; however, they concluded that SO₄²⁻ is adsorbed irreversibly. Potential-step experiments

were also performed, and the frequency decrease was measured as a function of time (t). They observed that f decreased linearly with $t^{1/2}$ for the unstirred solutions and concluded, for 0.1 M Br⁻ and 0.1 M I⁻, that the adsorption process occurs at a diffusion-limited rate, as described by the Cottrell equation for unstirred solutions.

Angerstein-Kozłowska *et al.* [13]-[14] applied cyclic voltammetry and chronoamperometry in a study of the formation and dissolution of surface oxides at single crystal and polycrystalline Au in the presence of adsorbing anions. They concluded, for increasing potential in the region of oxide formation, that AuOH is formed first at surface sites not occupied by adsorbed anions. Furthermore, they concluded that ultimately, with increasing potential, a monolayer of AuO is formed over the entire electrode surface with concomitant desorption of all adsorbed anions.

Whereas Angerstein-Kozłowska *et al.* focused their study at the very negative potential limit of oxide formation [13,14], Burke *et al.* studied the preoxide region [15]-[16]. They interpreted their results on the basis of formation of a sub-monolayer of hydrous oxide (AuOH) at Au atoms in low coordination sites, i.e., adatoms. They estimated that < 1 % of the surface sites are converted to AuOH in the preoxide region. They also considered the possibility that electrosorption of anions can contribute to the total observed electrode current. Here, we conclude that the magnitude of the frequency decrease observed during the positive scan in the preoxide region is inconsistent with the mere electrosorption of anions. Instead, we propose that the increased surface mass is primarily the result of a net increase in surface hydration as the result of H-bonding of H₂O to AuOH sites generated in the preoxide region.

EXPERIMENTAL

Reagents - Chemicals were reagent grade (Fisher Scientific). Solutions were prepared by dilution of concentrated acids with distilled water that had been purified in a NANOpure-I system (SYBRON/Barnstead). Gold (99.999%) and titanium (99.7%) (Johnson Matthey) were used for vapor deposition onto the quartz crystals.

Apparatus - The EQCM instrumentation has been described previously [17]. Planar (2.5-cm dia.), overtone-polished, AT-cut quartz crystals (Valpey-Fisher) were operated at their fundamental resonance frequency (*ca.* 5 MHz). Films of Ti (15-nm thick) were vapor deposited on the quartz disks to serve as an adhesive substrate for Au films. Gold films (*ca.* 200-nm thick) were subsequently vapor deposited on both sides of the quartz crystals to serve as contacts for the high-frequency oscillator circuitry. Vapor deposition was performed in an E306A coating system (Edwards).

The potentiostat was controlled and data acquired using an IBM-compatible PC/AT computer (APEX) connected to the EQCM by a DT2801-A interface with ASYST software (Data Translation). A Pt wire was used as the counter electrode. Capacitance measurements were made with a Model 137 potentiostat (EG&G Princeton Applied Research) and a SR530 lock-in amplifier (Stanford Research System).

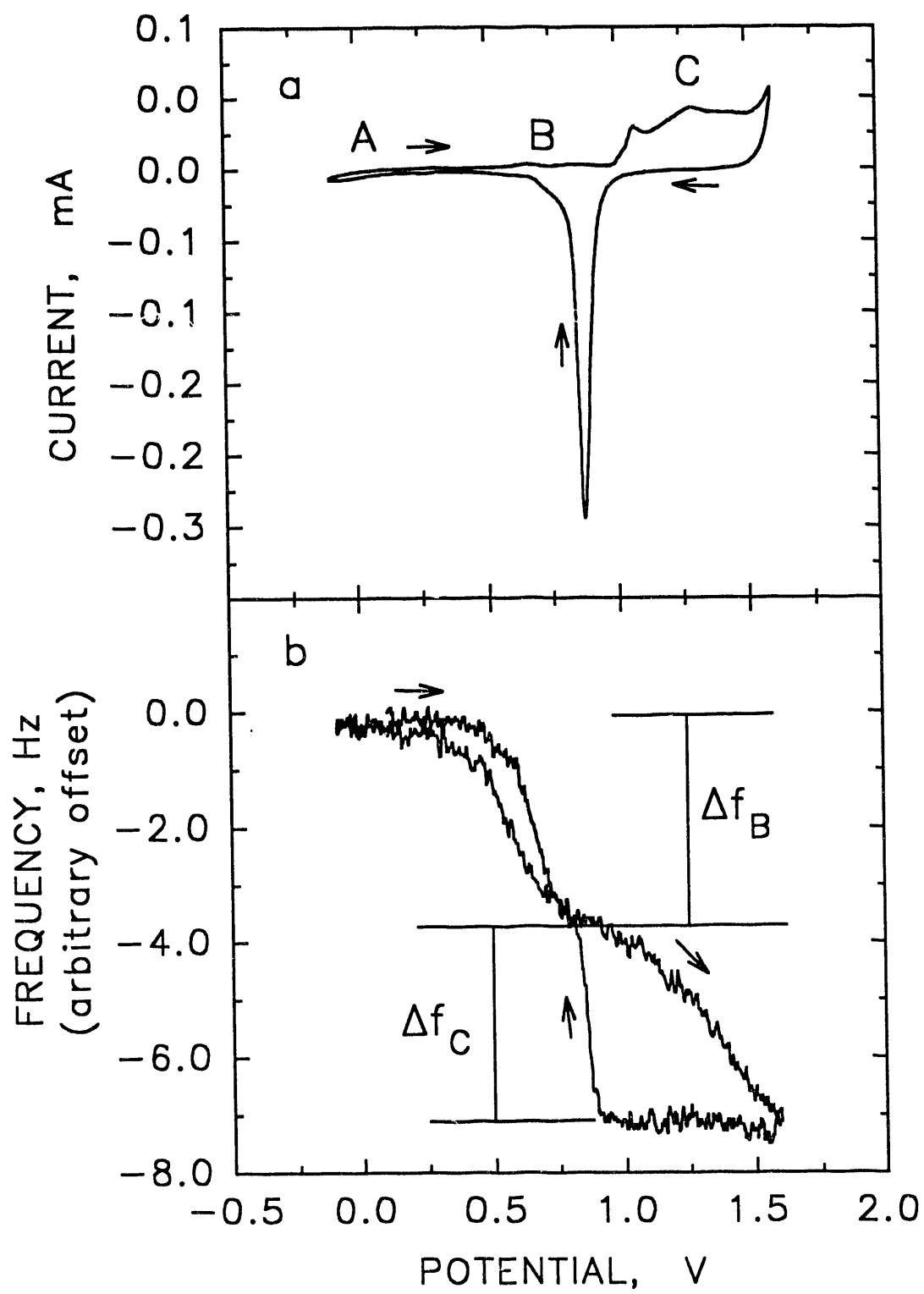
Procedures - Potentials were measured and are reported versus a SCE reference electrode filled with a sat'd NaCl solution. Methods for cleaning and calibrating EQCM electrodes were discussed previously [3].

RESULTS AND DISCUSSION

Figure 1a contains a typical current-potential (i - E) curve obtained at a Au-film electrode in 0.10 M HClO₄. The very small anodic current observed during the positive potential scan in Region A (-0.1 to *ca.* +0.5 V) corresponds to charging of the electrical double layer. Region B (*ca.* +0.5 to +1.0 V) during the positive scan corresponds to the preoxide region under discussion, and the slight increase in anodic current is concluded to result primarily from formation of a sub-monolayer of hydrous oxide, designated here as Au(OH)_a ($a \ll 1$). The large wave in Region C (*ca.* +1.0 to +1.6 V) corresponds to anodic formation of the inert surface oxide, designated here as AuO_c ($c \approx 1$). Scan reversal at +1.6 V results in rapid cessation of anodic current followed by a cathodic peak in the region *ca.* +1.2 to +0.7 V, corresponding to reductive dissolution of AuO_c.

Figure 1b contains the frequency-potential (f - E) curve recorded simultaneously with the i - E curve in Figure 1a. During the positive scan from -0.1 V, there is no detectable change in frequency corresponding to double-layer charging (Region A). However, a rapid decrease in frequency (mass increase) by the amount designated Δf_B is observed in Region B concomitantly with formation of Au(OH)_a. Continuation of the positive scan through Region C results in a further decrease in frequency by the amount Δf_C concomitantly with formation of AuO_c. Following scan reversal at +1.6 V, the frequency remains constant until increasing very rapidly in region *ca.* +1.0 to +0.7 V which corresponds to cathodic dissolution of AuO. Continuation of the negative scan

Figure 1. (a) Current-Potential (i - E) curve and (b) Frequency-Potential (f - E) for Au EQCM film in 0.1 M HClO₄. Scan rate: 75 mV/s. No convective mixing.

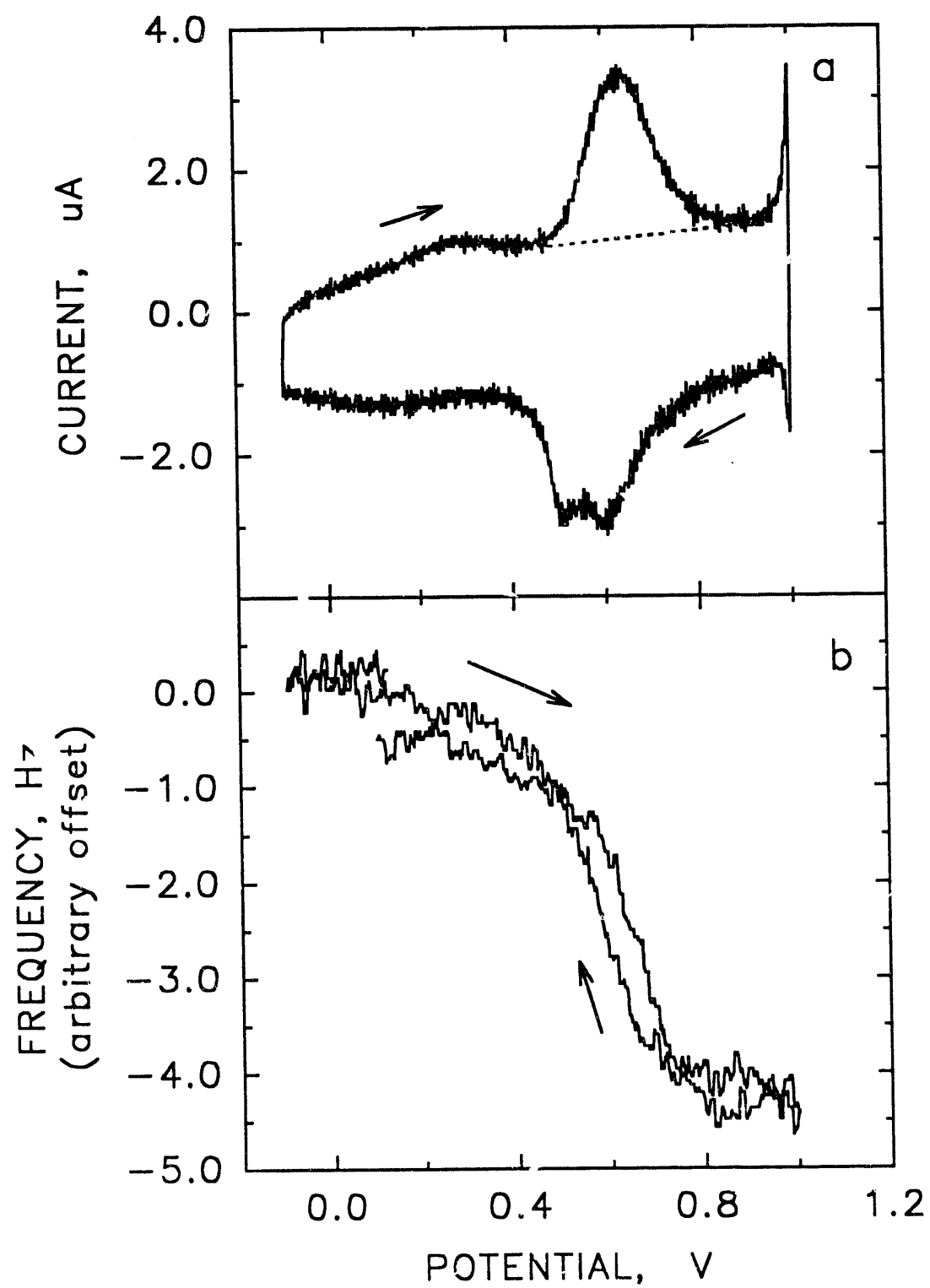


back through the preoxide region (**B**) results in further increase of frequency until the original value of f is attained in the double-layer region (**A**).

The i - E response in Regions **A** and **B** (-0.10 to +0.90 V) was recorded using a very high current sensitivity, and the results are shown in Figure 2a. During the positive scan, a peak-shaped anodic wave is observed in the region *ca.* +0.5 to +0.8 V, designated **B** in Figure 1a, which corresponds to the potential region of most rapid change in f in Figure 1b. This peak is concluded to correspond to formation of $\text{Au}(\text{OH})_a$. The estimated contribution from double-layer charging current (i_{dl}) in Region **B** is indicated by the dashed line in Figure 2a. Upon scan reversal at +1.0 V, reductive dissolution of $\text{Au}(\text{OH})_a$ results in the peak-shaped cathodic wave in the region *ca.* +0.8 to +0.4 V. The similarity of the peak potentials (E_{peak}) for the cathodic and anodic processes is indicative of quasireversible kinetics for these surface processes. Shown in Figure 2b is the f - E curve obtained simultaneously with the i - E curve in Figure 2a. The conclusion of quasireversibility for the surface processes in Region **B**, based on data in Figure 2a, is supported by the virtual superposition of the corresponding f - E curves in Figure 2b. The current response obtained for the positive scan throughout Regions **B** and **C** was corrected for double-layer charging by subtraction of the i_{dl} value indicated in Figure 2a. Then, the total frequency change (Δf_{tot}) was predicted corresponding to the scan from -0.1 to +1.6 V on the basis of the time integral of the corrected i - E curve according to:

$$\Delta f = \left(\frac{M}{\gamma F}\right)\left(\frac{K}{A_e}\right) \int i dt \quad (2)$$

Figure 2. (a) Current-Potential (i - E) curve and (b) Frequency-Potential (f - E) curve for Au EQCM film in 0.1 M HClO₄. Scan rate: 75 mV/s. No convective mixing.



where γ is the number of electrons for oxide formation (2 eq/mol), F is the Faraday constant (96,485 coul/eq), M is the molecular weight of oxygen (16 g/mol), A_e/K (mg/Hz) is a proportionality constant relating Δm and Δf determined independently for each crystal [3], and $dt = dE/\phi$, where ϕ is the potential scan rate ($V\ s^{-1}$). The predicted value of Δf_{tot} is 2.8 Hz for formation of a monolayer of AuO, which is significantly smaller than the observed value of $\Delta f_B + \Delta f_C = 7.1$ Hz shown in Figure 1b. It is doubtful that so large a difference between the predicted and observed decrease in frequency can be the result of incorrect choice of γ and/or M , or the assumed surface coverage by AuO.

The i - E and f - E curves were obtained also in solutions of HNO_3 and CF_3SO_3H . These acids were chosen because their anions have significantly different masses from that of $HClO_4$ and, furthermore, because they do not chemisorb at Au surfaces. The value of Δf_B obtained for repetitive measurements in the various media are summarized in Table 1. These data are virtually independent of the identity and concentration of the acids chosen. Hence, we conclude, in contradiction to Bruckenstein and Shay [10], and Shumacher and Stockel [12], that the observed change in apparent surface mass is not the primary result of adsorption of anions from these supporting electrolytes.

We propose that the anomalously large values obtained for Δf_B and Δf_C throughout

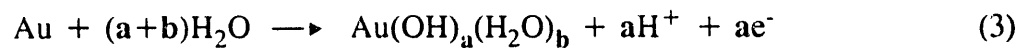
Table 1. Average Δf_B for various electrodes and electrolytes

Electrolyte	Δf_B (Hz)*	n**
0.1 M $\text{CF}_3\text{SO}_3\text{H}$	5.8 ± 0.3	5
1.0 M HClO_4	5.2 ± 0.8	9
0.1 M HClO_4	5.4 ± 1.0	4
1.0 M HNO_3	5.1 ± 0.8	5
0.1 M HNO_3	6.0 ± 1.1	4

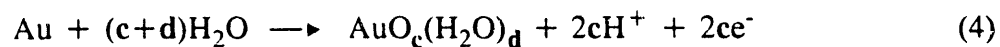
* Uncertainty indicated is standard deviation.

** Value of n represents number of data sets sampled.

Regions **B** and **C**, respectively, are the result of increased surface hydration as a consequence of formation of $\text{Au}(\text{OH})_a$ ($a \ll 1$; Region **B**) and AuO_c ($c \approx 1$; Region **C**). We represent the anodic process corresponding on the positive scan to *ca.* +0.9 V (Region **B**) by the reaction:



Furthermore, we represent the overall anodic process for the positive scan to +1.60 V (Regions **B** and **C**) by the reaction:



In Equations 3 and 4, **a** and **c** represent the fractional surface coverages by the hydroxyl and oxide species, respectively, and **b** and **d** represent the increase in the average effective number of H₂O molecules adsorbed per Au site as a consequence of the anodic reactions.

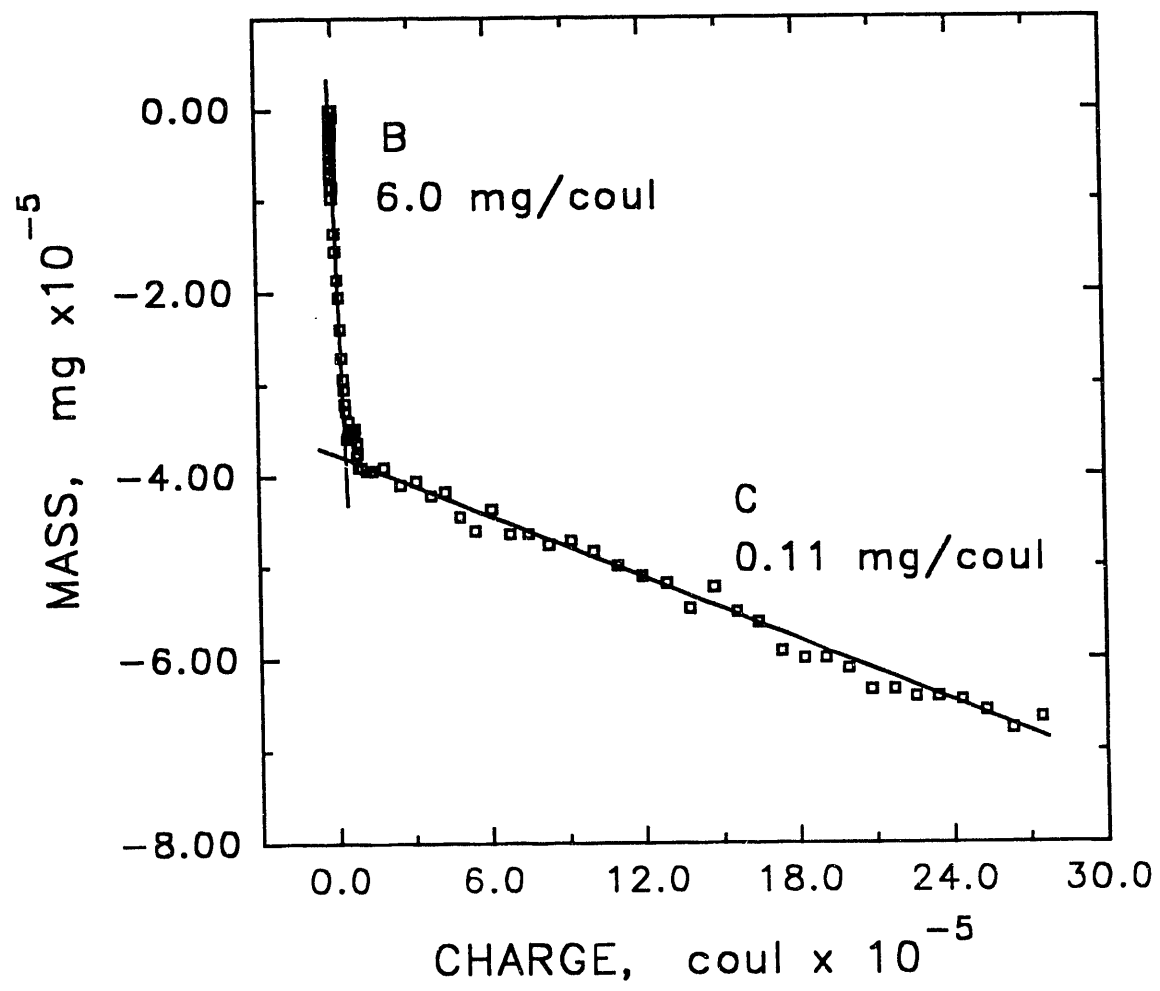
Values of the stoichiometric coefficients in Equations 3 and 4 can be calculated from *i*-*E* and *f*-*E* data, provided the true electrode area (A_{true}) is known. This value was calculated from the total faradaic charge for cathodic dissolution of surface oxide (AuO_c) obtained during the negative scan through the region +1.0 to +0.4 V (see Figure 1a), as described by:



For a positive scan to +1.60 V in 0.10 M HClO₄, the quantity of oxide formed corresponds virtually to one monolayer (*i.e.*, $c \approx 1.0$) and the cathodic charge required subsequently for dissolution of this oxide is 400 $\mu\text{coul}/\text{cm}^2$ [18]. Data are reported here for an electrode having $A_{\text{true}} = 0.57 \text{ cm}^2$. For this example, the geometric area (A_{geo}) was 0.34 cm^2 and, hence, the surface roughness ($A_{\text{true}}/A_{\text{geo}}$) is estimated to be 1.7.

Values of Δm were calculated from Δf -*E* data on the basis of Equation 1, and values of Δq were determined by digital integration of *i*-*E* curves after correction for i_{dl} . Values of Δm are plotted in Figure 3 as a function of Δq corresponding to the positive scan throughout the region +0.4 to 1.6 V. Two linear segments are readily apparent corresponding to Regions **B** and **C** (see Figure 1a and b) and have slopes ($\Delta m/\Delta q$) equal to 6.0 mg/coul for formation of Au(OH)_a(H₂O)_b (Region **B**) and 0.11 mg/coul for

Figure 3. Mass-Charge ($\Delta m/\Delta q$) curve for Regions **B** and **C** of the i - E curve in Figure 1.



formation of $\text{AuO}_c(\text{H}_2\text{O})_d$ (Region C). The linearity of the Δm - Δq plots corresponding to these two voltammetric regions is consistent with the speculation illustrated by Equations 3 and 4 that the change in surface hydration is a direct stoichiometric consequence of the anodic formation of $\text{Au}(\text{OH})_a$ and AuO_c in Regions A and B, respectively. Slopes of the two linear segments of the $\Delta m/\Delta q$ plots are given in Table 2 for three Au electrodes. The data in Figures 1 and 3 correspond to electrode #1 in Table 2.

Table 2. Values of $\Delta m/\Delta q$ determined for three electrodes in 1.0 M HClO_4 in Regions B and C, as specified in Figure 1

	REGION B	REGION C
Electrode	$\Delta m/\Delta q$ (mg/coul)	$\Delta m/\Delta q$ (mg/coul)
1	6.0 ± 0.1	0.11 ± 0.01
2	5.8 ± 0.1	0.10 ± 0.01
3	5.9 ± 0.1	0.08 ± 0.01

The numerical value of the coefficient a in Equation 3 (Region B) was calculated according to:

$$a = \Delta q_A (1/\gamma_h F) (N_A/d_{\text{Au}} A_{\text{true}}) \quad (6)$$

where Δq_A is the net anodic charge for Region A, $\gamma_h = 1$ eq/mol, $M_h = 17$ mg/mmol, $d_{\text{Au}} = 1.25 \times 10^{15} \text{ cm}^{-2}$ for the density of atoms on the Au surface [13], and N_A is Avogadro's number. The numerical value of the coefficient b in Equation 3 (Region B)

was calculated from $\Delta f_B = -3.7$ Hz (see Figure 1) according to:

$$b = [-(\Delta f_A)(A_e/K) - ad_{Au}A_{true}(M_h/N_A)](N_A/M_w)/(d_{Au}A_{true}) \quad (7)$$

where $M_w = 18$ mg/mmol, and the remaining terms are the same as used in Equation 6.

Values of a , b and b/a are given in Table 3 for three electrodes. For the electrode producing the data in Figures 1 and 3 (#1 in Table 3), $a = 0.050$, $b = 1.6$ and $b/a = 32$.

Table 3. Values of the stoichiometric coefficients shown in Equations 3 and 4 for three Au-film electrodes in 1.0 M HClO₄

Electrode	a	b	c	d	b/a
1	0.050	1.60	1.0	2.30	32
2	0.050	1.60	1.0	2.30	32
3	0.040	1.50	1.0	2.20	37

These data indicate an amazingly large increase in surface hydration as a result of the formation of the submonolayer of hydrous oxide, which is equivalent to a net increase in surface hydration equal to 3.14×10^{-9} mol/cm². We propose that the mechanism responsible for this increase in surface hydration is H-bonding by H₂O to the AuOH sites.

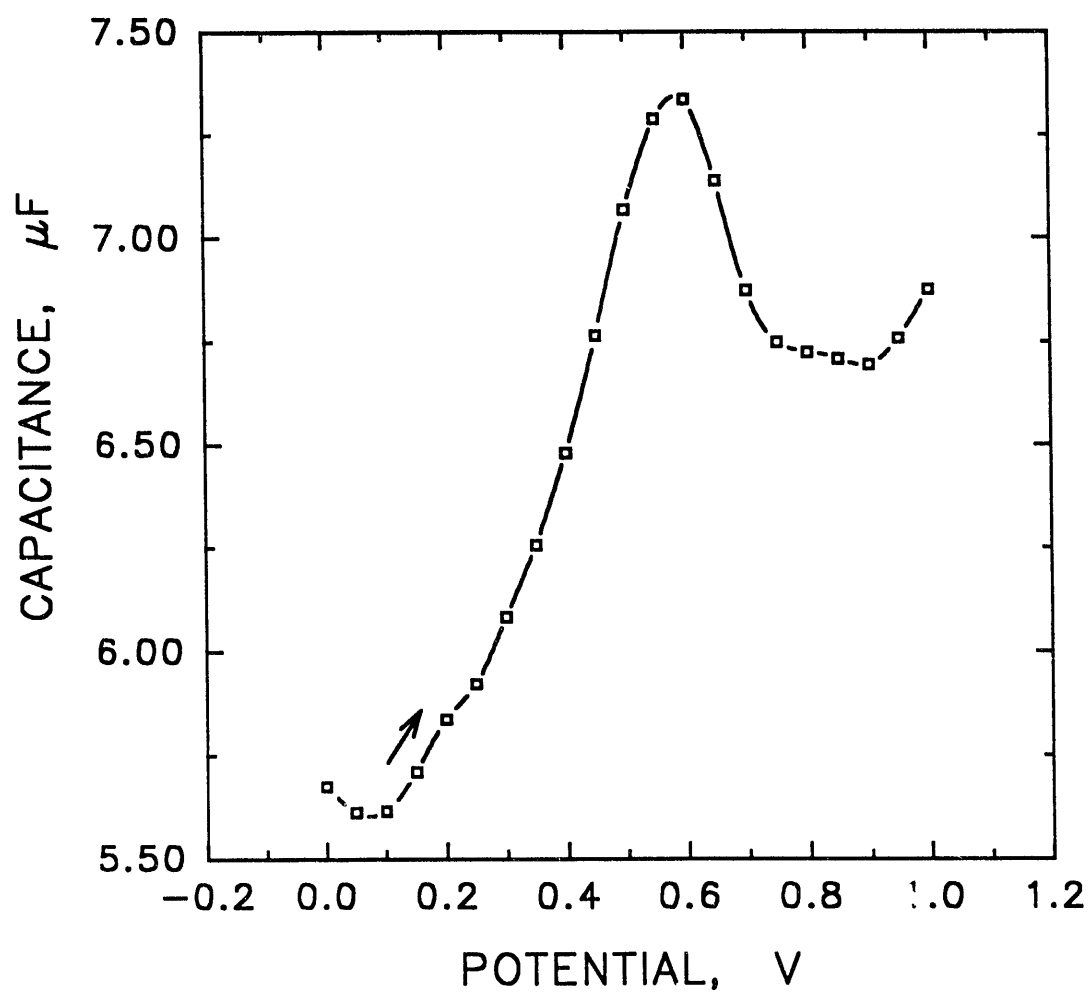
Numerical values for d in Equation 4 (Region C) were calculated from $\Delta f_C = 3.4$ Hz (see Figure 1b) according to:

$$d = -[(\Delta f_B)(A_e/K) - cd_{Au}A_{true}(M_{oxide}/N_A)](N_A/M_w)/(d_{Au}A_{true}) \quad (8)$$

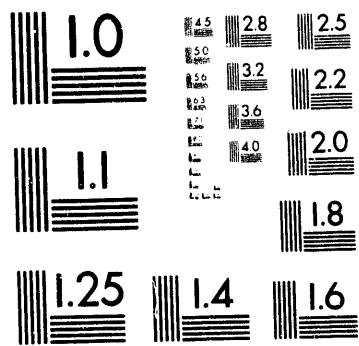
This calculation assumes $c = 1.0$, which is a reasonable estimate for a positive scan limit of +1.60 V vs. SCE in 0.10 M HClO₄. Values of d are included in Table 3 for three electrodes. For the electrode used to obtain data shown in Figures 1 and 3 (#1 in Table 3), $d = 2.3$ and $d/c = 2.3$. The corresponding net increase in surface coverage by H₂O in Region C is 1.41×10^{-9} mol/cm² for a total increase (Regions B and C) of 4.55×10^{-9} mol/cm², as compared to the oxide-free Au surface (Region A). This represents a relatively small net increase in surface hydration as a consequence of the conversion from Au(OH)_{0.050} to AuO_{1.0}.

AC voltammetric measurements were made in an effort to estimate the effective interfacial capacitance in Regions A and B. A staircase waveform with +50-mV steps was applied using a superimposed sinusoidal voltage with a frequency of 201 Hz and an amplitude of 3.2 mV. Figure 4 contains a plot of the apparent capacitance (C_{app}) vs. E as determined for the positive scan at a Au-film electrode. A dramatic increase in C_{app} is observed with a peak value at *ca.* +0.60 V, which corresponds to the peak potential for hydrous oxide formation in the preoxide region (see Figure 2a). If H-bonding occurs as a result of the formation of Au(OH)_a in Region B (see Equation 3), the increased ordering of water molecules at the electrode surface might be expected to cause a decrease in the dielectric constant for the interfacial region and, therefore, a decrease in the double-layer capacitance (C_{dl}). This expectation is contrary to our observation for C_{app} . However, recent work in our laboratory [19] has revealed that the kinetics for the Au-Au(OH)_a redox couple are sufficiently fast so that the quasi-reversible nature of the associated anodic and cathodic peaks obtained by cyclic voltammetry (Figure 2a) is

Figure 4. Capacitance-Potential curve at an Au EQCM film electrode in 1.0 M HClO₄. Conditions: 50-mV steps, AC frequency: 201 Hz, AC voltage 3.2 mV.



maintained even at scan rates in excess of 200 mV/s. Hence, we conclude the increase in C_{app} in Figure 4 is a result of so-called "pseudo capacitance" resulting from the contribution of the surface faradaic process to the AC-correlated signal obtained by this technique. This conclusion is contrary to that of Schumacher and Stockel [12] who concluded the increase in apparent capacitance is indicative of anion adsorption in this potential region.



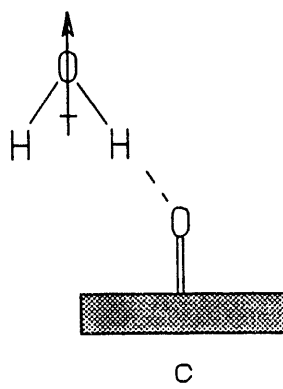
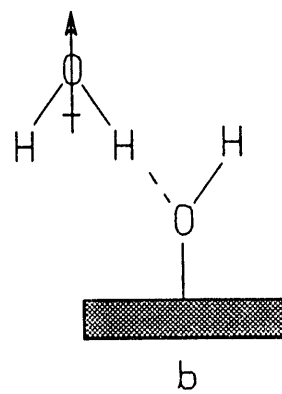
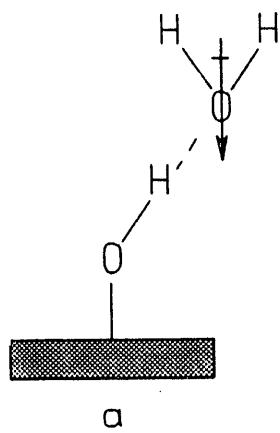
3 of 3

CONCLUSIONS

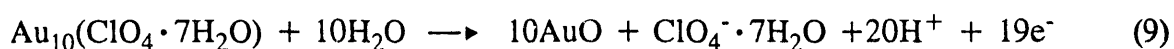
A large increase in surface mass is observed to occur concomitantly with anodic formation of $\text{Au}(\text{OH})_a$ ($a \ll 1$) during the positive scan through Region **B** of the i - E curve (see Figures 1a and b). Whereas we cannot totally discount the possibility of adsorption of ClO_4^- at Au in HClO_4 media, we cannot be convinced that anion adsorption is a significant factor in dictating either the anodic peak in Region **B** or the concomitant increase in apparent surface mass. Significant qualitative support for this conclusion comes from the observation that changes in surface mass are virtually identical whether measured in HClO_4 , HNO_3 or $\text{CF}_3\text{SO}_3\text{H}$, in spite of large differences in the equivalent weights of the corresponding anions. We also note that Yeager *et al.* [20] reported, on the basis of *in situ* FT-IR data, that there is no evidence for adsorption of ClO_4^- or NO_3^- at Au electrodes in these HClO_4 media. Hence, we conclude for Region **B**, that the increase in surface mass is the result of increased surface hydration *via* a mechanism involving H-bonding of H_2O to the hydroxyl species adsorbed at Au atoms in low coordination sites, as is suggested in Figures 5a and 5b. As shown, two orientations are possible within this consideration; however, these data do not indicate a preferred orientation.

A further increase in surface mass is observed concomitantly with formation of surface oxide (AuO) during the positive scan through Region **C** (see Figures 1a and b). Angerstein-Kozłowska [13-14] proposed for $\text{Au}(111)$ that as many as 10 surface sites can be blocked by adsorption of a single hydrated ClO_4^- anion, *i.e.*, $\text{ClO}_4^- \cdot 7\text{H}_2\text{O}$.

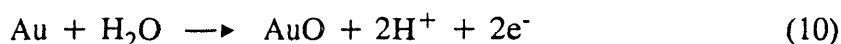
Figure 5. Diagram suggesting possible hydrogen bonding of H_2O to AuOH (a and b) formed in Region **B**, and to AuO (c) in Region **C** of *i-E* curve in Figure 1a.



Furthermore, they concluded that adsorbed anions are desorbed concomitantly with formation of surface oxide [13]. If hydrated ClO_4^- is electrosorbed in Region **B** and if the Angerstein-Kozłowska conclusion is relevant for these polycrystalline surfaces, then the desorption of a single $\text{ClO}_4^- \cdot 7\text{H}_2\text{O}$ (225 g/mol) in Region **C** occurs with the simultaneous uptake of ten oxygen atoms (10·16 g/mol), as indicated by:



Hence, the surface mass would be expected to decrease with a corresponding total frequency increase calculated to be *ca.* 0.8 Hz for these electrodes. Contrary to this scenario, an increase is observed in surface mass corresponding to a frequency decrease (Δf_C) of 3.4 Hz (Figure 1b). Furthermore, for formation of surface oxide without change in surface hydration, as indicated by:



$\Delta m/\Delta q = 0.083$ mg/coul. In contrast, for Region **C** (see Figure 3), $\Delta m/\Delta q = 0.11$ mg/coul. Hence, for Region **C** the large increase in surface mass is concluded to be the result of formation of a monolayer of oxide (AuO) with a further increase in surface hydration *via* H-bonding to the surface oxide, as suggested in Figure 5c.

According to our conclusion, the scan of potential from Region **A** to Region **B** results in a rather dramatic change at the electrode surface in which H_2O molecules become arranged into three-dimensional (perhaps hemispherical) clusters centered at widely separated AuOH sites. Workers in our laboratory have noted the electrocatalytic nature

of Au surfaces in the preoxide region for various anodic reactions which occur with transfer of oxygen from H_2O to the oxidation product(s) [21]. Speculation has been offered that the adsorbed hydroxyl species (AuOH) can assist in the adsorption of polar organic molecules and, furthermore, the hydroxyl species might represent the intermediate state of oxygen from H_2O being transferred to the oxidation products. Burke *et al.* [22]-[23] also have considered the electrocatalytic function of Au adatoms for anodic reactions in the preoxide region. We now add to the electrocatalytic speculations the possibility that the clusters of oriented H_2O dipoles centered at catalytic AuOH sites might contribute to observed voltammetric phenomena by way of their influence on the orientation of electroactive functional groups in reactants that must diffuse to these catalytic sites.

REFERENCES

1. Nomura, T.; and Iijima, M., *Anal. Chim. Acta*, **131**, 97 (1981).
2. Deakin, M. R.; Melroy, O., *J. Electroanal. Chem.*, **239**, 321 (1988).
3. Larew, L. A.; Gordon, J. S.; Hsiao, Y.; Johnson, D. C., *J. Electrochem. Soc.*, **137**, 3071 (1990).
4. Delong, H. C.; Donohue, J. J.; Buttry, D. A., *Langmuir*, **7**, 2196 (1991).
5. Hillman, A. R.; Loveday, D. C.; Bruckenstein, S., *J. Electroanal. Chem.*, **300**, 67 (1991).
6. Schumacher, R.; Gordon, J. G.; Melroy, O., *J. Electroanal. Chem.*, **216**, 127 (1987).
7. Sauerbrey, G., *Z. Phys.*, **155**, 206 (1959).
8. Johnson, D. C.; Chang, H.; Feng, J.; Wang, W.; "Electrochemistry for a Cleaner Environment", J. D. Genders and N. L. Weinberg (Eds.), The Electrosynthesis Co., Inc.: East Amherst, NY; (1992) Chapter 17.
9. Gordon, J. S.; Johnson D. C., in preparation. Paper II, this dissertation.
10. Bruckenstein S.; Shay, M., *J. Electroanal. Chem.*, **188**, 131 (1985).
11. Schumacher, R.; Stockel, W., *Ber. Bunsenges. Phys. Chem.*, **91**, 345 (1987).
12. Stockel, W.; Schumacher, R., *Ber. Bunsenges. Phys. Chem.*, **93**, 600 (1989).
13. Angerstein-Kozłowska, H.; Conway, B. E.; Hamelin, A.; Stoicoviciu, L., *Electrochim. Acta*, **31**, 1051 (1986).
14. Angerstein-Kozłowska, H.; Conway, B.E.; Telefsen, K.; Barnett, B., *Electrochim. Acta*, **34**, 1045 (1989).
15. Burke, L. D.; O'Sullivan, J. G., *Electrochem. Acta*, **37**, 2987 (1992).

16. Burke, L. D.; Lee, B. H., *J. Electroanal. Chem.*, **330**, 637 (1992).
17. Ostrom, G. S.; Buttry, D. A., *J. Electroanal. Chem.*, **256**, 41 (1988).
18. Angerstein-Kozłowska, H.; Conway, B. E.; Hamelin A.; Stoicoviciu, L., *J. Electroanal. Chem.*, **228**, 29 (1987).
19. Roberts, R; Johnson, D.C.; unpublished.
20. Yeager, E. B.; Scherson, D.; Xing, X.; Bae, I. T., *Anal. Chem.*, **61**, 1154 (1989).
21. Vitt, J. E.; Larew, L. A.; Johnson, D. C., *Electrocatalysis*, **2**, 21 (1990).
22. Burke, L. D.; O'Sullivan, J. G., *Electrochem. Acta*, **37**, 2087 (1992).
23. Burke, L. D.; Lee, B. H., *J. Electroanal. Chem.*, **330**, 637 (1992).

GENERAL CONCLUSIONS

In this research the EQCM was used to increase the fundamental understanding of the electrode/electrolyte interface processes occurring as a result of the deposition of various metal oxide films onto gold electrode surfaces.

Within the Bi-PbO₂ films, the Bi was concluded to be primarily incorporated as Bi⁺⁵ in the form of BiO₂A, where A is an electrolyte anion (NO₃⁻ or ClO₄⁻). This is in agreement with earlier work on the speciation of Bi within the films. Complications of water incorporation into these films prohibited a definitive identification of the Bi species. Further work is suggested using higher ratios of [Bi⁺³]/[Pb⁺²] to produce a higher loading of Bi within the films in order to determine more precisely the speciation of the Bi. Bulk PbO₂ films deposited on the electrode surface with values of $\Delta m/\Delta q$ that agreed well with the theory. No evidence of water incorporation within the bulk of those films was observed.

Oxidation of the gold film electrodes was found to produce a low surface coverage (< 1%) of AuOH prior to formation of the surface oxide (AuO). This formation was concluded to result in an increase in surface hydration due to hydrogen bonding of H₂O with the surface AuOH in the preoxide region. It is speculated that clusters of oriented H₂O dipoles might influence the orientation of the reactant's electroactive functionality group to enhance or inhibit diffusion to the catalytic sites. This could have a profound effect in the pulsed electrochemical detection research for understanding the selectivity in oxidation of various organic species.

The EQCM is a valuable tool in examining the electrode/electrolyte interface and processes occurring therein and should continue to be used to study the deposition of the PbO_2 and other metal oxide films. However, while being extremely sensitive to interfacial changes in mass, density and viscosity, the EQCM is nonselective. These results are concluded to indicate that changes in surface hydration and water inclusion within the oxide films as they deposit contribute significantly to the EQCM signal. Therefore, the convoluted information obtained from EQCM experiments necessitates careful interpretation of results in considering all of the possible interactions occurring at the electrode surface.

LITERATURE CITED

1. Johnson, D. C.; LaCourse, W. R., *Anal. Chem.*, **62**, 589A (1990).
2. LaCourse, W. R.; Johnson, D. C.; Rey, M. A.; Slingsby, R. W., *Anal. Chem.*, **63**, 134 (1991).
3. LaCourse, W. R.; Johnson, D. C., *Carbohydrate Research*, **215**, 159 (1991).
4. Tarasevich, M. R.; Sadkowski, A.; Yeager, E., in "Comprehensive Treatise of Electrochemistry", Conway, B. E.; Bockris, J. O'M.; Yeager, E.; Khan, S. U. M.; White, R. E., Eds., Elsevier: Amsterdam, Vol. 26, 301 (1987).
5. LaCourse, W. R.; Hsiao Y. L.; Johnson, D. C., *J. Electrochem. Soc.*, **136**, 3714 (1989).
6. Chang, H.; Johnson, D. C., *J. Electrochem. Soc.*, **137**, 2452 (1990).
7. Chang, H.; Johnson, D. C., *Analytica Chimica Acta*, **248**, 85 (1991).
8. Wels, B., Ph.D. Dissertation, Iowa State University, Ames, IA, 1990.
9. Feng, J.; Johnson, D. C., *J. Electrochem. Soc.*, **137**, 507, (1990).
10. Chang, H.; Johnson, D. C., *J. Electrochem. Soc.*, **137**, 2452 (1990).
11. Hsiao, Y. L.; Johnson, D. C., *J. Electrochem. Soc.*, **136**, 3704 (1989).
12. Hsiao, Y. L.; Vitt, J. E.; Johnson, D. C., *J. Electrochem. Soc.*, **139**, 377 (1992).
13. Yeo, I. H.; Johnson, D. C., *J. Electrochem. Soc.*, **134**, 1973 (1987).
14. Chang, H.; Johnson, D. C., *J. Electrochem. Soc.*, **136**, 17 (1989).
15. Yeo, I. H.; Kim, S.; Jacobson, R.; Johnson, D. C., *J. Electrochem. Soc.*, **136**, 1395 (1989).

16. Nielsen, B. S.; Davis, J. L.; Theil, P. A., *J. Electrochem. Soc.*, **137**, 1017 (1990).
17. Curie, J.; Curie, P., *Rendu*, **91**, 294 (1880).
18. Sauerbrey, G. Z., *Z. Phys.* **155**, 206 (1959).
19. King, W. H., *Anal. Chem.*, **36**, 1735 (1964).
20. Ho, M. A.; Guilbault, G. G.; Reitz, B., *Anal. Chem.*, **54**, 1998 (1982).
21. Jordan, J. M., M.S. Thesis, University of New Orleans, New Orleans, 1985.
22. Guilbault, G. G.; Lopez-Roman, A., *Environ. Lett.* **2**, 35 (1971).
23. Karmarkar, K. H.; Guilbault, G. G., *Anal. Chim. Acta*, **75**, 111 (1975).
24. Olin, J. G.; Sern, G. J., *Atmos. Environ.*, **5**, 653 (1971).
25. Guilbault, G. G.; Jordan, J. M., *CRC Critical Reviews of Analytical Chemistry*, **19**, 1 (1988).
26. Schulz, W. W.; King, W. H., *J. Chromatogr.*, **11**, 343 (1973).
27. Bastiaans, G. T.; Konash, P. L., *Anal. Chem.*, **52**, 1929 (1980).
28. Buttry, D. A.; Lasky, S. J., *Am. Biotech. Lab.*, **8**, 8 (1990).
29. Guilbault, G. G.; Suleiman, A., *Am. Biotech. Lab.*, **8**, 28 (1990).
30. Jones, J. L.; Meiore, T., *Anal. Chem.*, **41**, 484 (1969).
31. Nomura, T.; Ijima, M., *Anal. Chim. Acta.*, **131**, 97 (1981).
32. Deakin, M. R.; Melroy, O., *J. Electroanal. Chem.*, **239**, 321 (1988).
33. Bruckenstein, S.; Shay, M., *J. Electroanal. Chem.*, **188**, 131 (1985).
34. Muller, A.; Wicker, M.; Schumacher, R.; Schindler, R. N., *Bunsenges Phys. Chem.* **92**, 1395 (1988).
35. Schumacher, R.; Gordon, J. G.; Melroy, O., *J. Electroanal. Chem.*, **216**, 127

- (1987).
36. Schumacher, R.; Gordon, J. G.; Melroy, O., *J. Electroanal. Chem.*, **216**, 127 (1987).
 37. Varineau, P. T.; Buttry, D. A., *J. Phys. Chem.*, **91**, 1292 (1987).
 38. Buttry, D. A.; Orata, D., *J. Am. Chem. Soc.*, **109**, 3574 (1987).
 39. Hillman, A. R.; Loveday, D. C.; Bruckenstein, S., *J. Electroanal. Chem.*, **300**, 67 (1991).
 40. Hillman, A. R.; Loveday, D. C.; Bruckenstein S., *Langmuir*, **7**, 191 (1991).
 41. Lasky, S.; Buttry, D. A., *J. Am. Chem. Soc.*, **110**, 6258 (1988).
 41. Mizunuma, M.; Ohsaka, T.; Miyamoto, H.; Oyama, N., *Bull. Chem. Soc. Japan*, **64**, 2887 (1991).
 42. De Long, H. C.; Donohue, J. J.; Buttry, D. A., *Langmuir*, **7**, 2196 (1991).
 43. Deakin, M. R.; Buttry, D. A., *Anal. Chem.*, **61**, 1147A (1989).
 44. Buttry, D. A., in "Electroanalytical Chemistry, A Series of Advances Vol. 17", Ed. Allen J. Bard, Marcel Dekker, INC, New York New York, 1991, pp. 2-85.
 45. Schumacher, R., *Angewandte Chemie*, **29**, 329 (1990).
 46. Ward, M. D.; Buttry, D. A., *Science*, **249**, 1000 (1990).
 48. Buttry, D. A.; Ward, M. D., *Chem. Rev.*, **92**, 1355 (1992).
 49. Burke, L. D.; Lee, B. H., *J. Electroanal. Chem.*, **330**, 637 (1992).
 50. Deakin, M. R.; Li, T. T.; Melroy, O. R., *J. Electroanal. Chem.*, **243**, 343 (1988).
 51. Melroy, O. R.; Kanazawa, K.; Gordon, J. G.; Buttry, D. A., *Langmuir*, **2**, 697

(1985).

52. Hillier, A. C.; Ward, M., *Anal. Chem.*, **64**, 1289 (1992).
53. Goss, C. A.; Charych D. H.; Majda, M., *Anal. Chem.*, **63**, 85 (1991).

APPENDIX

EQCM OPERATIONS MANUAL

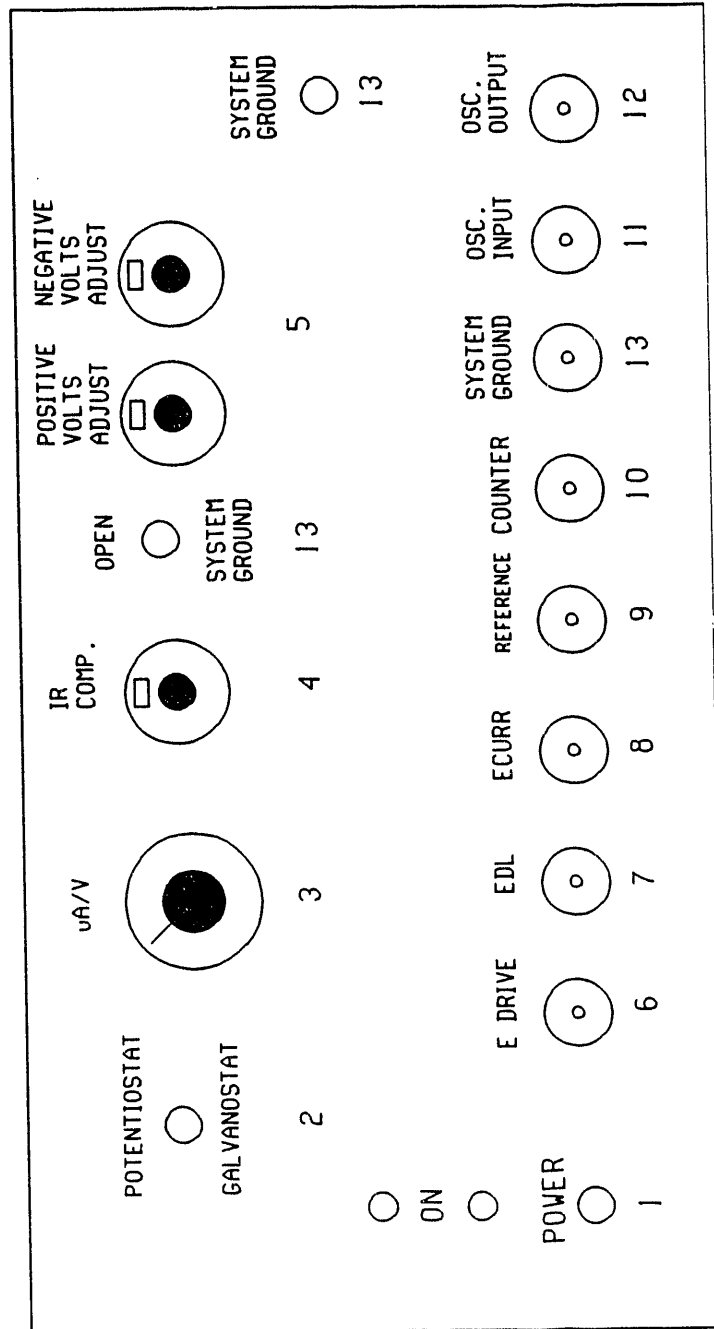
Introduction

The EQCM is used to measure mass changes occurring on the surface of a Au EQCM electrode during electrochemical experiments [1-4]. The heart of this device is a dual potentiostat/oscillator that was built in Ames Laboratory's Instrument Services. This manual is a condensed guide for the proper operation of the EQCM.

A diagram of the front panel of the potentiostat/oscillator is seen in Figure 1. The power switch (1), with its positive (+) and negative (-) lights, indicates when the device is ON and being powered appropriately by both batteries. If both lights are not lit after the instrument is turned on, check the battery connections to insure that they are secure and are properly attached to the correct pole. The potentiostat/galvanostat switch (2) allows operation in either the constant-potential (potentiostatic) or constant-current (galvanostatic) mode.

The current-to-voltage converter (3) is used to control the current sensitivity for the experiment via a set of resistors. The IR-compensation adjust (4) is used only for experiments performed in nonaqueous solutions with high resistance. Finer control of the oscillator circuit is provided using the positive and negative voltage adjusts (5), to produce a more stable oscillation. The E Drive BNC (6) connects the A/D board through

Figure 1. An illustration of the front panel for the potentiostat/oscillator.

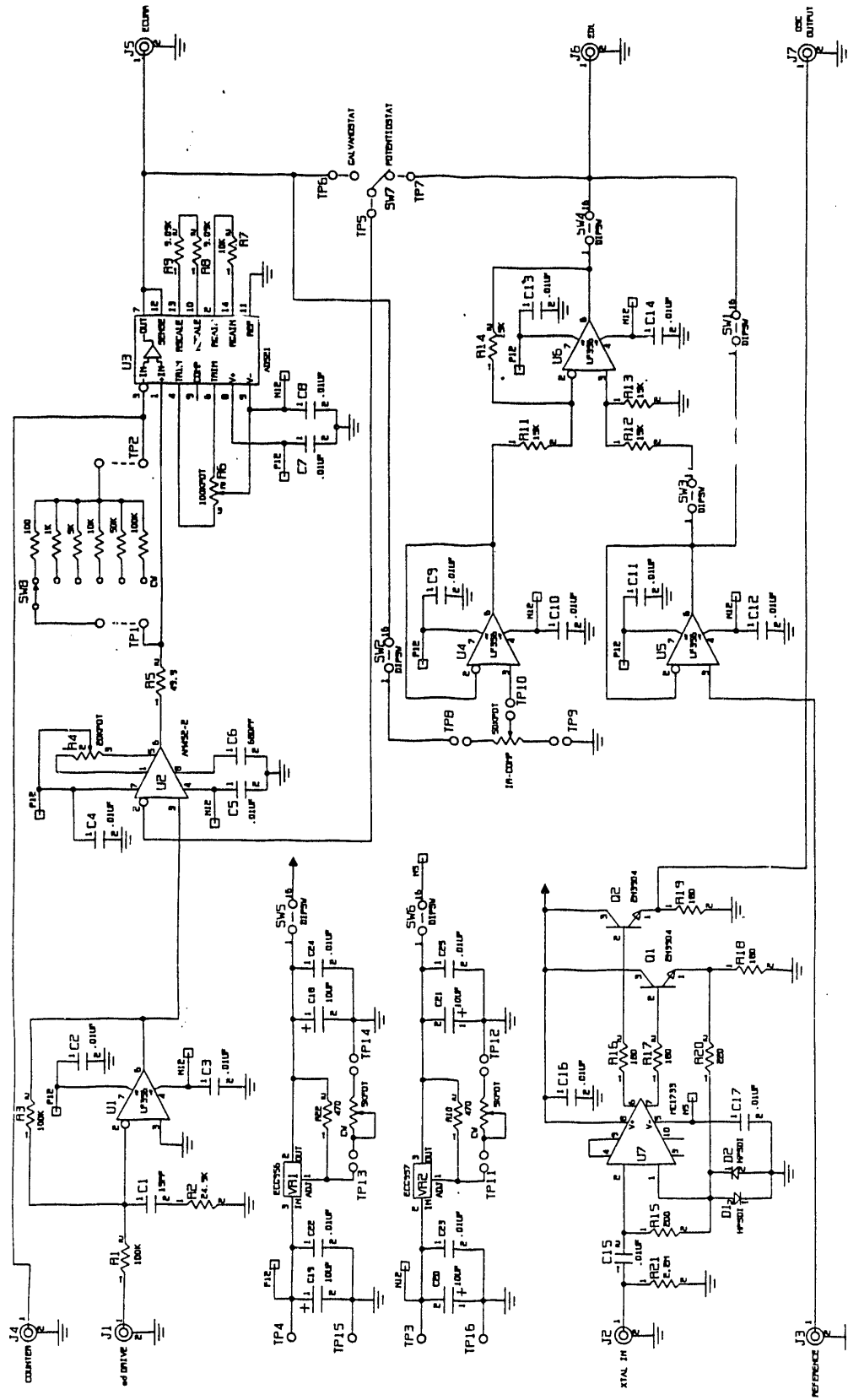


the screw terminal board to the computer (D/A Channel 0) or Pine Instruments RDE4 potentiostat for controlling the potential applied to the electrochemical cell. The potential being applied to the electrochemical cell is monitored through A/D Channel 6.

The EDL BNC (7) is used in conjunction with the IR compensator for computer potential control when experiments are performed in nonaqueous solutions. The electrochemical cell current is monitored with ECURR BNC (8) through A/D Channel 4. The Reference and Counter BNC, (9) and (10) respectively, are leads to the appropriate electrodes in the electrochemical cell. The OSC Input BNC (11) couples the oscillator circuit to the quartz crystal. The grounded side of this lead is connected to the Au film on the crystal serving as the working electrode for electrochemical experiments. This film is on the side of the crystal referred to as the "solution" side because it will be in contact with the solution during the experiment. The other lead is connected to the Au film serving to generate the oscillating electric field causing the crystal to oscillate. This film is on the "air" side of the crystal because it faces away from the solution and contacts only air.

The OSC Output BNC (12) links the oscillator circuit and the frequency counter (Phillips PM 6654C). The output from the frequency counter is monitored through A/D Channel 5. The grounding of the circuitry is accomplished with the grounding switch and either of two grounding terminals (13). The system ground is connected to the screw terminal board. A 286 IBM-compatible computer and the EQCM are interfaced using a Data Translations DT2801 12 bit data acquisition board. The circuit diagram for the EQCM is shown in Figure 2.

Figure 2. The schematic circuit diagram for the potentiostat/oscillator.



Operation

1. The computer is turned **ON** by depressing the red switch on the right-hand side of the multi-socketed surge protector.
2. At this point, it is advantageous to check the voltage of the batteries used to power the system. Leads for the multimeter may be disconnected from the screw terminal board and connected to the batteries, one at a time, to determine their output voltage. This value should be $12\text{V} \pm 1\text{V}$; if not, the batteries are to be recharged, one at a time, using a recharger. Commercial rechargers are available for these batteries; however, with care a typical car battery recharger can be used. The lowest possible constant current setting for the car battery recharger is used (typically 2A) because the maximum amperage that can be applied to the batteries is 8.3A. Each battery is recharged until its output voltage is $> 11.5\text{V}$. This usually requires 4 - 6 hours. Care should be taken not to overcharge the batteries. Therefore, it is recommended that the charging be supervised and located in a fume hood. A car battery recharger is obtainable, on loan, from the Research Equipment Assistance Program (R.E.A.P.), 93 Physics.
3. After checking the batteries and before turning **ON** the EQCM, the appropriate software must be loaded into the computer because the A/D board outputs 2.5V to the circuitry as a default value. Prolonged exposure to this voltage could damage the electrode surface. The appropriate software is loaded by typing the following commands

into the computer:

(the commands you will type are in bold print):

a. The command prompt in DOS is "C:\", at the prompt
C:\ **ASYST**

b. The command prompt in ASYST is "OK" (Note the spacing, capitalized letters and period's)

OK LOAD SETUP. to establish the necessary arrays and variables.

c. **OK LOAD ANALOGCV.** to perform a cyclic voltammetric experiment.

OK LOAD GCHRO. to perform a chronoamperometric experiment.

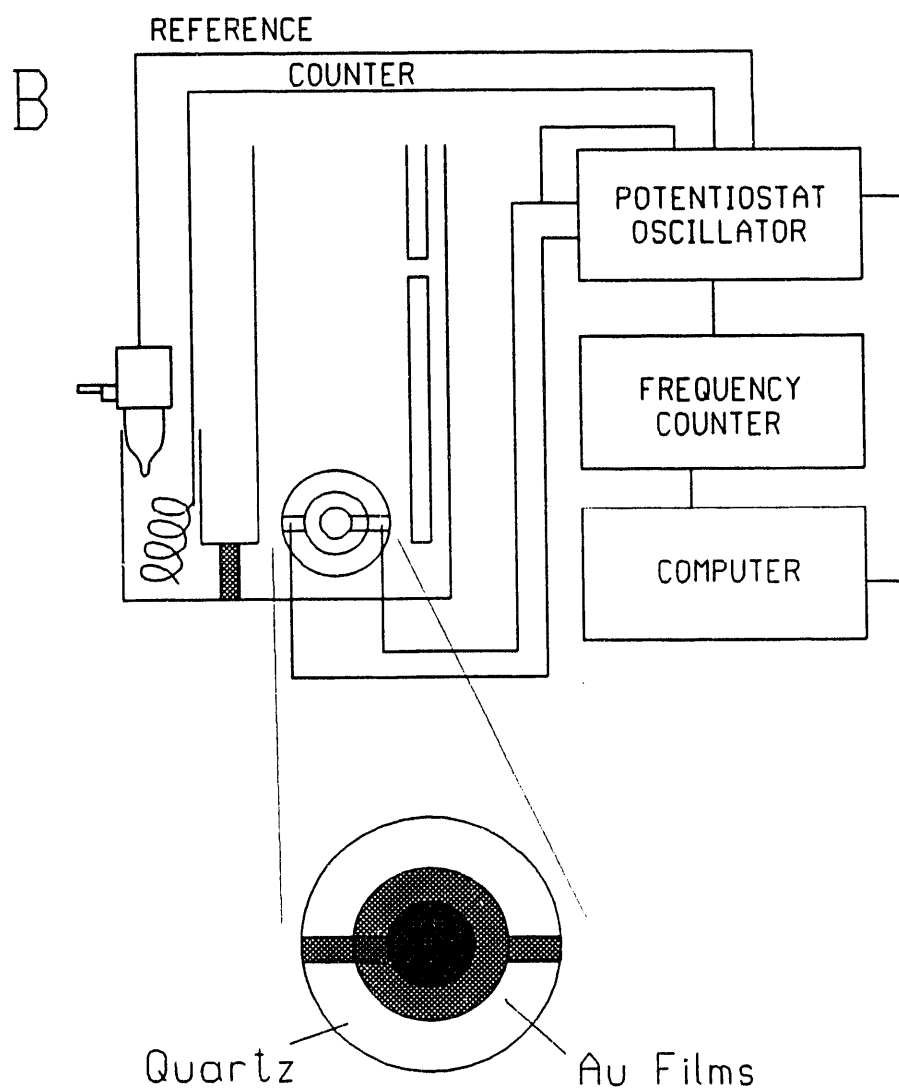
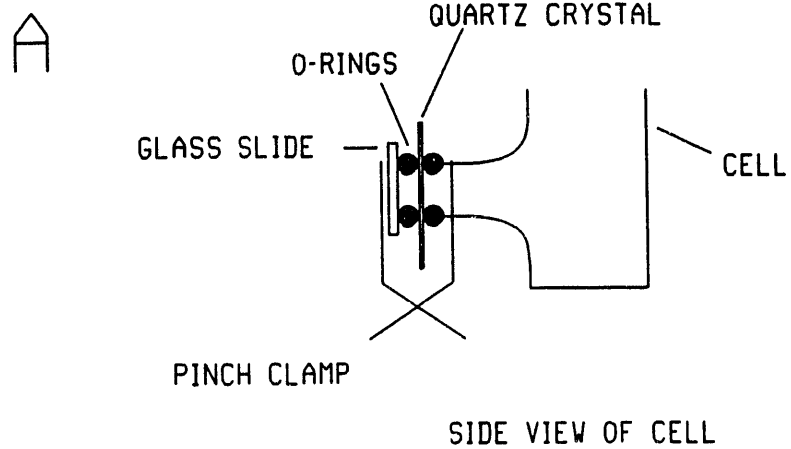
TYPICAL VALUES

<u>ANALOGCV.</u>		<u>GCHRO.</u>	
UPPER POT.	1.0 V	FREQ SCALE	100 F. S.
LOWER POT.	-1.0 V	CURR. CONVERT	5.555 mA/V
START POT.	0.0 V	DELAY TIME	5 SEC
SCAN RATE	100 mV/S	TIME 1	30 SEC
FREQ SCALE	100 F. S.	TIME 2	30 SEC
CURR. CONVERT	0.555 mA/V	TIME/PT	65 SEC
		INITIAL POT.	0.0 V
		FINAL POT.	1.0 V

These are reasonable values, but specific values depend on the particular reactant being investigated and the type of information desired from the experiment. In setting the frequency scale (FREQ SCALE), "F. S." is the abbreviation for Full Scale.

4. After the programs are loaded, the EQCM cell is assembled according to the following procedure: (The fully assembled cell is illustrated in Figure 3A)

Figure 3. (A) An illustration of the fully assembled EQCM cell. (B) An illustration of all of the EQCM components with an expanded view of a quartz crystal with Au films vapor deposited onto both sides. The large electrode area = 1.21 cm^2 and the small electrode area = 0.28 cm^2 .



- a. One of the small black O-rings is placed into the O-ring seal joint on the EQCM.
 - b. A quartz crystal with the large Au contact side facing into the cell is placed onto the O-ring so that the entire circular portion of the contact is inside the O-ring.
 - c. A second O-ring is placed on the back side of the quartz wafer exactly eclipsing the first O-ring to avoid cracking the crystal.
 - d. One half of a microscope slide is placed onto the second O-ring so that the quartz wafer is sandwiched between the two O-rings.
 - e. Finally, a pinch clamp is carefully placed onto the assembly to secure the quartz wafer. Again, care must be taken to ensure that the O-rings are properly aligned to avoid breaking the crystal.
 - f. The cell is now ready to be filled with reactant/electrolyte. The small cell volume requires only 20 - 25 ml of solution. Caution should be exercised to carefully check the surface of the quartz crystal to ensure that no air bubbles are trapped on the Au electrode which could adversely affect the frequency measurements.
5. After assembling and filling the cell, electrical connection to the reference (sat'd. calomel electrode) and counter (Pt wire) electrodes should be made before turning **ON** the EQCM. After these connections are made, the EQCM may be turned **ON**. Once the EQCM is **ON**, the OSC input is connected to the metal film on the "air" side of the crystal first. Finally, the grounded side of the OSC input is connected to the metal film on the "solution" side of the crystal, i.e. the working electrode. Figure 3B illustrates the EQCM equipment and arrangement. Care must be taken that the leads from the OSC

Input do not break the crystal by placing an inordinate amount of strain on it.

6. The multimeter and frequency counter are used to determine if the appropriate potential and frequency are being registered. [NOTE: The Keithley Model 197 Digital Multimeter Operator's Manual and the Philips PM6654C Programmable Timer and Frequency Counter Operator's Manual should be consulted for their proper operation.] If the expected potential and a frequency value of $ca. 5 \pm 0.3$ MHz is not obtained, first, the working electrode should be disconnected and all of the other connections should be checked. If this does not alleviate the problem, disconnect the working electrode, reload the program, reconnect the working electrode, and check again. It may be necessary also to adjust the negative and/or positive voltage controls (5) on the front panel to produce a stable oscillation frequency. If this is the problem only a slight adjustment will be required. Perform this last procedure as a last effort. If the problem is not alleviated, the crystal should be replaced.

7. The programs are executed with the following commands:

OK RUNCV to execute ANALOGCV.

OK CHRONOG to execute GCHRO.

All the data is stored in predefined arrays, and after collection can be viewed with the following commands:

OK SHOWC to plot potential vs. current for data collected with ANALOGCV.

OK SHOWF to plot potential vs. frequency for data collected with ANALOGCV.

OK PLOT C to plot time vs. current for data collected with GCHRO.

OK PLOT to plot time vs. frequency for data collected with GCHRO.

After collection, the data can be stored on the computer's hard disk or a floppy disk for future reference with the commands:

OK LOAD STOCV. when ANALOGCV. has been executed

OK LOAD STOCHRO1. when GCHRO. has been executed

A file name is required followed by an optional short description of the experimenters choosing.

8. The two programs ANALOGCV. and GCHRO. operate under different potential control mechanisms. In ANALOGCV., the program is written such that the Pine RDE4 potentiostat controls the potentials applied to the electrochemical cell. Under this analog potential control, the computer acts as a sophisticated recorder reading in potential, current, and frequency from the oscillator/potentiostat and the RDE4 potentiostat. This means that the potential values input to initiate the program (p. 162) **MUST** be the same as those set on the front of the RDE4 potentiostat in order for data to be collected in the proper range and at the proper time interval. The E Drive BNC is connected to the RDE4 potentiostat through the output voltage terminal, label E1 on the RDE4's front panel. In GCHRO., the program is written such that the computer outputs potential values digitally at given times. For computer controlled potential application, the E Drive BNC is connected to D/A Channel 0. The RDE4 potentiostat is not a component in this configuration.

9. To shutdown the system, first disconnect the working electrode and then the turn **OFF** the potentiostat/oscillator. All other leads are disconnected at this time, in no specific order. If the EQCM is not to be used for a prolonged period of time (> 30 min.), the working electrode should be disconnected and the potentiostat/oscillator turned **OFF** (All other connects may be left intact). This decreases unnecessary drain on the batteries and helps prevent the application of spurious potentials. ***NOTICE*** In case of an emergency the potentiostat/oscillator can be simply turned **OFF**.

10. Once data has been stored it can be recalled into the ASYST environment by using the program GETCV. To recall a previously saved file:

OK LOAD GETCV.

This command is used regardless of the whether ANALOGCV. or GCHRO. was used to collect the data. With GETCV. loaded, the commands

OK SHOWC

OK SHOWF

are used to view the current and frequency data, respectively, regardless of which program was used to collect the data.

11. Once all work is completed, the command to exit the ASYST is

OK BYE

The DOS command prompt should appear on the screen. ***IMPORTANT*** The EQCM should be completely shutdown and the cell disassembled before exiting the ASYST

environment (see step 7).

12. Before turning the computer **OFF**, it is necessary to park the hard drive to prevent damage to stored data. This is accomplished with the following commands:

- a. C:\ **PCTOOLS**
- b. then press the F3 key followed by **P**. A note should appear that the hard drive is parked and that the computer may be shut off.

The computer can be turned **OFF** by depressing the red switch on the right side of the surge protector.

References

1. Deakin, M. R.; Buttry, D. A., *Anal. Chem.*, **61**, 1147A (1989).
2. Buttry, D. A.; in "Electroanalytical Chemistry, A Series of Advances, Vol. 17", Ed. Allen J. Bard, Marcel Dekker, Inc., New York, New York, 1991, p. 2-85.
3. Schumacher, R., *Angewandte Chemie*, **29**, 329 (1990).
4. Buttry, D. A.; Ward, M. D., *Chem. Rev.*, **92**, 1355 (1992).

**DATE
FILMED**

11 / 5 / 93

END

